Multiresolution analysis of electronic structure: semicardinal and wavelet bases

T.A. Arias
Department of Physics
Massachusetts Institute of Technology
Cambridge Massachusetts

Reviews of Modern Physics, in press for January 1999.

Abstract

This article reviews recent developments in multiresolution analysis which make it a powerful tool for the systematic treatment of the multiple length-scales inherent in the electronic structure of matter. Although the article focuses on electronic structure, the advances described are useful for non-linear problems in the physical sciences in general. Among the reviewed developments is the construction of *exact* multiresolution representations from extremely limited samples of physical fields in real space. This new and profound result is the critical advance in finally allowing systematic, all electron calculations to compete in efficiency with state-of-the-art electronic structure calculations which depend for their celerity upon freezing the core electronic degrees of freedom. This review presents the theory of wavelets from a physical perspective, provides a unified and self-contained treatment of non-linear couplings and physical operators and introduces a modern framework for effective single-particle theories of quantum mechanics.

PACS numbers: 71.15.-m, 31.15.-p, 02.30.Mv

Contents

List of Figures

List of Tables

I Introduction

The focus of this review is the application of wavelet theory to the determination of electronic structure. Wavelet theory has at its foundation a single, simple idea: *multiresolution analysis*[Mal89, Mey86, Mey90], a relatively recent and mathematically rigorous theory of the description of functions which provides simultaneously for a homogeneous underlying description of space and the capacity to control and vary the resolution of this description at will.

Interest in multiresolution analysis and wavelet theory has mushroomed dramatically since their introduction. Over seventy-two monographs have been written on the general subject of wavelets within the last six years. (For a comprehensive review of the literature of the field prior to 1993, see [PSU93].) In addition to several recent introductory texts[Kai94, HW96, SN96, GGBB97], specialized monographs are now available which discuss applications to such wide-ranging fields as chemical engineering[MJ94], bio-medical engineering[Aka97] and applied science[DFB97], as well as the traditional areas of application in mathematics[MCC97] and signal processing[Sut98]. In terms of recent monographs, those of the greatest relevance to the present discussion describe the application of wavelets methods to partial differential equations[DKO97, ALM$^+$97].

The well-known fact that the electronic wave functions in molecular and condensed-matter systems vary much more rapidly near the atomic nuclei than in interatomic regions calls for precisely the capabilities of multiresolution analysis. Figure 1 illustrates the multiscale behavior of electronic wave functions, using the carbon atom as an example. The curves in the figure show the Kohn-Sham orbitals of the atom as computed within the local density approximation[KS65] to density functional theory[HK64]. In the immediate vicinity of the nucleus and its strong attractive potential, the electrons possess large kinetic energies, as reflected by high spatial frequencies evident in the orbitals. In this example, the high-frequency "core" region extends only approximately 0.5 Bohr radii out from the nucleus in the case of carbon, beyond which the variations in the wave functions are quite smooth. Resolving the cusps in the s states of this atom requires a resolution on the order of 0.03 Bohr (corresponding to a plane wave cutoff[PTA$^+$92] of nearly 160,000 Rydberg). To provide this resolution uniformly throughout a computational cell of 8 Bohr on a side would require a basis with 16 million coefficients. The vast majority of these basis functions would be wasted as they would serve to provide unnecessarily high resolution outside the core region; only about sixteen thousand functions would be needed to provide the required resolution uniformly throughout the core region defined above.

Multiresolution analysis allows us to add resolution precisely into the core in a systematic, hierarchical manner. The solid curves in Figure 1 come from the earliest reported application of multiresolution analysis to self-consistent electronic structure calculations in three dimensions[ACLT95]. Despite the high resolution needed in the core, these multiresolution calculations required fewer that three thousand basis functions and yet produce results nearly indistinguishable from the output of atomic calculations carried out at essentially infinite resolution by exploiting spherical symmetry to produce an effective one-dimensional problem and then using a very fine radial grid.

Figures 2-3 present similar all-electron calculations for the N_2 molecule[Ari95]. Figure 2 shows the lowest energy Kohn-Sham orbital. The 1σ symmetry of the state and the cusps near the nuclei

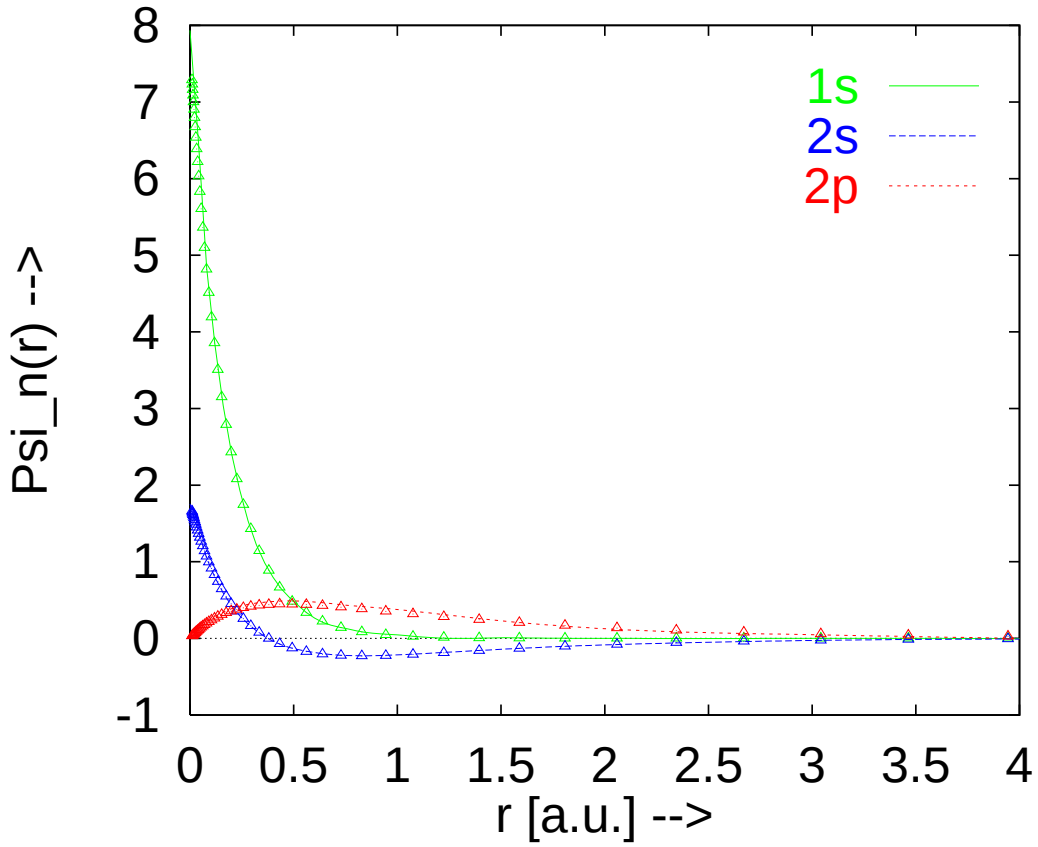

Figure 1: Early electronic structure calculations using multiresolution analysis[ACLT95]: Kohn-Sham orbitals of the carbon atom within the local density approximation from standard atomic software (diamonds) and multiresolution analysis (curves).

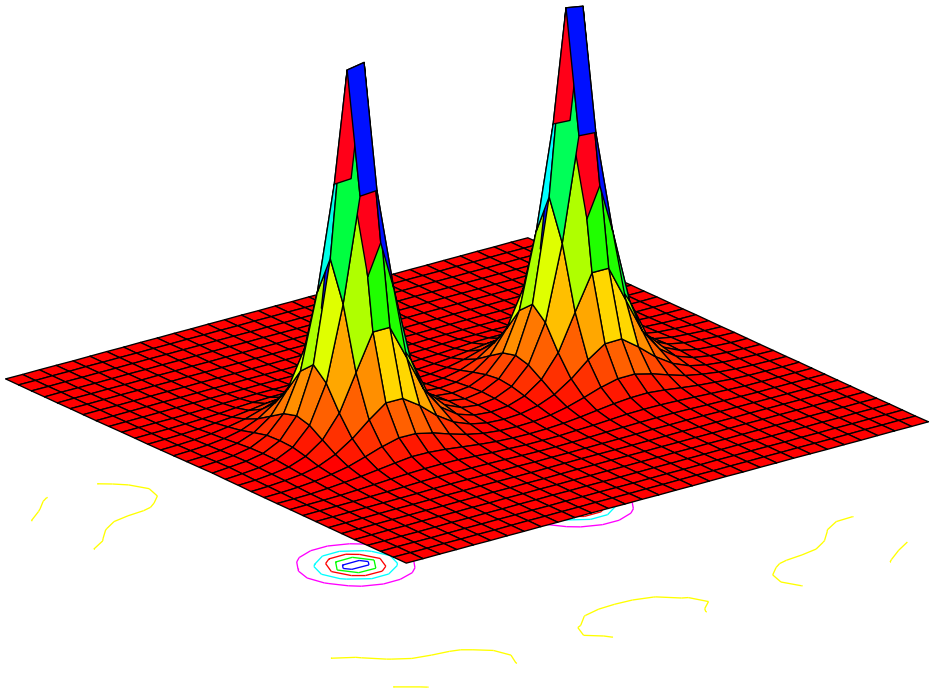

Figure 2: 1σ Kohn-Sham orbital of N_2 in plane containing both nuclei.

are clearly visible. Figure 3 shows results for the bond length and vibrational frequency of the molecule. Using the cubic fit in the figure, we find a bond length and a spring constant within 0.1% and 7% of experiment, respectively. Both these and the preceding atomic calculations were carried out in the same 8 Bohr periodic cell at an effective resolution resolution of corresponding to 16 million coefficients. Both sets of calculations used the $l = 3$ interpolating scaling functions of the product form discussed in Sec. V-C.4 and the basis restriction strategy described in Sec. III-A with seven levels of resolution.

The succeeding pages lay out the explicit details of how these and other calculations of electronic structure have been performed using multiresolution analysis. Although the emphasis of this review is the calculation of electronic structure, the techniques we describe are widely applicable to other physical problems involving coupled sets of linear and non-linear partial differential equations. Shortly after the initial reports of the above applications to electronic structure calculations, independent applications of the ideas of wavelet theory to physical problems described by partial differential equations appeared in a variety of areas, including combustion[FS94, FS97] and fluid mechanics[VYP97, CD97]. General model problems have also been explored[BK95, BN96, BK97]. And, more recently, the solution of Poisson's equation has been studied[GI98, LAE98].

The issue of multiple length-scales in electronic structure is not new. It has driven the development of a variety of techniques which are now quite mature, including the linear muffin tin orbital (LMTO) method[And75], the linearized augmented plane wave (LAPW) method[Sin94], the full potential LAPW (FLAPW) method[WKWF81] and the plane wave pseudopotential approach[PTA$^+$92]. The first three methods use one type of basis set inside of a set of spheres organized around the nuclei and another type of basis set outside of the spheres. The wave functions are then matched at the spherical boundaries to determine the solution. The plane wave

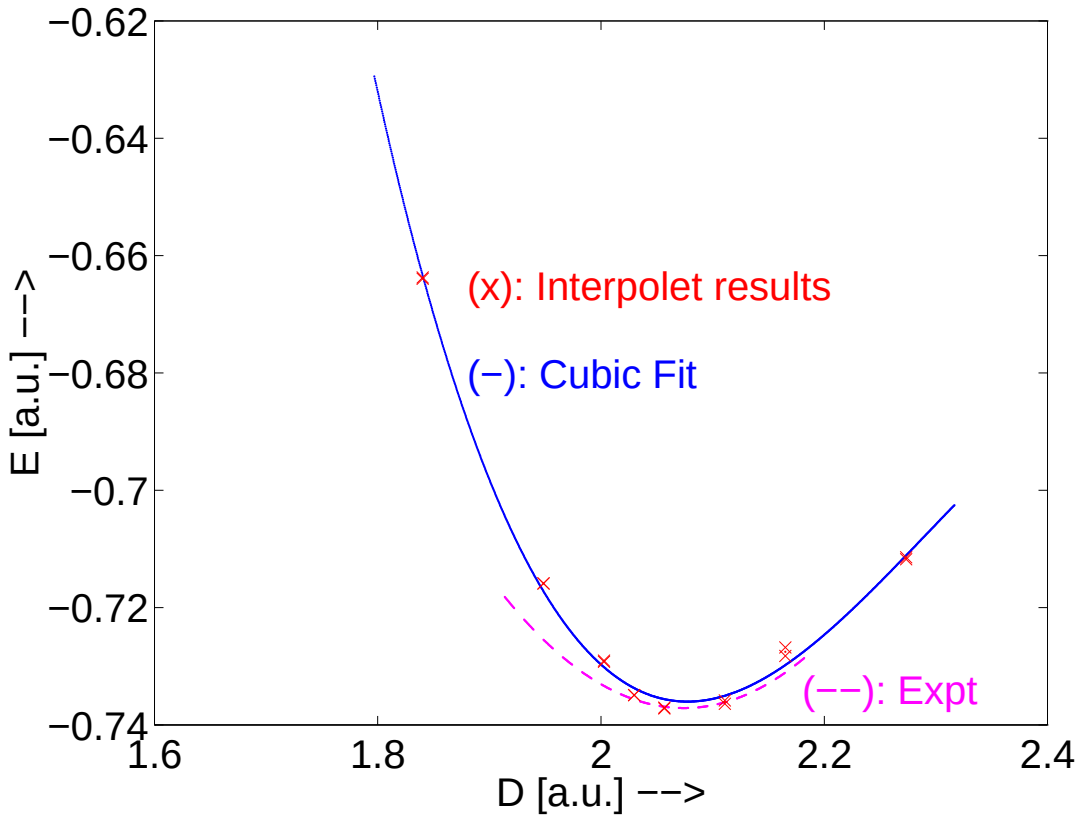

Figure 3: Energy of N_2 as a function of inter-nuclear separation: results of multiresolution analysis (crosses), cubic fit and quadratic with experimental curvature and minimum (solid and dashed curves, respectively).

pseudopotential approach replaces the atomic core with an effective potential manufactured to have similar scattering properties. While each of these approaches has had great success, none is systematically improvable to complete convergence in a simple, practical manner, and each requires great care and expertise in the selection and construction of the atomic spheres or in the development of appropriate pseudopotentials. As a result, a general method is still needed to obtain unambiguous results to a sufficient accuracy to permit direct and systematic study of the relative accuracy of competing density functionals and alternate theories of electronic structure.

As illustrated briefly above and discussed in depth below, multiresolution analysis provides a systematic approach which can replace millions of grid points with merely thousands of basis functions. The development of the multiresolution analysis of electronic structure therefore holds the promise of at last enabling the systematic evaluation of different theories of electronic structure at high precision. In addition, the mathematical structure of multiresolution analysis is sufficiently rich so that new algorithms and techniques are constantly being developed, making it probable that multiresolution approaches will prove to be not only more accurate and systematic, but also more computationally efficient than present approaches.

This review is organized as follows. Section II overviews the equations of density functional theory and gives an extremely brief review of other modern, systematically improvable approaches to the calculation of electronic structure. Section III introduces a new basis-set independent matrix language to express the equations of density functional theory. Section IV lays down the mathematical framework of multiresolution analysis in a language suited for physical applications in multiple dimensions, and Sec. V gives specific examples of basis functions which fit into this framework. Secs. VI-VII then describe new methods which are needed to make the application of the operators and transforms associated with these functions feasible in physical calculations of complex systems. Finally, the review concludes in Sec. VIII with a few brief remarks.

II Electronic Structure

II-A Kohn-Sham Lagrangian

Over the last several decades, density functional theory has proven an accurate, reliable and effective tool for predicting electronic structure. It has found application in such diverse areas as the study of surfaces, point defects, melting, diffusion, plastic deformation, disorder, catalysis, phase transitions and chemical reactions. For reviews see [Coh84, AFO85, Pic89, PTA$^+$92].

In standard atomic units, $\hbar = m = e = 1$, the equations of density functional theory in the local density approximation (LDA) [KS65] are equivalent to finding the *saddle* point of lowest energy of the Lagrangian functional,

$$\begin{aligned}\mathcal{L}_{LDA}(\{\psi_i\},\phi) &= \frac{1}{2}\sum_i f\int d^3r\,||\nabla\psi_i(r)||^2 + \int d^3r\,V_{\rm ion}(r)n(r) \\ &\quad + \int d^3r\;\epsilon_{xc}(n(r))n(r) - \Re\int d^3r\,\phi(r)(n(r)-n_0) \\ &\quad - \frac{1}{8\pi}\int d^3r\,||\nabla\phi(r)||^2, \end{aligned} \tag{1}$$

where the electron density is defined as

$$n(r) \equiv \sum_i f|\psi_i(r)|^2, \tag{2}$$

the orbitals $\{\psi_i\}$ obey the orthonormality constraint

$$\int d^3r \ \psi_i^*(r)\psi_j(r) = \delta_{ij}, \tag{3}$$

and $\Re(z)$ denotes the real part of the complex number z. Here, $V_{\text{ion}}(r)$ is the potential of each electron due to the presence of the nuclei (and core electrons in the case of pseudopotential calculations) in the system, and $\epsilon_{xc}(n)$ is the exchange-correlation energy per electron in a uniform electron gas of density n. For simplicity, in this review we hold the occupation factors f in (1) and (2) fixed at $f \equiv 2$ to reflect the fact that two electrons of spin 1/2 may occupy each orbital. For calculations in periodic systems, we introduce n_0, which corresponds to a positive charge background neutralizing the electronic charge density. The effect of this background on the total energy is properly accounted when the Ewald summation is used to compute the interionic interactions.

At the saddle point, the value of $\mathcal{L}_{LDA}$ is the total Kohn-Sham energy of the system[KS65], and the fields $\{\psi_i(r)\}$ and $\phi(r)$ are the Kohn-Sham orbitals (electronic wave functions) and the Hartree potential (the electrostatic field arising from the mean electron density), respectively. Taking the real part of the integral coupling the electron density $n(r)$ to the Hartree field $\phi(r)$ ensures that $\phi(r)$ is real at the saddle point. This Lagrangian formalism for density functional theory, introduced in [LAE98], has the advantage over the standard energy functional approach of rendering local in space all couplings among the physical fields. This not only dramatically simplifies formal manipulations but also allows for the practical strategy of a direct search for the saddle point to solve the Schrödinger and Poisson equations simultaneously.

Three factors make locating the saddle point of (1) challenging. First, the Lagrangian deals with continuous fields which must be describe in terms of a finite number of coefficients for the purpose of calculation. Second, the solutions we seek exhibit multiscale behavior. Finally, the Lagrangian couples the fields *non-linearly*, both through the exchange-correlation energy density $\epsilon_{xc}(n) \cdot n$ and through the term coupling the Hartree field and the electronic charge density, $\phi(r)n(r)$.

A variety of systematically improvable approaches have appeared in the literature to meet these challenges. To place the development of multiresolution analysis in context, we now give a brief overview of these other approaches. We shall not discuss the muffin-tin families of approaches, which are not so closely related to multiresolution analysis, beyond their brief mention in the introduction.

II-B Systematic basis approaches

II-B.1 Plane wave approach

The plane wave approach is reviewed in detail in [PTA$^+$92]. In this approach, the Kohn-Sham orbitals and the Hartree potential are expanded in a discrete basis of plane waves (complex exponentials) consistent with periodic boundary conditions. The resulting discrete set of expansion coefficients for the orbitals $\{\psi_i\}$ and Hartree potential ϕ are well-suited for computation.

In a plane wave basis, differential operators are diagonal, making their implementation particularly simple. The remaining couplings in the Lagrangian (1) are the non-linear, spatially local couplings. When using a plane wave basis, one implements these couplings on a point by point basis in real space, using the fast Fourier transform (FFT) to convert efficiently between the real space and the plane wave representations.

Plane wave calculations may be brought to convergence simply by increasing a single parameter, the kinetic energy below which all plane waves are included in the basis. This makes systematic basis set convergence studies straightforward. However, the extremely high resolution required

near atomic nuclei combined with the uniform resolution afforded by plane waves makes the direct application of this method prohibitive for all but the lightest elements. The introduction of pseudopotential theory overcomes this limitation, but at the cost of introducing the pseudopotential approximation, which is uncontrolled. One great advantage of multiresolution analysis is that it maintains the regularity of plane wave expansions while allowing variable resolutions and thus the direct treatment of heavier elements.

Finally, even the wave functions in pseudopotential calculations at times require significant resolution near ionic cores, particularly when dealing with first-row elements or transition metals. This opens the exciting possibility of combining the pseudopotential approach with multiresolution analysis, an issue which has begun to be explored[WC96].

II-B.2 Finite element and adaptive mesh approaches

There is an extensive literature dedicated to the finite element approach, particularly in the fields of solid[Bra97] and fluid[Chu92b] mechanics. See [Whi97] for a review of recent developments, and [CB97] for an introduction.

The application of the finite element approach to electronic structure calculations began in the late eighties[WWT89] and has undergone a recent revival[TT95b, TT95a, TT96]. As in the plane wave approach, the finite element method expands the electronic orbitals in terms of a set of basis functions. By using localized basis functions concentrated in the regions of space requiring high resolution, these bases can provide a much more efficient description of electronic wave functions.

Finite elements also represent an extremely efficient method for dealing with non-linear interactions by providing, as do plane waves, highly efficient rapid transforms. For finite elements, these transforms are based on two properties of the basis functions, cardinality and interpolation[Whi97]. Below, we shall discuss how to construct multiresolution analyses which maintain these two highly desirable properties.

One great difficulty with the application of finite elements to electronic structure is that finite elements basis sets must be uprooted and reformed as the nuclei move. Each coefficient in a finite element representation corresponds to the value or weight of a function over the region of one basis function and thus cannot be taken to be small where the electronic orbitals themselves are non-negligible. As a result, coefficients associated with the basis functions which are uprooted as the atoms moves carry large values, and this process must be managed with extreme care. Multiresolution analysis provides an elegant solution to this difficulty which we discuss briefly immediately below and in more depth in Sec. III-A.

Another potential solution to variations in the basis as the atoms move is provided by a branch of finite element methods particularly attractive for the calculation of electronic structure, the "Riemannian metric"[Gyg93, Gyg95, GG95, DKCJ94] or "adaptive curvilinear-coordinate"[Ham95, Ham96b, Ham96a, Ham97, ZMK96, NC97, TT96] approach. This approach lays down the finite element mesh according to a smooth mapping from a underlying cubic grid of points, thereby ameliorating the problems of uprooting the finite element grid as the atoms move. Because it preserves the underlying cubic topology of the grid, the Riemannian metric approach falls into the class of "structured mesh" methods, for which it is difficult to generate very strongly graded meshes[Ran93], a limitation which multiresolution analyses do not suffer.

II-B.3 Multigrid algorithms

Multigrid algorithms provide an extremely effective means of solving equations whose convergence is limited by a wide range of length-scales. This approach too has an extensive literature associated

with its application in a wide variety of fields. For an in-depth introduction, see [Wes92].

Explorations of the multigrid approach as applied to electronic structure calculations also date back to the late eighties[WWT89] and have become much more common in the last few years[GG95, BSB96, TB95, BBSB97]. Multigrid algorithms do not specify a basis set and leave open the issue of how best to discretize physical problems. The mathematical structure of multigrid algorithms parallels very closely the ideas of multiresolution analysis, and multigrid algorithms can be applied directly or easily generalized to the solution of differential equations expressed in wavelet bases[RJZ94, Yes97, YA98].

II-B.4 Multiresolution analysis

Wavelet bases place functions of varying resolution on a multiresolution grid while maintaining a uniform resolution throughout all of space in the precise mathematical sense of multiresolution analysis[Mal89, Mey86, Mey90]. The mathematical regularity of the resulting basis leads to efficient fast transforms[Dau92, Chu92a] and methods to apply differential operators[BCR91, LAE98].

In contrast to the expansion coefficients of a finite-element expansion which reflect directly the values of a function, the coefficients of a multiresolution analysis separate information into different length-scales. This subtle but critically important difference means that, so long as a function varies smoothly, the fine-scale coefficients will be quite small even where the value of a function is quite large. As described in Sec. III-A, this means that, as the atoms move, one may arrange for the changes in the basis to involve the truncation of only coefficients which are small, thereby effectively providing a high resolution throughout all of space with an extremely limited number of coefficients. This also means that no particular care is needed to handle the regriding as the atoms move.

The first electronic structure calculations to use such a basis employed a discrete frame of non-orthogonal Gaussian-Mexican hat basis functions[CAJL93]. This work established the efficacy of such bases for representing electronic wave functions, but the calculations were limited to one-electron systems. The first reported self-consistent, multiple-electron density functional calculations[ACLT95, Ari95] used the semicardinal bases described in Sec. V and employed the analytically continued conjugate gradient approach[APJ92] to solve the Kohn-Sham equations. How Poisson's equation was solved in these calculations is described in more detail in [LAE98]. Wei and Chou[WC96] carried out the first calculations employing orthogonal Daubechies wavelets[Dau92]. This work studied molecular dimers within the local density approximation using Daubechies D6 wavelets, employed self-consistent iteration to solve of the Kohn-Sham equations, and represented the first use of pseudopotentials in the multiresolution analysis of electronic structure. Since that time, Tymczak and Wang[TW97] used Daubechies D8 wavelets and introduced the innovations of dynamically refining the basis and the use of the Car-Parrinello approach to solve the Kohn-Sham equations. Most recently, Goedecker and Ivanov [GI98] have applied lifted wavelets[Swe96] to the solution of Poisson's equation.

Until recently, the primary bottleneck in multiresolution analysis calculations of electronic structure had involved the performance of transforms and the application of differential operators. The standard transforms associated with orthogonal wavelet bases require or produce the values of the electronic orbitals on a uniform grid at the finest resolution. To use these transforms, one "unpacks" each electronic orbital from its stored coefficients, operates on the unpacked version, and then "repacks" the result. Although this gives great benefit in terms of the use of memory, processing the wave functions in their highly redundant unpacked representation still involves significant memory and also much wasted computation. For example, applying this approach to the

nitrogen dimer calculations described in the introduction expends hundreds of millions of floating point operations to process each electronic orbital, each of which are represented in terms of only six thousand coefficients.

Workers interested in electronic structure therefore have sought different methods. One approach has been to take techniques from the wavelet literature such as the "non-standard" multiply approach of Beylkin, Coifman and Rokhlin[BCR91], which has been applied to the solution of Poisson's equation in multiresolution bases with the processing of some additional coefficients but still leading to an efficient scheme[GI98]. Workers also have developed new methods specifically for physical calculations[LAE98]. These new methods allow operators to be applied to the electronic wave functions directly in their "packed" representation without processing any additional information and have been shown to be several times more efficient than the non-standard matrix approach in situations typical of electronic structure[LAE98]. The associated transforms have been shown to have the novel property that the process of (a) unpacking the physical fields at a number of points in space equal to only the number of packed coefficients, (b) coupling the physical fields in any local, non-linear fashion at these points, and (c) repacking the result always yields coefficients *identical* to what would be obtained with a fully unpacked function on a grid of *arbitrarily* fine resolution[LAE98]. With these latest advances, the field now stands poised to see the first applications of multiresolution analysis to large-scale electronic structure calculations.

III Multiresolution Analysis of Electronic Structure

III-A Multiresolution analysis and restriction

Section IV reviews the mathematical structure of multiresolution analysis in detail. Here, we give a conceptual overview sufficient to discuss the use of multiresolution analysis in the calculation of electronic structure.

Figure 4 illustrates the concept of multiresolution analysis and its application to electronic structure. Throughout this work we shall use the variables Q, R and P to denote different levels of resolution and will take the coarsest and finest levels of resolution in a given calculation to be M and N, respectively. As [Mal89, Mey90, Dau92, Chu92a, SN96] describe, a multiresolution analysis begins with a basis of coarse resolution $Q = M$, which consists of basis functions laid out on a regular grid across the region of interest (larger circles in the figure). The *span* of this set of functions, the vector space of all functions formed by their linear combinations, is denoted V_M. For reasons which will become clear below, the basis functions of this coarse space are referred to as the *scaling functions*.

The next conceptual step is to increase the resolution of the basis by adding finer resolution functions at the points of a finer grid (smaller circles in the figure). The basis consisting of both the original coarse scaling functions and the new finer functions now spans V_{M+1}, a space of increased resolution $Q = M + 1$. The added functions are referred to as the *detail functions* or the *wavelets*.

One may continue adding finer levels of detail functions to reach the final desired level of resolution, $Q = N$. We shall designate as W_{Q+1} the space spanned by the detail functions which bring the resolution from level Q to the next level $Q + 1$, so that $V_{Q+1} = V_Q \oplus W_{Q+1}$. (Note that some authors prefer to designate the above detail space as W_Q, rather than W_{Q+1}.) Here, as throughout this work, by the addition of vector subspaces "$\oplus$", we mean the space of all vectors which may be written as a sum of a pairs of vectors, one from each subspace. The space of all functions which can be described by functions on all of the scales included in the basis is thus

$$V_N \equiv V_M \oplus W_{M+1} \oplus \ldots \oplus W_N.$$

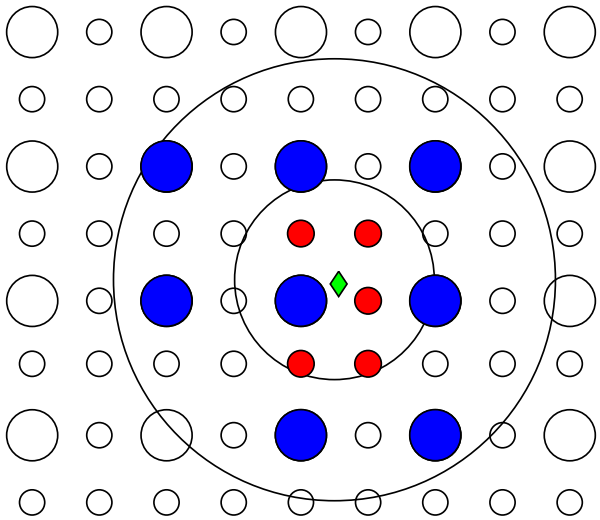

Figure 4: Multiresolution analysis and the application of restriction to electronic structure: coarse grid (larger circles), detail points of finer grid (smaller circles), atomic nucleus (diamond), spheres of resolution (large circles centered on the nucleus), basis functions restricted from basis (empty circles), surviving basis functions (filled circles).

Figure 5 shows the behavior of the expansion coefficients in such a multiresolution basis for the 1σ state of the nitrogen molecule, which appeared in Figure 2 in the introduction. Figure 5 displays, on a logarithmic scale, the magnitude of the expansion coefficients for this state as a function of the two parameters characteristic of each basis function: location in space $\vec{r}$ and resolution Q. The three dimensional location $\vec{r}$ is projected onto the one-dimensional horizontal axis r as the distance from the center of the basis function to the nearest atomic nucleus. The scales Q of the basis functions are coded by different symbols. As evident in the figure, the separation of information into different length-scales afforded by the multiresolution analysis results in separate characteristic exponential decay envelopes with distance from the nuclei for the coefficients of each scale. These envelopes illustrate the fact that the finest scale coefficients need only be kept for basis functions in the immediate vicinity of the nuclei. This is precisely the behavior which makes multiresolution analysis so attractive for the calculation of electronic structure.

The strategy introduced by[CAJL93] to exploit this behavior is illustrated in Figure 4: about each nucleus we draw a set of successively inscribed spheres of appropriate radii for the scales $M, M+1, \ldots, N$, and we keep in the basis only those functions of a given scale which fall within the corresponding sphere. The grid points whose associated functions appear in the final basis set according to this prescription appear as filled circles in the figure. (Calculations with periodic boundary conditions generally include all functions on the coarsest scale.) We refer to this process of selecting grid points and their associated functions as *restriction*. For other applications, it is not always known *a priori* how to restrict the basis. For adaptive restriction approaches, the reader may wish to consult[LPT89, LT90, BK97, BK97]. Tymczak and Wang[TW97] have also developed an adaptive restriction technique specifically for electronic structure calculations.

Selecting the cutoff spheres so as to discard only coefficients below a given tolerance gives a systematic procedure for working with a dramatically reduced number of coefficients while maintaining a description equivalent, for any given tolerance, to the full basis V_N. In contrast to finite

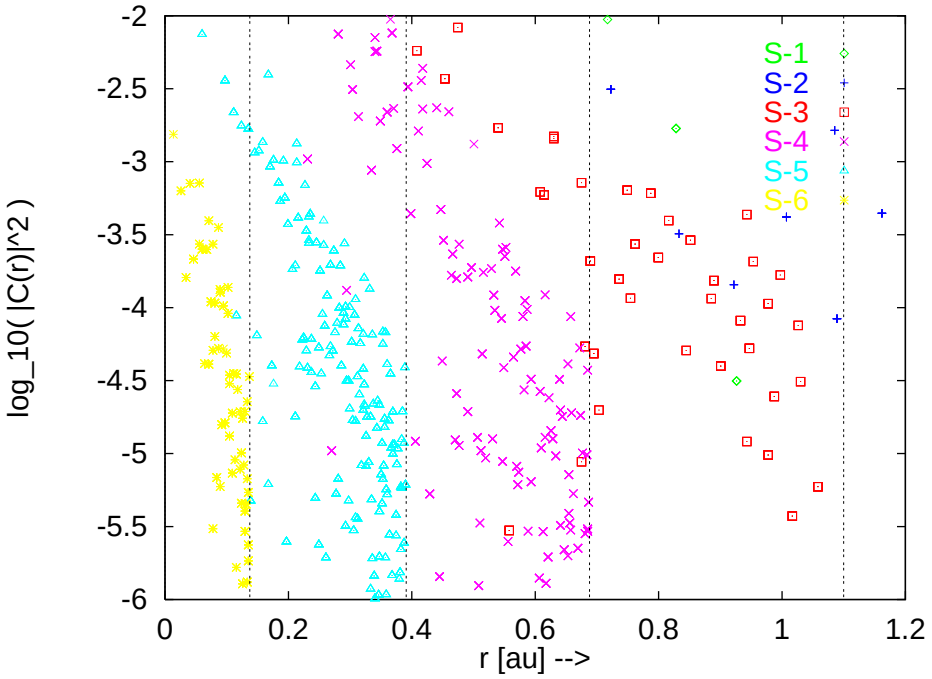

Figure 5: Coefficients of the multiresolution analysis of the 1σ orbital of N_2: radii of restriction are denoted by vertical lines.

element approaches, in multiresolution analysis there are no basis set derivative corrections in the Hellman-Feynman theorem because the basis functions of a multiresolution analysis remain fixed in space as the atoms move. The only effect of the motion of the atoms is to turn on or turn off basis functions whose coefficients are below the selected tolerance. As a result, the discontinuous effects from such on-off switching events are controllable and generally quite small. For example, in the calculations of [CAJL93], although the basis was chosen only to produce correct total energies without regard to the calculation of forces, the small jumps in the forces calculated from the Hellman-Feynman theorem were only on the order of 1 $meV/$Å.

III-B Algebraic structure

The main step in implementing a density functional calculation is to express each term of the LDA Lagrangian (1) in terms of the coefficients d_α and $c_{\alpha,i}$ for the Hartree field $\phi(r)$ and the Kohn-Sham orbitals $\{\psi_i(r)\}$, which appear in the expansions

$$\begin{aligned} \psi_i(r) &= \sum_\alpha c_{\alpha,i} b_\alpha(r) \\ \phi(r) &= \sum_\alpha d_\alpha b_\alpha(r), \end{aligned} \tag{4}$$

where $\{b_\alpha(r)\}$ is the basis set used in the calculation. Once the Lagrangian is represented in terms of these coefficients, the gradients of the Lagrangian with respect to d_α and $c_{\alpha,i}$ may be calculated so as to locate the saddle point and thereby determine the orbitals $\{\psi_i(r)\}$, potential $\phi(r)$ and total electronic energy $\mathcal{L}$ of the system. Several different approaches for expressing the Lagrangian have

been used in the application of multiresolution analysis to electronic structure. Here we present an overview of these approaches and the operators and transformations which they involve. Explicit details and formulae are given in Secs. III-D-III-E.

The simplest terms in the LDA Lagrangian are the electronic kinetic energy T and the Hartree field self-energy V_{H-H}, the first and final terms of (1). These are bilinear in the coefficients and may be evaluated exactly in terms of two-center integrals of the Laplacian operator between the basis functions. Because the matrix elements of the Laplacian operator are known explicitly for functions making up multiresolution analyses (Sec. V-C.2), all implementations of multiresolution analysis to date use this simple two-center form to evaluate T and V_{H-H}[CAJL93, ACLT95, WC96, TW97].

The electron-ion potential energy V_{e-i}, the second term in $\mathcal{L}_{LDA}$, is also bilinear in the expansion coefficients $c_{\alpha,i}$, but the matrix elements of the ionic potential needed to compute V_{e-i} consist of three-center integrals, each involving two basis functions and one ion, and thus require special care. To date, V_{e-i} has been handled through the introduction of a grid G of points p in real space. Two prescriptions for employing this grid exist. The first prescription (used in [ACLT95]) follows the spirit of the energy functional and computes the electron-ion interaction as a functional of the electron density. This recipe first uses a forward transform to determine the values of the wave functions on the grid. From these, the single particle density $n(r) = \sum_i f|\psi_i(r)|^2$ is computed on the grid and the corresponding expansion coefficients are determined through an inverse transformation. From the resulting expansion coefficients, the final step is to compute the total potential energy in terms of known overlaps between the basis functions and the ionic potential. This approach has the advantage that the grid need only be able to resolve the electron density $n(r)$ and not necessarily the potential $V_{\rm ion}(r)$, which may vary much more rapidly. We refer to this approach below as the *energy functional prescription.*

The second prescription (used in [WC96, TW97]) follows the spirit of the effective Schrödinger equation for the Kohn-Sham orbitals and applies the electron-ion interaction as a diagonal operator in real space. This recipe also begins with a forward transform to evaluate the wave functions $\psi_i(r)$ on the points of the grid. It then applies the potential operator at each point p of the grid G to produce $V_{\rm ion}(p)\psi_i(p)$ and inverse transforms the result to coefficient space. Finally, the overlap of $\psi_i^*(r)$ and $V_{\rm ion}(r)\psi_i(r)$ is computed using the known overlaps between the basis functions. We refer to this approach below as the *operator prescription.*

The fourth term of (1) describes the coupling between the electrons and the Hartree field, V_{e-H}. This term is cubic in the expansion coefficients and involves three-center integrals. In principle, a treatment in terms of direct three-point interactions is possible using analytic results for the integrals of triple products of scaling and detail functions developed in [BK97]. To date, this direct route has not been pursued in the calculation of electronic structure. Instead, one may exploit the fact that the coupling V_{e-H} has the same structure as the electron-ion coupling and compute it in the same manner, either as a functional of the electron density or as the result of the application of $\phi(r)$ as a local operator.

The final remaining term, the third term in (1), gives the local density approximation to the total exchange-correlation energy of the system, E_{xc}. This is known only in terms of the non-algebraic function $\epsilon_{xc}(n)$, which is tabulated in [PZ81], and thus cannot be evaluated in terms integrals of products of basis functions using the formalism of [BK97]. For this term, there is no choice but to evaluate the electron density on a grid G and evaluate the tabulated function $\epsilon_{xc}(n)$ on a point by point basis in real space. Once this is done, there are a variety of choices for how to use the exchange-correlation field to determine the total exchange-correlation energy E_{xc}. One could proceed directly and evaluate the exchange-correlation energy density per unit volume $\epsilon_{xc}(n(p)) \cdot n(p)$ at each point and then integrate the result numerically, which would introduce an

additional class of approximation in the evaluation of the Lagrangian. What has been done, instead, is to follow the same prescriptions as used in computing the electron-ion interaction, following either the energy functional prescription and computing E_{xc} as the integral of the product of $n(r)$ and $\epsilon_{xc}(n(r))$[ACLT95] or following the operator prescription and computing E_{xc} as the expectation of $\epsilon_{xc}(n(r))$ as an operator acting on the Kohn-Sham orbitals[WC96, TW97].

III-C Matrix language

To discuss the various approaches available for evaluating the LDA Lagrangian in terms of the expansion coefficients for the physical fields, we now introduce a matrix language for electronic structure methods which are based on single-particle orbitals. In analogy with Dirac's bra-ket language, this matrix language is completely explicit but keeps the expressions for physical quantities independent of the details of the underlying basis set. This allows us to discuss the various strategies for applying multiresolution analysis to electronic structure without obscuring the discussion with irrelevant details. This new language is useful in its own right for both formal manipulations and the development of highly portable, efficient software. Plane wave calculations performed with software developed by translating this language directly into the C++ include [IBA98, CIBA98].

For simplicity, we consider below cases where the Fermi occupations f are constant and the sampling of the Brillouin zone is carried out at the Γ point. More general cases including variable fillings and multiple k-points may be worked out with some additional complexity[APJ92]. For systems sufficiently large that the Brillouin zone may be sampled at the Γ point alone, the formulae below may be used directly.

III-C.1 Fundamental basis-dependent operations

We begin by introducing two operators, diag and Diag. The operator diag converts a matrix to a column vector containing the elements along the diagonal of the matrix, and the operator Diag converts a column vector to a diagonal matrix with the components of the vector placed along the diagonal. In terms of components, for a matrix M and a vector v, these operators are

$$\begin{aligned} (\,\mathrm{diag}\, M)_\alpha &\equiv M_{\alpha\alpha} \\ (\,\mathrm{Diag}\, v)_{\alpha\beta} &\equiv v_\alpha \delta_{\alpha\beta}, \end{aligned} \tag{5}$$

respectively, where $\delta_{\alpha\beta}$ is the Kronecker δ. Note that while $\mathrm{diag}\,\mathrm{Diag}\, v = v$ for any vector v, $\mathrm{Diag}\,\mathrm{diag}\, M = M$ if and only if the matrix M is diagonal. Two identities involving these operators which we shall use freely are

$$\begin{aligned} (\,\mathrm{diag}\, M)^\dagger v &= \mathrm{Tr}\left(M^\dagger\,\mathrm{Diag}\, v\right), \\ v^\dagger\,\mathrm{diag}\, M &= \mathrm{Tr}\left((\,\mathrm{Diag}\, v)^\dagger M\right). \end{aligned} \tag{6}$$

Next, it is useful to regard the Hartree field expansion coefficients, the d_α from (4), as the components of a column vector d and the electronic wave function coefficients, the $c_{\alpha,i}$ from (4), as the elements of a matrix C, each of whose columns contains the expansion for a single electronic orbital, $C_{\alpha i} \equiv c_{\alpha,i}$ For formal manipulations, it is convenient to define also

$$P \equiv f C C^\dagger, \tag{7}$$

the representation of the single particle density matrix in the space of basis functions $\{b_\alpha(r)\}$.

As Sec. III-B describes, evaluation of the Lagrangian (1) in terms of the expansion coefficients contained in d and C requires knowledge both of the overlaps of the basis functions among themselves and of their matrix elements through the Laplacian operator,

$$\mathcal{O}_{\alpha\beta} \equiv \int d^3r\, b^*_\alpha(r) b_\beta(r) \tag{8}$$

$$L_{\alpha\beta} \equiv \int d^3r\, b^*_\alpha(r) \nabla^2 b_\beta(r). \tag{9}$$

The first two non-trivial basis-dependent operations which require careful implementation are multiplication by the inner product matrix $\mathcal{O}$ and by the Laplacian matrix L, to which we refer below as *application of the overlap operator* and *application of the Laplacian operator*, respectively. Section V-C.2 discusses how to compute the required matrix elements, and Sec. VI describes efficient techniques for applying these operators. Note that in the special case of orthonormal bases[WC96, TW97], we have simply $\mathcal{O} = I$, where I is the identity matrix.

The *forward transform* operation described in the previous section converts the expansion coefficients of a function into the values of the function on the points p of the grid G in real space. This operation simply amounts to multiplication of a column vector containing the expansion coefficients by the matrix

$$\mathcal{I}_{p\alpha} \equiv b_\alpha(p), \tag{10}$$

whose α^{th} column consists of the values of the α^{th} basis functions at all of the points p of the grid. In the case where different bases are used for the wave functions and for the Hartree field[WC96, TW97], the columns of $\mathcal{I}$ consist of two subsets, one for each of the two basis sets.

As described in Sec. III-B, it is at times necessary to find the expansion coefficients for a function from its values on the grid G. We denote this linear *inverse transform* operator as $\mathcal{J}$. In implementations where the number of grid points equals the number of basis functions[ACLT95, LAE98, Yes97], the natural choice is to take $\mathcal{J} \equiv \mathcal{I}^{-1}$. However, we maintain the distinction between $\mathcal{J}$ and $\mathcal{I}^{-1}$ because in implementations where a full uniform grid G of sampling points is used[WC96, TW97], there are generally more grid points p than basis functions $b_\alpha(r)$, and $\mathcal{I}$ and $\mathcal{J}$ cannot be inverses. In the case where more that one basis set is used[WC96, TW97], formally, $\mathcal{J}$ computes the inverse transform separately for each basis set. In practice, however, as seen below, only one inverse generally need be computed because $\mathcal{J}$ will be needed only on one basis set.

Finally, as we shall see in Secs. III-D and III-E, two further transforms appear in the calculation of the gradients of the Lagrangian. These two *conjugate* transforms represent multiplication by the Hermitian conjugates $\mathcal{I}^\dagger$ and $\mathcal{J}^\dagger$ of the standard transforms. The reader should bear in mind that the relation $\mathcal{I}^\dagger = \mathcal{I}^{-1} = \mathcal{J}$ for the discrete Fourier transform is quite special. Because orthogonality with respect to integration does not ensure orthogonality with respect to a discrete sampling of the functions the above relation for the discrete Fourier transform is not generally true, even for orthonormal bases. In particular, $\mathcal{I}^\dagger \neq \mathcal{I}^{-1}$ for the multiresolution bases of Daubechies wavelets used in [WC96, TW97].

In summary, six non-trivial basis-set dependent operations are needed in the calculation of electronic structure: the application of two operators (the Laplacian and overlap operator) and four transforms (forward, inverse, and the conjugates to each), which we denote as L, $\mathcal{O}$, $\mathcal{I}$, $\mathcal{J}$, $\mathcal{I}^\dagger$ and $\mathcal{J}^\dagger$, respectively.

III-C.2 Identities

Although the action of the six operations L, $\mathcal{O}$, $\mathcal{I}$, $\mathcal{J}$, $\mathcal{I}^\dagger$ and $\mathcal{J}^\dagger$ depend on the specific choice of basis, they obey several important identities of which we shall make use. In addition to their use in

formal manipulations, these identities provide a useful practical tool to verify the implementation of the various operators.

The most important among these identities involve the constant function. To represent the constant function on the grid, we introduce $\mathbf{1}$, a column vector containing unity as each entry on the grid:

$$\mathbf{1}_p \equiv 1. \tag{11}$$

Plane waves, finite element bases, and proper multiresolution analyses all have the property of being able to represent this function exactly. For these bases, we have that for all points r, $\sum_\alpha (\mathcal{J}\mathbf{1})_\alpha b_\alpha(r) = 1$. Evaluating this on the points p of the grid G yields that, in particular,

$$\mathcal{I}\mathcal{J}\mathbf{1} = \mathbf{1}. \tag{12}$$

For other sufficiently descriptive bases, such as Gaussian bases, this and the relations below should hold at least approximately in the regions described by the basis.

There is a close relationship between the inner product matrix $\mathcal{O}$ and the integrals of the basis functions. The vector

$$s \equiv \mathcal{O}\mathcal{J}\mathbf{1}, \tag{13}$$

is a column vector containing the integrals of each of the basis functions:

$$\begin{aligned} s_\alpha &\equiv (\mathcal{O}\mathcal{J}\mathbf{1})_\alpha \\ &= \int d^3r\; b^*_\alpha(r) \left(\sum_\beta (\mathcal{J}\mathbf{1})_\beta b_\beta(r) \right) \\ &= \int d^3r\; b^*_\alpha(r). \end{aligned}$$

Thus, if g is a vector of expansion coefficients, the integral of the function represented by g is

$$\int d^3r\, g(r) = \int d^3r \sum_\alpha g_\alpha b_\alpha(r) = s^\dagger g. \tag{14}$$

From this, we may also derive the normalization condition

$$s^\dagger \mathcal{J}\mathbf{1} = \int 1\, d^3r = \Omega, \tag{15}$$

where Ω is the volume in which the calculation is carried out.

In solving Poisson's equation for the Hartree potential, care always must be taken with the null space of the operator L. Integrating the identity $\nabla^2 1 = 0$ against the complex conjugate of each basis function gives

$$L\mathcal{J}\mathbf{1} = 0. \tag{16}$$

In periodic systems, where the only solution to Laplace's equation is the constant function, the entire null space of the operator L consists of the vector $\mathcal{J}\mathbf{1}$. Below, we use this to determine the precise value of the compensating average density n_0 needed to avoid divergences in the Lagrangian in periodic calculations.

Finally, although there is no *a priori* relationship between $\mathcal{I}^\dagger$ and $\mathcal{J}$, an approximate relation exists when the grid G is uniform and of high resolution. Under these conditions, we have

$$\mathcal{O}\mathcal{J} \approx \omega \mathcal{I}^\dagger, \tag{17}$$

where ω is the volume per grid point. To see this, consider two arbitrary functions $g(r)$ and $h(r)$, where $g(r)$ is represented by the vector $\tilde{g}$ of its expansion coefficients and $h(r)$ is represented by the vector h of its values on the points p of the grid G. There are then two ways of approximating the integral $\int d^3r\, g(r)^* h(r)$, both of which should give nearly the same result. First, one could inverse transform h to find appropriate expansion coefficients and then evaluate the overlap in coefficient space, giving the result $\tilde{g}^\dagger \mathcal{O}\mathcal{J} h$. Alternately, one could determine the values of g on the grid by the forward transform and then approximate the integral as the sum $\omega(\mathcal{I}\tilde{g})^\dagger h$. Equating these two expressions for general vectors $\tilde{g}$ and h leads to (17).

III-D Lagrangian and energy functionals

As described above, the cornerstone of all density functional calculations which use basis set expansions is the explicit expression of the LDA Lagrangian (1) in terms of the coefficients d and C of the expansions (4). The language and operators defined in the previous section were created specifically so that the expression of the Lagrangian is identical for most basis sets, including plane wave, Gaussian orbital, and multiresolution bases. As described in Sec. III-B two common strategies exist for expressing the Lagrangian in terms of the expansion coefficients in multiresolution analyses, the energy functional prescription and the operator prescription. We now give explicit expressions for these two prescriptions.

III-D.1 Energy functional prescription

III-D.1(a) Lagrangian The only terms in the Lagrangian (1) which cannot be written directly as a functional of the electron density are the electronic kinetic energy and the Hartree field self-energy. These two terms are simple bilinear forms in the expansion coefficients and are best evaluated exactly by the direct substitution of the expansions (4) into (1), giving

$$T = -\frac{1}{2}\sum_i f \sum_{\alpha\beta} c^*_{\alpha,i} L_{\alpha\beta} c_{\beta,i} = -\frac{1}{2}\,\mathrm{Tr}\, f C^\dagger L C = \mathrm{Tr}\left((-\frac{1}{2}L)P\right) \tag{18}$$

$$V_{H-H} = \frac{1}{8\pi}\sum_{\alpha\beta} d^*_\alpha L_{\alpha\beta} d_\beta = \frac{1}{8\pi} d^\dagger L d, \tag{19}$$

where we have detailed the explicit conversion to matrix language and made use of cyclic property of the trace to give a representation of T in terms of the density matrix P defined in (7).

The remaining terms in the Lagrangian all may be written directly in terms of the electron density. In our matrix representation, each column of the matrix $\mathcal{I}C$ contains the values of one of the electronic orbitals when evaluated on the grid. The electron density at each point p of the grid is thus

$$\begin{aligned} n(p) &= \sum_i f (\mathcal{I}C)^*_{pi} (\mathcal{I}C)_{pi} \\ &= \left(f(\mathcal{I}C)(\mathcal{I}C)^\dagger\right)_{pp}. \end{aligned}$$

From this, we may gather the real space charge density into the column vector n as

$$n = \mathrm{diag}\left(\mathcal{I}P\mathcal{I}^\dagger\right). \tag{20}$$

Finally, the expansion coefficients for the function $n(r)$ are just $\mathcal{J}n$.

Using this last result to evaluate V_{e-i}, we find

$$\begin{aligned} V_{e-i} &= \int d^3r\, V_{\rm ion}(r) n^*(r) \\ &= (\mathcal{J}n)^\dagger v \\ &= \mathrm{Tr}\left(\mathcal{I}^\dagger(\,\mathrm{Diag}\,\mathcal{J}^\dagger v)\mathcal{I}P\right), \end{aligned} \tag{21}$$

where the vector

$$v_\alpha \equiv \int d^3r\, b_\alpha^*(r) V_{\rm ion}(r) \tag{22}$$

represents the ionic potential as its overlap with each function of the basis. (In conjunction with the appearance of n_0 and the use of the Ewald summation, the zero wave-vector component of $V_{\rm ion}$ should be subtracted when evaluating these overlaps in calculations with periodic boundary conditions.) Although $n(r)$ is real, we introduced $n^*(r)$ above as a formal device to reduce the number of complex conjugations appearing in the final expression. The conversion to density-matrix form in the last line of (21) may be carried out using the identities (6).

The evaluation of the next term in the Lagrangian, the total exchange correlation energy E_{xc}, is similar. Given access to the values of n on the grid points, it is a simple matter to also evaluate the exchange-correlation energy per particle $\epsilon_{xc}(n(p))$ at those points. Collecting these into the column vector $\epsilon_{xc}(n)$, inverse transforming both this and the charge density and taking the overlap in coefficient space gives the final result,

$$\begin{aligned} E_{xc} &= \int d^3r \epsilon_{xc}(n(r)) n^*(r) \\ &= (\mathcal{J}n)^\dagger \mathcal{O}(\mathcal{J}\epsilon_{xc}(n)), \end{aligned} \tag{23}$$

where again we introduce the conjugation of n to reduce the number of complex conjugations appearing in the final result. E_{xc} may also be converted to density-matrix form using (6).

The final term remaining in (1), V_{e-H}, also has the overlap form

$$\begin{aligned} V_{e-H} &= -\Re\left[\int d^3r\, \phi(r)\,(n(r)-n_0)^*\right] \\ &= -\Re\left[(\mathcal{J}(n-n_0\mathbf{1}))^\dagger\, \mathcal{O}d\right], \end{aligned} \tag{24}$$

where $\mathbf{1}$ is as defined in (11). Again, the conjugation of the density term has no effect but to yield the simplest final expression.

To determine the proper choice of n_0 for periodic supercell calculations, we note that the Hartree self-energy term V_{H-H} has no contribution from the projection of d in the null space of L, which Sec. III-D showed lies along the direction $\mathcal{J}\mathbf{1}$. Thus, in order for a saddle point to exist for the Lagrangian (1), there can be no coupling of this component of d to the electron density in (24). Hence, we must have $(\mathcal{J}(n-n_0\mathbf{1}))^\dagger\mathcal{O}\cdot\mathcal{J}\mathbf{1}=0$. With the identities of Sec. III-C.2, this means that $n_0 = s^\dagger(\mathcal{J}n)/\Omega$, in accord with our interpretation of n_0 as the integral of $n(r)$ divided by the volume of the supercell. With this result, V_{e-H} is

$$V_{e-H} = -\Re\left[n^\dagger\mathcal{J}^\dagger(\mathcal{O}-\frac{ss^\dagger}{\Omega})d\right]. \tag{25}$$

Putting the preceding results together, the final expression for the LDA Lagrangian under the energy functional prescription is

$$\begin{aligned}\mathcal{L}_{LDA}(C,d) &= \mathrm{Tr}\left(fC^\dagger(-\frac{1}{2}L)C\right)+(\mathcal{J}n)^\dagger v \\ &\quad +(\mathcal{J}n)^\dagger\mathcal{O}\mathcal{J}\epsilon_{xc}(n) \\ &\quad -\Re\left[n^\dagger\mathcal{J}^\dagger(\mathcal{O}-\frac{ss^\dagger}{\Omega})d\right]+\frac{1}{8\pi}d^\dagger Ld \qquad (26)\\ &= \mathrm{Tr}\left((-\frac{1}{2}L)P\right)+\mathrm{Tr}\left(\mathcal{I}^\dagger(\,\mathrm{Diag}\,\mathcal{J}^\dagger v)\mathcal{I}P\right) \qquad (27)\\ &\quad +\mathrm{Tr}\left(\mathcal{I}^\dagger\left(\,\mathrm{Diag}\,\mathcal{J}^\dagger\mathcal{O}\mathcal{J}\epsilon_{xc}(n)\right)\mathcal{I}P\right) \\ &\quad -\mathrm{Tr}\,\mathcal{I}^\dagger\Re\left[\,\mathrm{Diag}\,\mathcal{J}^\dagger(\mathcal{O}-\frac{ss^\dagger}{\Omega})d\right]\mathcal{I}P+\frac{1}{8\pi}d^\dagger Ld,\end{aligned}$$

where n is defined as in (20). Here we have given two forms. The form (26) is more efficient for evaluating the value of the Lagrangian in terms of the coefficients C and d. The form (27), which is expressed almost entirely in terms of the density matrix, is most useful in formal manipulations which determine the gradients of the Lagrangian with respect to the electronic coefficients.

III-D.1(b) Poisson's equation To determine the expansion coefficients of the Hartree field ϕ, one sets to zero the variation of the Lagrangian with respect to all possible infinitesimal variations δd in the Hartree field coefficients. Taking the real part of (25) explicitly, this variation is

$$\begin{aligned}\delta\mathcal{L}_{LDA} &= -(\delta d)^\dagger\left(\frac{1}{2}(\mathcal{O}-\frac{ss^\dagger}{\Omega})\mathcal{J}n+\frac{1}{8\pi}Ld\right) \qquad (28)\\ &\quad -\left(\frac{1}{2}(\mathcal{O}-\frac{ss^\dagger}{\Omega})\mathcal{J}n+\frac{1}{8\pi}Ld\right)^\dagger\delta d.\end{aligned}$$

The gradient with respect to the real and imaginary parts of d are thus the real and imaginary components of

$$\partial_d\mathcal{L}_{LDA}=-\left((\mathcal{O}-\frac{ss^\dagger}{\Omega})\mathcal{J}n+\frac{1}{4\pi}Ld\right), \qquad (29)$$

respectively. Setting this to zero, we arrive at the basis independent representation of Poisson's equation,

$$Ld=4\pi(\mathcal{O}-\frac{ss^\dagger}{\Omega})\mathcal{J}n. \qquad (30)$$

The positive sign of the right side of this equation reflects the negative unit charge of the electron.

Care must be taken in solving this equation because, as described above, L has a null space along the direction $\mathcal{J}\mathbf{1}$. However, by the construction of (25), the right-hand side of the equation has no projection in this space. Thus, in the solution

$$d=4\pi L^{-1}(\mathcal{O}-\frac{ss^\dagger}{\Omega})\mathcal{J}n, \qquad (31)$$

L^{-1} is understood to mean inversion of the linear operator L in the sub-space orthogonal to the null space and leaving zero projection along the null-space in the result.

III-D.1(c) Energy functional Substituting the explicit result for d into the Lagrangian (1) gives the following explicit expression for the LDA energy functional $E_{LDA}(C)$,

$$\begin{aligned} E_{LDA}(C) &= \mathrm{Tr}\left(fC^\dagger(-\frac{1}{2}L)C\right) + (\mathcal{J}n)^\dagger v \\ &\quad +(\mathcal{J}n)^\dagger \mathcal{O}\mathcal{J}\epsilon_{xc}(n) \\ &\quad +\frac{1}{2}n^\dagger \mathcal{J}^\dagger(\mathcal{O}-\frac{ss^\dagger}{\Omega})(-4\pi L^{-1})(\mathcal{O}-\frac{ss^\dagger}{\Omega})\mathcal{J}n. \end{aligned} \tag{32}$$

Note that Hermitian symmetry has ensured that the Hartree term is explicitly real.

III-D.2 Operator prescription

III-D.2(a) Lagrangian The alternative prescription for expressing the Lagrangian, followed in [WC96, TW97], is to view it as the sum of the expectations of an energy operator $\hat{\mathcal{L}}$ among the orbitals, $\mathcal{L}_{LDA} = \sum_i f \int d^3r\, \psi_i^* \hat{\mathcal{L}}\psi_i$. The only term which cannot be taken to involve involve the electrons in this way is the Hartree self-energy term, which is best represented in the exact form (19). Note that we have already expressed the electronic kinetic energy in its operator form in (18).

The remaining contributions to $\hat{\epsilon}$ are local operators in real space and thus all take on the same form as does the electron-ion interaction V_{e-i}. The technique which Wei and Chou[WC96] introduced to treat V_{e-i} is to first compute $\mathcal{I}C$, the values of the wave functions on the grid points and then multiply the result by a diagonal matrix containing the values of the potential at the grid points. This results in $(\,\mathrm{Diag}\,\tilde{v})\mathcal{I}C$, where $\tilde{v}$ is the vector containing the values of the ionic potential at the grid points,

$$(\tilde{v})_p \equiv V_{\mathrm{ion}}(p),$$

where the tilde on $\tilde{v}$ distinguishes this vector of values from the vector v of overlaps defined in (22). To compute the energy, this result is transformed into expansion coefficients by the operation of $\mathcal{J}$ and the overlaps with the $\psi_i^*(r)$ are computed using the known overlaps between basis functions. The total of the resulting potential energy among all of the orbitals is

$$\begin{aligned} V_{e-i} &= \sum_i f \int d^3r\, \psi_i^*(r)\,(V_{\mathrm{ion}}(r)\psi_i(r)) \\ &= \mathrm{Tr}\, fC^\dagger \cdot \mathcal{O}\cdot\mathcal{J}\,((\,\mathrm{Diag}\,\tilde{v})\mathcal{I}C) \\ &= \mathrm{Tr}\, fC^\dagger VC = \mathrm{Tr}\, VP, \end{aligned} \tag{33}$$

where $V \equiv \mathcal{O}\mathcal{J}(\,\mathrm{Diag}\,\tilde{v})\mathcal{I}$. A potential difficulty with this approach is that the inherently asymmetric roles played by ψ^* and ψ have resulted in a potential energy operator V which is not Hermitian and thus may lead to complex energies. Taking the Hermitian part of V corresponds to taking just the real part of (33) and gives the proper form for the electron-ion energy. After some manipulation and using the fact that $\tilde{v}$ is real, we have the following equivalent forms for V_{e-i}

$$\begin{aligned} V_{e-i} &\equiv \Re\,\mathrm{Tr}\,(\mathcal{O}\mathcal{J}\,\mathrm{Diag}\,\tilde{v}\mathcal{I}\cdot P) \\ &= \tilde{v}^\dagger \Re\,\mathrm{diag}\,(\mathcal{I}P\mathcal{O}\mathcal{J}) \\ &= \omega\tilde{v}^\dagger\tilde{n}, \end{aligned} \tag{34}$$

where we have defined

$$\tilde{n} \equiv \Re\,\mathrm{diag}\,(\mathcal{I}P\mathcal{O}\mathcal{J})/\omega,$$

as an effective charge density, and ω as the volume per grid point. With these definitions, the electron-ion interaction takes on precisely the appearance of a numerical integration in real space of the product of potential and the *effective* electron density. Indeed, from (17) and (20), as long as a fine, uniform grid is used, we have $\Re\,\mathrm{diag}\,(\mathcal{I}P\mathcal{O}\mathcal{J}) \approx \omega n$, so that $\tilde{n}$ approximates the physical electron density. As we shall see, the effective density $\tilde{n}$ replaces the physical density in all energy expressions of the operator prescription.

The remaining terms from (1) have the same structure as V_{e-i} and thus may be evaluated in the same way to yield

$$\begin{aligned} E_{xc} &= \omega\epsilon_{xc}^{\dagger}\tilde{n} \\ V_{e-H} &= -\omega\Re[(\mathcal{I}d)^{\dagger}(\tilde{n} - n_0\mathbf{1})]. \end{aligned}$$

To determine n_0, we again ensure that there be no coupling between the electron density and the projection of d along the null space of L: $(\mathcal{I}\cdot\mathcal{J}\mathbf{1})^{\dagger}(\tilde{n} - n_0\mathbf{1}) = 0$. This simplifies to

$$n_0 = \frac{\mathbf{1}^{\dagger}\tilde{n}}{\mathbf{1}^{\dagger}\mathbf{1}}, \tag{35}$$

the mean value of $\tilde{n}$ among the points of the grid.

We shall find in Sec. III-E.2 that the the exchange-correlation energy should also be evaluated using the *effective density* $\tilde{n}$, so that the final expressions for the Lagrangian in the operator prescription are

$$\begin{aligned} \mathcal{L}_{LDA}(C,d) &= \mathrm{Tr}\left(fC^{\dagger}(-\frac{1}{2}L)C\right) + \omega\tilde{v}^{\dagger}\tilde{n} \qquad (36)\\ &\quad +\omega(\epsilon_{xc}(\tilde{n}))^{\dagger}\tilde{n} \\ &\quad -\omega\Re\left[d^{\dagger}\mathcal{I}^{\dagger}\left(I - \frac{\mathbf{1}\mathbf{1}^{\dagger}}{\mathbf{1}^{\dagger}\mathbf{1}}\right)\tilde{n}\right] + \frac{1}{8\pi}d^{\dagger}Ld \\ &= \mathrm{Tr}\left((-\frac{1}{2}L)P\right) + \Re\,\mathrm{Tr}\,(\mathcal{O}\mathcal{J}(\,\mathrm{Diag}\,\tilde{v})\mathcal{I}P) \qquad (37)\\ &\quad +\Re\,\mathrm{Tr}\,(\mathcal{O}\mathcal{J}\,\mathrm{Diag}\,(\epsilon_{xc}(\tilde{n}))\mathcal{I}P) \\ &\quad -\Re\,\mathrm{Tr}\left(\mathcal{O}\mathcal{J}\left(\,\mathrm{Diag}\,\Re\left[(I - \frac{\mathbf{1}\mathbf{1}^{\dagger}}{\mathbf{1}^{\dagger}\mathbf{1}})\mathcal{I}d\right]\right)\mathcal{I}P\right) + \frac{1}{8\pi}d^{\dagger}Ld. \end{aligned}$$

III-D.2(b) Poisson's equation Following the same procedure as (28) to compute the variation of (36) with differential changes in the Hartree field coefficients δd gives, in the operator prescription,

$$\partial_d\mathcal{L}_{LDA} = -\omega\mathcal{I}^{\dagger}\left(I - \frac{\mathbf{1}\mathbf{1}^{\dagger}}{\mathbf{1}^{\dagger}\mathbf{1}}\right)\tilde{n} + \frac{1}{4\pi}Ld. \tag{38}$$

Thus,

$$Ld = 4\pi\omega\mathcal{I}^{\dagger}\left(I - \frac{\mathbf{1}\mathbf{1}^{\dagger}}{\mathbf{1}^{\dagger}\mathbf{1}}\right)\tilde{n} \tag{39}$$

is the representation of Poisson's equation in the orbital approach. Note that the effective electron density $\tilde{n}$, rather than the actual density n is the source term.

In solving this equation for d, the inversion of L^{-1} is again understood to take place in the space orthogonal to the null space of L, giving the result,

$$d = 4\pi\omega L^{-1}\mathcal{I}^{\dagger}\left(I - \frac{\mathbf{1}\mathbf{1}^{\dagger}}{\mathbf{1}^{\dagger}\mathbf{1}}\right)\tilde{n}. \tag{40}$$

III-D.2(c) Energy functional With the result (40), the expression for the LDA energy functional $E_{LDA}(C)$ in the operator prescription is

$$\begin{aligned} E_{LDA}(C) &= \mathrm{Tr}\left(fC^\dagger(-\frac{1}{2}L)C\right) + \omega\tilde{v}^\dagger\tilde{n} \\ &\quad +\omega(\epsilon_{xc}(\tilde{n}))^\dagger\tilde{n} \\ &\quad +\frac{1}{2}(\omega\tilde{n})^\dagger\left(I - \frac{\mathbf{1}\mathbf{1}^\dagger}{\mathbf{1}^\dagger\mathbf{1}}\right)\mathcal{I}(-4\pi L^{-1})\mathcal{I}^\dagger\left(I - \frac{\mathbf{1}\mathbf{1}^\dagger}{\mathbf{1}^\dagger\mathbf{1}}\right)\omega\tilde{n}. \end{aligned} \tag{41}$$

III-E Kohn-Sham equations

In the preceding sections, we computed the gradient of the LDA Lagrangian (26,36) with respect to the Hartree field coefficients to derive the Poisson equation. In this section, we consider the gradient with respect to the electronic coefficients to determine the effective Schrödinger equation for the electronic orbitals.

Before proceeding, we first note that as a consequence of the Hellman-Feynman theorem, the expression for the gradient with respect to the electronic coefficients of the LDA Lagrangian may also be used for the gradient of the LDA energy functional, so long as one substitutes the appropriate expression (31 or 40) for the Hartree potential coefficients in terms of the electronic coefficients C. This follows from the fact that the solutions (31,40) ensure $\partial_d\mathcal{L}_{LDA}(C, d(C)) = 0$ and thus

$$\begin{aligned} \frac{d}{dC}E_{LDA}(C) &= \frac{d}{dC}\mathcal{L}_{LDA}(C, d(C)) \\ &= \partial_C\mathcal{L}_{LDA}(C, d(C)) + \partial_d\mathcal{L}_{LDA}(C, d(C)) \cdot \partial_C d(C) \\ &= \partial_C\mathcal{L}_{LDA}(C, d(C)). \end{aligned} \tag{42}$$

It thus suffices for us to determine the gradient of the Lagrangian with respect to C.

This is done most efficiently by expressing all contributions to the variation of $\mathcal{L}_{LDA}$ in the form $\mathrm{Tr}\, M\delta P$ where M is a Hermitian matrix and δP is the variation in the density matrix defined in (7). In terms of the variations in C, such a variation takes the form

$$\mathrm{Tr}\,(M\,\delta P) = \mathrm{Tr}\left((fMC)^\dagger\,\delta C\right) + \mathrm{Tr}\left(\delta C^\dagger\,(fMC)\right). \tag{43}$$

The contribution from such a variation to the total gradient with respect to the real and imaginary parts of of C are therefore the real and imaginary components of $2fMC$, respectively.

The final consideration when varying the wave function coefficients is the orthonormality constraint (3), which in our matrix language becomes

$$C^\dagger\mathcal{O}C = I. \tag{44}$$

The analytically continued functional approach[APJ92] deals with these constraints by introducing a set of orbital expansion coefficients Y which are *unconstrained* and may have any set of overlaps,

$$U \equiv Y^\dagger\mathcal{O}Y. \tag{45}$$

The coefficients C are then defined as dependent variables through the mapping $C = YU^{-1/2}$, which ensures that the constraints (44) are always satisfied automatically, as easily verified by direct substitution.

In terms of the independent variables Y, the density matrix appearing in the functionals (27,37) is

$$P \equiv fCC^\dagger = fYU^{-1}Y^\dagger. \tag{46}$$

After some manipulation, the variations with respect to the Y take the form

$$\begin{aligned} TrM\delta P &= \mathrm{Tr}\, M\delta(fYU^{-1}Y^\dagger) \\ &= \mathrm{Tr}\left(f\bar{P}MYU^{-1}\right)^\dagger \delta Y + \mathrm{Tr}\,\delta Y^\dagger \left(f\bar{P}MYU^{-1}\right), \end{aligned} \tag{47}$$

where we have used the relation $\delta(U^{-1}) = -U^{-1}(\delta U)U^{-1}$ and defined

$$\bar{P} \equiv (I - \mathcal{O}YU^{-1}Y^\dagger) = (I - \mathcal{O}CC^\dagger), \tag{48}$$

an idempotent projection operator onto the subspace spanned by the unoccupied wave functions. From these considerations, we have that the contributions from such a variation to the gradient of $\mathcal{L}_{LDA}$ with respect to the real and imaginary parts of the unconstrained variables Y are the real and imaginary parts of $2f\bar{P}MYU^{-1}$, respectively.

III-E.1 Energy functional prescription

All but one of the dependencies of (27) with the wave functions are already explicitly in the form $\mathrm{Tr}\, MP$, so that their contribution to the gradient may be evaluated immediately according to (43,47). The one remaining dependency of (27) on the electrons is through the density dependence of $\epsilon_{xc}(n)$. This variation may also be cast into the form of (43,47). To do so, we consider the effect of this variation on E_{xc} when expressed in the form (23). Using the definition of n (20) and one of the identities (6), this leads to

$$\begin{aligned} n^\dagger \mathcal{J}^\dagger \mathcal{O}\mathcal{J}\delta\epsilon_{xc}(n) &= n^\dagger \mathcal{J}^\dagger \mathcal{O}\mathcal{J}\left((\mathrm{Diag}\,\epsilon'_{xc}(n))\delta n\right) \\ &= \mathrm{Tr}\left[\mathcal{I}^\dagger \mathrm{Diag}\left((\mathrm{Diag}\,\epsilon'_{xc}(n))\mathcal{J}^\dagger\mathcal{O}\mathcal{J}n\right)\mathcal{I}\delta P\right]. \end{aligned}$$

The total variation of (27) as the wave functions vary is thus,

$$\delta\mathcal{L}_{LDA} = \mathrm{Tr}\,\left(H_{sp}\delta P\right),$$

where

$$\begin{aligned} H_{sp} \equiv\; & -\frac{1}{2}L + \mathcal{I}^\dagger \mathrm{Diag}\left\{\mathcal{J}^\dagger v + \mathcal{J}^\dagger\mathcal{O}\mathcal{J}\epsilon_{xc}(n)\right. \\ & + \left(\mathrm{Diag}\,\epsilon'_{xc}(n)\right)\mathcal{J}^\dagger\mathcal{O}\mathcal{J}n \\ & \left. -\Re\left(\mathcal{J}^\dagger(\mathcal{O} - ss^\dagger/\Omega)d\right)\right\}\mathcal{I} \end{aligned} \tag{49}$$

is the energy functional prescription for the representation of the single-particle Kohn-Sham Hamiltonian. Using (43,47), the gradients which we seek are therefore

$$\begin{aligned} \partial_C\mathcal{L}_{LDA}(C,d) &= 2fH_{sp}C \\ \partial_Y\mathcal{L}_{LDA}(Y,d) &= 2f\bar{P}H_{sp}YU^{-1}, \end{aligned} \tag{50}$$

where U and $\bar{P}$ are defined in (45) and (48), respectively.

III-E.2 Operator prescription

The results for the orbital approach are directly analogous. All of the dependencies of the Lagrangian in the operator prescription on the wave functions, except for that of ϵ_{xc}, are already explicitly in the form $\mathrm{Tr}\, MP$. If we take ϵ_{xc} as a function of $\tilde{n}$, then this variation of E_{xc} (second line of (41)) is

$$\begin{aligned}\omega(\delta\epsilon_{xc}(\tilde{n}))^\dagger\tilde{n} &= \omega(\,\mathrm{Diag}\,\epsilon'_{xc}\cdot\delta\tilde{n})^\dagger\tilde{n}\\ &= \omega\left((\,\mathrm{Diag}\,\epsilon'_{xc})\tilde{n}\right)^\dagger\delta\tilde{n}\\ &= \Re\,\mathrm{Tr}\,\left(\mathcal{O}\mathcal{J}(\,\mathrm{Diag}\,(\,\mathrm{Diag}\,\epsilon'_{xc}\cdot\tilde{n}))\mathcal{I}\delta P\right).\end{aligned}$$

This combines with the explicit dependency of the exchange-correlation term in (37) on P to produce the total exchange-correlation energy dependency in the form

$$\begin{aligned}\delta E_{xc} &= \delta(\omega\epsilon_{xc}(\tilde{n})^\dagger\tilde{n})\\ &= \Re\,\mathrm{Tr}\,\left(\mathcal{O}\mathcal{J}(\,\mathrm{Diag}\,v_{xc})\mathcal{I}\delta P\right),\end{aligned}$$

where v_{xc} is the usual exchange-correlation potential operator,

$$v_{xc}\equiv\partial_{\tilde{n}}(\epsilon_{xc}(\tilde{n})\,\tilde{n})=\epsilon'_{xc}(\tilde{n})\,\tilde{n}+\epsilon_{xc}(\tilde{n}). \tag{51}$$

Note that, as referred to in Sec. III-D.2 this form is obtained only when the exchange correlation energy per particle ϵ_{xc} is evaluated as a function of the *effective density* $\tilde{n}$, not as a function of the physical density n.

Combining this result for E_{xc} with the remaining dependencies in the operator prescription for the Lagrangian (37) gives the total variation in the form $\delta\mathcal{L}_{LDA}=\mathrm{Tr}\, H_{sp}\delta P$, where

$$H_{sp}=-\frac{1}{2}L+\frac{1}{2}\left[\mathcal{O}\mathcal{J}\,\mathrm{Diag}\left\{\tilde{v}+\left[(\,\mathrm{Diag}\,\epsilon'_{xc}(\tilde{n}))\;\tilde{n}+\epsilon_{xc}(\tilde{n})\right]-\Re\left[(I-\frac{\mathbf{1}\mathbf{1}^\dagger}{\mathbf{1}^\dagger\mathbf{1}})\mathcal{I}d\right]\right\}\mathcal{I}+\mathrm{h.c.}\right], \tag{52}$$

and "h.c." stands for the Hermitian conjugate of the entire matrix product to the immediate left. Again, once given this expression for H_{sp}, the expressions (50) gives the gradients with respect to the wave functions.

III-F Solution techniques

Locating the saddle point of the LDA Lagrangian (1) corresponds to the simultaneous, self-consistent solution of the Poisson and Schrödinger equations. Although the Lagrangian formulation allows for a direct search for the saddle point, most calculations to date have solved Poisson's equation explicitly at each iteration and then followed the gradients in (50) to solve the Schrödinger equations using standard electronic structure approaches. The approaches applied to solve the Schrödinger equations include conjugate gradient minimization with respect to Y[ACLT95] and iterative matrix diagonalization[WC96] and Car-Parrinello simulated annealing[TW97] to find C. The solution of Poisson's equation in multiresolution analyses, on the other hand, has garnered special attention.

To solve the Poisson (40), Wei and Chou[WC96] introduced the innovation of using a separate Fourier representation for the operator L in the self-energy term of the Hartree field. The interpretation of (40) when using such a representation is the following procedure. First, subtract the average value from the effective density $\tilde{n}$, then perform a discrete Fourier transform $\mathcal{I}^\dagger$ of the result

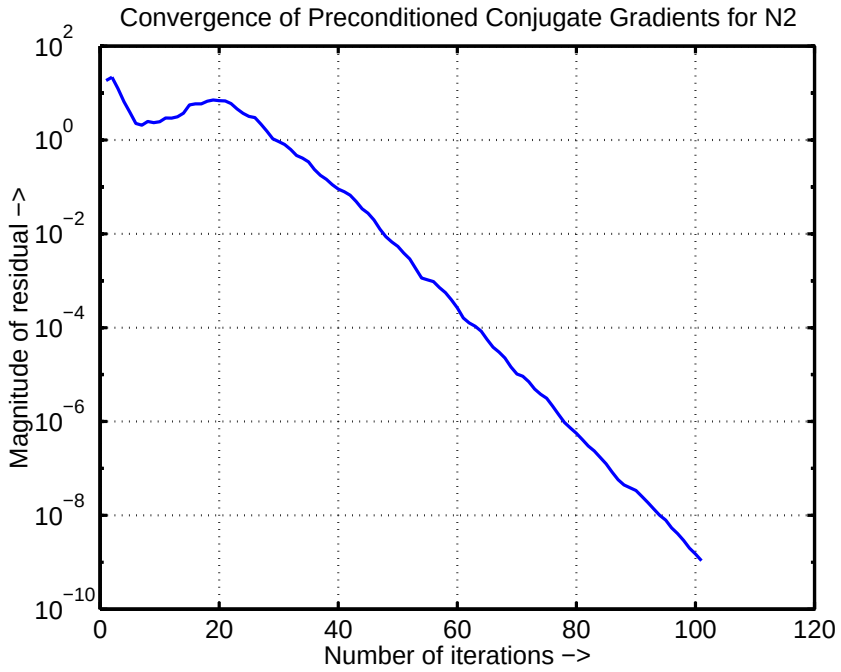

Figure 6: Convergence of iterative conjugate-gradient solver used in [ACLT95] (results from [LAE98]).

into Fourier space, divide by the familiar factor of negative squares of wave vectors $-q^2$ (ignoring the $q = 0$ term), and scale by $4\pi\omega$ to obtain the final result. The disadvantage of this procedure is that one must store and process data associated with an unrestricted grid of points at the highest resolution.

When working only with the points of a restricted grid, no such direct solution is known. Instead, iterative solutions have been used. In [ACLT95], a conjugate gradient solver with simple diagonal preconditioning was used to solve Poisson's equation in a semicardinal multiresolution analysis of the type described in Section V-B.3. Figures 6 and 7 show the results of a study of the performance of this algorithm[LAE98]. Figure 6 shows the root mean square magnitude of the residual as a function of iteration as this algorithm is applied to the nitrogen molecule in a basis with seven levels of refinement. After an initial phase of about twenty iterations, the convergence of the solution of Poisson's equation becomes nearly perfectly exponential and reduces the residual by over ten orders of magnitude in one hundred iterations, very good performance for a system consisting of 14,000 degrees of freedom in which the Laplacian operator has a nominal condition number of 2×10^6.

The slope of the exponential portion of the convergence curve in Figure 6 corresponds to a reduction in the error at each iteration by 25%. Defining the effective condition number of the procedure as the inverse of this fractional improvement gives an effective condition number $c \approx 4$. Figure 7 explores the behavior of this effective condition number as a function of the number of refinement levels k. Beyond about five refinement levels, the effective condition number remains essentially constant, implying that a constant number of iterations suffices to produce a result of a given accuracy. With the methods described in Sec. VI-B, the computational work involved in

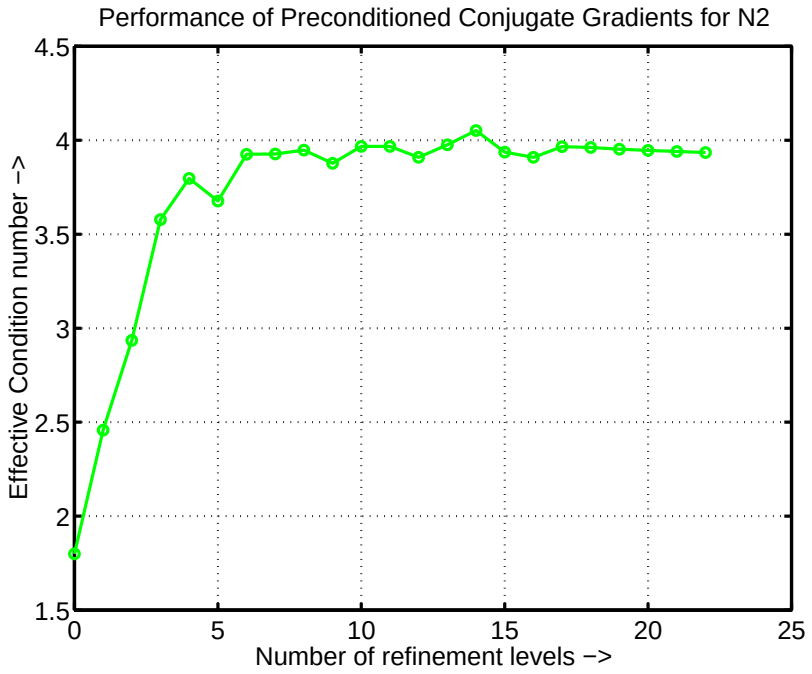

Figure 7: Effective condition number of iterative conjugate-gradient solver used in [ACLT95] as a function of resolution. (Results from [LAE98].)

each iteration is linear in the number of coefficients n_r in the restricted multiresolution analysis. For these problems, this simple preconditioned conjugate gradient approach therefore produces the solution to Poisson's equation with $O(n_r)$ operations.

Working with special linear combinations of the basis functions from [LAE98] known as lifted wavelets[Swe96], Goedecker and Ivanov have also used preconditioned conjugate gradients to solve Poisson's equation and report similar convergence rates and an $O(n_r)$ solution as well[GI98].

Finally, multigrid techniques have been combined with multiresolution analysis[RJZ94, Yes97]. This approach has also been shown to produce $O(n)$ solutions of Poisson's equation in tests carried out in one dimension[Yes97, YA98].

IV Theory of Multiresolution Analysis

In this section we review multiresolution analysis, the conceptual basis of wavelet theory. Our presentation below departs somewhat in notation and perspective from the traditional discussion[Dau92, Chu92a, SN96] to provide a presentation more suited to physical calculations in multiple dimensions.

The basic idea behind multiresolution analysis is to provide a framework for systematically increasing the resolution of a basis in such a way as to always maintain a uniform description of space. Each stage of a multiresolution analysis doubles the resolution of the basis in the precise mathematical sense described in Secs. IV-A and IV-B. In order for this to be possible, the basis functions at the coarsest scale must be chosen from among a special class of functions known as *scaling functions*, whose explicit construction we describe in Sec. IV-C. To analyze a function into

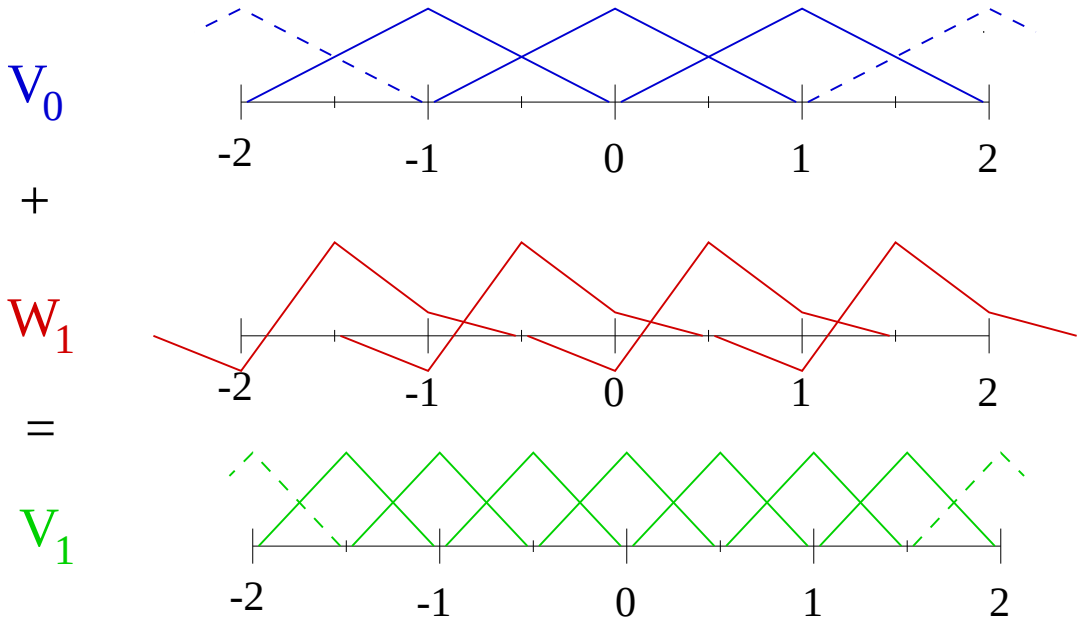

Figure 8: Bases involved in two-scale decomposition: coarse resolution space (V_0), fine resolution space (V_1), detail space (W_1).

contributions on separate scales and thus make possible the efficient representation of electronic structure described in Sec. III , a second type of basis function, known as either as a *wavelet* or a *detail function*, is needed to carry the finer scale information. For a given choice of scaling function for the coarsest scale, the use of only certain detail functions results in the systematic doubling of resolution at each stage in the multiresolution analysis. Sections IV-D and IV-E discuss this doubling process, known as *two-scale decomposition*, and specify the allowable classes of detail functions. The last paragraph of Section IV-E sketches an alternate, more basis-set oriented, viewpoint on two-scale decomposition which the reader may find illuminating. Once suitable scaling and detail functions are decided upon, including them into the multilevel framework described in Sec. IV-B completes the construction of the multiresolution analysis. Our review of multiresolution analysis concludes in Section IV-F with the introduction a matrix representation which is useful for developing and describing techniques for electronic structure and other physical applications.

IV-A Bases of successive resolution

The top panel of Figure 8 illustrates a typical coarse resolution basis. In a multiresolution analysis, this starting basis consists of a set of $d-$dimensional functions $\phi(x-n)$ translated to be centered on the points n of Z^d, the cubic lattice of integer spacing in $d-$dimensions. The vector space of functions which may be expressed as linear combinations of these basis functions is denoted V_0. All functions $F(x)$ in V_0 thus may be expanded with expansion coefficients F_n as

$$F(x) = \sum_{n \in Z^d} F_n \phi(x-n). \tag{53}$$

Starting from V_0, one approach to produce a set of bases of successively higher resolution is to reduce the scale of space by increasing powers of two, compressing both the lattice on which the

functions are centered and the basis functions themselves. This process defines a sequence of lattices $C_0, C_1, \ldots, C_N, \ldots$, associated with a sequence of bases of increasing resolution, $V_0, V_1, \ldots, V_N, \ldots$,

$$\begin{aligned} C_Q &\equiv \left\{ \frac{n}{2^Q} \right\}_{n \in Z^d}, \\ V_Q &\equiv \text{span} \left\{ \phi\left(2^Q(x-p)\right) \right\}_{p \in C_Q} = \text{span} \left\{ \phi(2^Q x - n) \right\}_{n \in Z^d}. \end{aligned} \tag{54}$$

Note that the two representations for the basis functions of V_Q given in the second line of (54) are equivalent. Below, we shall use whichever form is most suitable. The top and bottom panels of Figure 8 serve to illustrate the effect of going from V_0 to V_1.

As we will see in Secs. IV-C—IV-E, it is possible under quite general circumstances to find additional basis functions, referred to as *detail functions* or *wavelets*, which when combined with the basis functions for the space V_Q span the space of next higher resolution, V_{Q+1}. The advantage of this approach for increasing the resolution is that it clearly separates the description into different length scales. The original coarse basis functions will continue to carry information about coarse scale behavior, and the new functions carry the higher frequency details. Accordingly, the space spanned by the detail functions is referred to as the *detail space* W_{Q+1}. The center panel of Figure 8 illustrates the appearance of such a detail space.

All functions in V_{Q+1} may be decomposed into the sum of one function from the coarser space V_Q and another from the detail space W_{Q+1}, which means

$$V_Q \oplus W_{Q+1} = V_{Q+1}, \tag{55}$$

where the addition is in this sense of combining vector spaces. We shall refer to this representation of the functions in V_{Q+1} as the sum of a function in V_Q and a function in W_{Q+1} as the *two-scale representation* or the *two-scale decomposition*. We refer to the alternate representation of the same space functions in terms of the compressed scaling functions of scale $Q+1$ as the *single-scale* representation.

Clearly, for the single- and two-scale representations to be equivalent, the spaces V_{Q+1} and $V_Q \oplus W_{Q+1}$ must be of the same dimension. The basis spanning the finer space contains one function for each point in C_{Q+1}, and the basis spanning the coarser space has one function for each point in C_Q. Therefore, the basis spanning W_{Q+1} must consist of one function for each point in

$$D_{Q+1} \equiv C_{Q+1} - C_Q.$$

In Figure 8 for example, C_0 consists of all integer points, C_1 contains all integer and odd half-integer points, and D_1 consists of only the odd half-integer points. Figure 9 illustrates the appearance of these sets of points in $d = 2$ dimensions.

These various periodic sets of points appearing in the discussion of multiresolution analysis may be described simply in the language of crystallography. The set D_{Q+1} contains the "decoration" points which when added to the lattice C_Q produce the lattice C_{Q+1}. D_{Q+1} therefore is a crystal of points with a crystalline basis containing $2^d - 1$ points and with C_Q as the underlying Bravais lattice. When dealing with a finite number of levels of resolution, $C_M \subset C_{M+1} \subset \ldots \subset C_N$, it proves convenient to have a notation for the set of points beyond a given level Q,

$$B_Q \equiv C_N - C_Q = D_{Q+1} \cup \ldots \cup D_N. \tag{56}$$

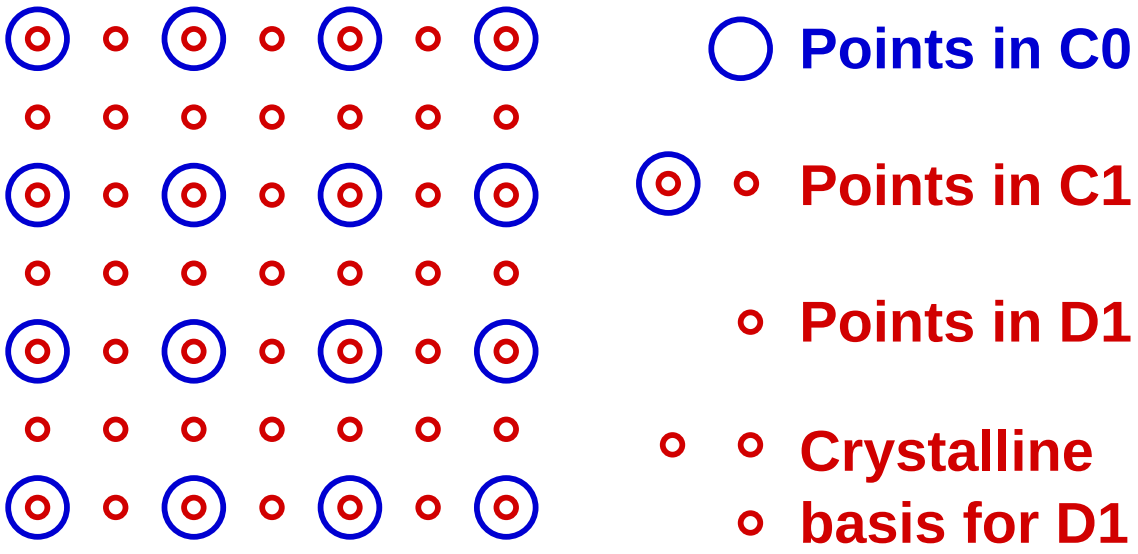

Figure 9: Lattices C_0, C_1 and detail "crystal" D_1 in $d = 2$ dimensions.

IV-B Multiresolution analysis

Given suitable detail spaces W_Q, iterative application of two-scale decomposition can augment a space V_M of fixed coarse resolution to a space V_N of *arbitrarily* high resolution,

$$\begin{aligned} V_N &= (V_0 \oplus W_1 \oplus \ldots \oplus W_M) \oplus W_{M+1} \oplus \ldots \oplus W_N \\ &= V_M \oplus W_{M+1} \oplus \ldots \oplus W_N, \end{aligned}$$

where $M < N$ in accord with the convention introduced in Sec. III-A. Correspondingly, all physical functions may be described by a sequence of evermore detailed components,

$$f(x) = F_M(x) + G_{M+1}(x) + \ldots + G_N(x) \tag{57}$$

where $F_M(x)$ is a function in V_M and the $G_Q(x)$ are functions from the detail spaces W_Q. We refer to the decomposition of a function in this form as the *multiresolution analysis* of the function.

The analysis of functions in the form (57) is what gives rise to the great advantages of using multiresolution analysis. As illustrated previously in Figures 4 and 5, the detail component functions $G_Q(x)$ are physically relevant only within the tiny volumes of the atomic cores and thus may be described by a dramatically restricted subset of the basis.

IV-C Scaling functions

For the condition (55) to apply, each basis function of the coarser basis V_Q, including in particular the function $\phi(2^Q y)$ centered at origin, must be among the functions in the space V_{Q+1}. Thus, there must exist some set of coefficients c_n for which

$$\phi(2^Q y) = \sum_{n \in Z^d} c_n \phi(2^{Q+1} y - n).$$

This condition is universal and independent of the scale Q as may be seen by the substitution $x = 2^Q y$, which re-scales the condition to scale $Q = 0$:

$$\phi(x) = \sum_n c_n \phi(2x - n). \tag{58}$$

Condition (58) is known as the *two-scale relation*. Those functions which satisfy (58) are known as *scaling functions*. It easily may be verified that if $\phi(x)$ satisfies condition (58), then all basis functions $\phi(2^Q y - n)$ in V_Q are also in the space V_{Q+1}, so that indeed $V_Q \subset V_{Q+1}$.

Because any multiresolution analysis must be based upon scaling functions, it is useful to have a prescription for generating *all* allowable scaling functions. The two-scale relation (58) expresses the function $\phi(x)$ as a convolution of the discrete sequence c_n and the continuous function $\phi(2x)$. This convolution takes the familiar form of a product in Fourier space,

$$\begin{aligned} \hat{\phi}(k) &\equiv \int \frac{d^d x}{(2\pi)^d}\ e^{-ik\cdot x}\phi(x) \\ &= \int \frac{d^d x}{(2\pi)^d}\ e^{-ik\cdot x}\sum_n c_n \phi(2x-n) \\ &= \left(\sum_n \frac{c_n}{2^d} e^{-i(k/2)\cdot n}\right)\hat{\phi}(k/2) \\ &= m_0(k/2)\hat{\phi}(k/2), \end{aligned} \tag{59}$$

where we have defined m_0, the *two-scale symbol* for the scaling function $\phi(x)$, as

$$m_0(k) \equiv \sum_n \frac{c_n}{2^d} e^{-ik\cdot n}. \tag{60}$$

By construction, the two-scale symbol is periodic on $2\pi C_0$, the hyper-cubic lattice of lattice constant 2π. Note that the first line of (59) gives the normalization convention which we shall use for Fourier transforms throughout this work.

The recursive nature of Eq. (59) implies that the Fourier transforms of scaling functions always take the form

$$\begin{aligned} \hat{\phi}(k) &= m_0(k/2)m_0(k/4)\ldots m_0(k/2^n)\ldots\hat{\phi}(0) \\ &= \left(\prod_{n=1}^{\infty} m_0(k/2^n)\right)\hat{\phi}(0). \end{aligned} \tag{61}$$

Conversely, substitution into the final lines of (59) verifies that any function constructed from (61) in conjunction with any $2\pi C_0$-periodic function m_0 satisfying $m_0(0) = 1$ (so that the infinite product converges) results in a proper scaling function. Eq. (61) therefore places the set of acceptable scaling functions as in one-to-one correspondence with $2\pi C_0$-periodic functions with value unity at the origin. The interested reader may wish to consult [Dau92] for a rigorous discussion of technical mathematical details related to the infinite product.

IV-D Two-scale decomposition theorem

With the allowable scaling functions $\phi(x)$ and hence the spaces V_Q defined, we now turn to the issue of what functions form appropriate bases for the detail spaces W_{Q+1}.

Before specifying a basis for $W_{Q+1} \equiv V_{Q+1} - V_Q$, we first determine what functions belong to this space by establishing the nature of the excess freedom which exists in V_{Q+1} over that which exists in V_Q. If F and f are two arbitrary functions from the spaces V_Q and V_{Q+1}, respectively, then

$$\begin{aligned} F(x) &= \sum_{n \in Z^d} F_n \phi(2^Q x - n) \\ f(x) &= \sum_{n \in Z^d} f_n \phi(2^{Q+1} x - n). \end{aligned}$$

These expressions are both convolutions of form similar to (58) and also give products in Fourier space:

$$\begin{aligned} \hat{F}(k) &= \left(\sum_n \frac{F_n}{2^{Qd}} e^{-i(k/2^Q)\cdot n} \right) \hat{\phi}(k/2^Q) \\ &\equiv m_F(k/2^Q) \hat{\phi}(k/2^Q) \\ &= m_F(k/2^Q) m_0(k/2^{Q+1}) \hat{\phi}(k/2^{Q+1}), \end{aligned} \tag{62}$$

where we have used the two-scale relation (59); and

$$\begin{aligned} \hat{f}(k) &= \left(\sum_n \frac{f_n}{2^{(Q+1)d}} e^{-i(k/2^{Q+1})\cdot n} \right) \hat{\phi}(k/2^{Q+1}) \\ &\equiv m_f(k/2^{Q+1}) \hat{\phi}(k/2^{Q+1}), \end{aligned} \tag{63}$$

where $m_F(q)$ and $m_f(q)$ are two new $2\pi C_0$-periodic functions defined from Fourier series constructed with the sequences F_n and f_n respectively. Thus, $F(x)$ and $f(x)$ are in V_Q and V_{Q+1} if and only if their Fourier transforms are of the forms in (62) and (63) with $2\pi C_0$-periodic functions m_F and m_f.

We can use these results to verify quickly that any function F in V_Q is also in V_{Q+1}. First note that if F is in V_Q, then there exists a suitable $2\pi C_0$-periodic function m_F to satisfy (62). Using this function, then clearly the choice

$$m_f(q/2) \equiv m_F(q) m_0(q/2), \tag{64}$$

will cast F in the form (63). All that remains to confirm that this places F in V_{Q+1} is to show that the function m_f defined as in (64) is indeed always $2\pi C_0$-periodic, as is easily verified using the fact that m_0 and m_F both have $2\pi C_0$-periodicity.

Naturally, it is not possible to describe a general fine-scale function f from V_{Q+1} as a function F from the coarser space V_Q. To write a function of the form (63) in the form (62), would require

$$m_F(q) \equiv m_f(q/2)/m_0(q/2), \tag{65}$$

to be a $2\pi C_0$-periodic function. The function $m_f(q/2)$, however, can be any $4\pi C_0$-periodic function of q. The failure of f to be in V_Q thus may be viewed as the inability of the $2\pi C_0$-periodic function $m_F(q)$ to describe the full freedom present in $m_f(q/2)$, a general $4\pi C_0$-periodic function of q.

As a hint as to how to capture the this full freedom, we note that the Monkhorst-Pack theory of Brillouin zone sampling[MP76] shows that any $4\pi C_0$-periodic function may be expressed as a sum of 2^d separate functions, each with a special $2\pi C_0$-periodicity. The particular $2\pi C_0$-periodicities

chosen by Monkhorst and Pack are those associated with points of the reciprocal lattice of $4\pi C_0$ which fall in the first Brillouin zone of the reciprocal lattice of $2\pi C_0$, namely the set of k-points $k_i \equiv \eta_i/2$ where

$$\eta_i \in \{0,1\}^d. \tag{66}$$

For instance, in $d = 3$ dimensions,

$$\{\eta_i\} \equiv \{(0,0,0),(0,0,1),(0,1,0),(0,1,1),(1,0,0),(1,0,1),(1,1,0),(1,1,1)\}.$$

Thus, all $4\pi C_0$-periodic functions of q may be written as a linear combination of functions $p_i(q)$ with the special $2\pi C_0$-periodicities described by the condition that

$$p_i(q+Q) = e^{-iQ\cdot(\eta_i/2)} p_i(q)$$

for all Q in $2\pi C_0$. For convenience, we will adopt the notation that $\eta_0 = 0$ and will index sums which omit this zero vector by α, except for two cases noted explicitly in the text in Sec. V-A.

From the theory Monkhorst and Pack, we thus conclude that if we take the $2\pi C_0$-periodic function $m_F(q)$, which has the same periodicity as $p_0(q)$ above, and augment it with $2^d - 1$ new functions $m_{G_\alpha}(q)$ with the periodicities of the $p_\alpha(q)$,

$$m_{G_\alpha}(q) \equiv \sum_{n\in C_0} G_{\alpha,n} e^{-i(n+\eta_\alpha/2)\cdot q} \tag{67}$$

for some set of Fourier coefficients $G_{\alpha,n}$, the collection of these functions represents the same freedom present in the $4\pi C_0$-periodic function $m_f(q/2)$. Thus, for any set of *fixed* 2π-periodic functions $m_\alpha(q)$ introduced to play roles parallel to that of $m_0(q)$, we may always find functions $m_{G_\alpha}(q)$ of the form (67) so that

$$m_f(q/2) = m_F(q)m_0(q/2) + \sum_{\alpha=1}^{2^d-1} m_{G_\alpha}(q)m_\alpha(q/2), \tag{68}$$

provided the choice of the fixed functions $m_\alpha(q)$ is not pathological. Eq. (68), for instance, will not hold in general if we choose $m_\alpha(q) = 0$ for all α. For reasons which will become clear in the next section, the $m_\alpha(q)$ are called the *detail* or *wavelet* symbols.

The *Two-Scale Decomposition Theorem* [Dau92, Chu92a] specifies precisely the conditions under which the choice of $m_\alpha(q)$ is not pathological so that $m_f(q/2)$ indeed may be decomposed in the form (68). Translating (68) by each of the 2^d vectors $2\pi\eta_i$ and simplifying the result using the periodicity properties of m_F and m_{G_α}, gives the following system of equations:

$$\begin{aligned}
m_f(q/2) &= m_F(q)m_0(q/2) + \sum_{\alpha=1}^{2^d-1} m_{G_\alpha}(q)m_\alpha(q/2) \qquad (69)\\
&\vdots \\
m_f(q/2+\pi\eta_i) &= m_F(q)m_0(q/2+\pi\eta_i) + \sum_{\alpha=1}^{2^d-1} (-1)^{\eta_i\cdot\eta_\alpha} m_{G_\alpha}(q)m_\alpha(q/2+\pi\eta_i)\\
&\vdots \\
m_f(q/2+\pi\eta_{2^d-1}) &= m_F(q)m_0(q/2+\pi\eta_{2^d-1}) + \sum_{\alpha=1}^{2^d-1} (-1)^{\eta_{2^d-1}\cdot\eta_\alpha} m_{G_\alpha}(q)m_\alpha(q/2+\pi\eta_{2^d-1}).
\end{aligned}$$

So long as this $2^d \times 2^d$ system is not singular, we may always solve directly for the variable functions m_F and m_{G_α} in terms the function m_f we are to reproduce and the 2^d fixed functions m_i and thus accomplish the two-scale decomposition (68). Replacing $k \equiv q/2$, the final condition for two-scale decomposition to obtain is therefore

$$\left| \begin{array}{ccc} m_0(k) & \dots & m_{2^d-1}(k) \\ \vdots & & \vdots \\ m_0(k+\pi\eta_i) & \dots & (-1)^{\eta_{2^d-1}\cdot\eta_i} m_{2^d-1}(k+\pi\eta_i) \\ \vdots & & \vdots \\ m_0(k+\pi\eta_{2^d-1}) & \dots & (-1)^{\eta_{2^d-1}\cdot\eta_{2^d-1}} m_{2^d-1}(k+\pi\eta_{2^d-1}) \end{array} \right| \neq 0 \quad \text{for all } k. \tag{70}$$

We conclude this section by observing the implications of (70) for functions in the spaces V_Q and V_{Q+1}. Making the replacement $q = k/2^Q$ in (68), which we now know holds whenever the determinant (70) is non-zero, multiplying through by $\hat{\phi}(k/2^{Q+1})$ and using (62), we obtain

$$\begin{aligned} \hat{f}(k) &= m_F(k/2^Q) m_0(k/2^{Q+1}) \phi(k/2^{Q+1}) + \sum_{\alpha=1}^{2^d-1} m_{G_\alpha}(k/2^Q) m_\alpha(k/2^{Q+1}) \phi(k/2^{Q+1}) \\ &\equiv \hat{F}(k) + \hat{G}(k), \end{aligned} \tag{71}$$

which decomposes a general function $f \in V_{Q+1}$ into a coarse function F in V_Q and an additional function G, which carries the finer scale, detailed information about f and thus lies in the space W_{Q+1}.

IV-E Wavelets

To determine the basis functions for W_{Q+1}, note that by its definition (55), the detail space contains precisely the functions $\hat{G}(k)$ from (71). Using the expansions (67) for the functions m_{G_α}, the Fourier transform of (71) gives

$$G(x) = \sum_{n \in C_0} \sum_\alpha \left(2^{Qd} G_{\alpha,n} \right) \psi_\alpha \left(2^Q (x - \frac{n + \eta_\alpha/2}{2^Q}) \right), \tag{72}$$

where

$$\hat{\psi}_\alpha(k/2^Q) \equiv m_\alpha(k/2^{Q+1}) \hat{\phi}(k/2^{Q+1}). \tag{73}$$

The detail space is therefore

$$W_{Q+1} \equiv \text{span} \left\{ \psi_\alpha \left(2^Q (x - \frac{n + \eta_\alpha/2}{2^Q}) \right) \right\}_{n \in C_0, \alpha = 1 \dots 2^d - 1}, \tag{74}$$

where the η_α are defined as the non-zero vectors in (66). The new functions $\psi_\alpha(x)$, defined in terms of the detail symbols m_α from (68), when scaled and centered appropriately, make up the basis for W_{Q+1} and are thus the detail functions, or wavelets. Note that the extra phase factors in (67) have ensured naturally that each detail function $\psi_\alpha(x)$ is associated with a unique point in D_{Q+1}, as anticipated in Sec. IV-A.

The functional form of the detail functions is revealed by Fourier expanding the $2\pi C_0$-periodic symbols m_α,

$$m_\alpha(q) \equiv \sum_{n \in C_0} \frac{d_{\alpha,n}}{2^d} e^{-iq\cdot n}, \tag{75}$$

and transforming the $Q = 0$ case of (73) to real space,

$$\psi_\alpha(x) \quad = \quad \sum_{n \in C_0} d_{\alpha,n} \phi(2x - n), \tag{76}$$

Thus, as $V_Q \oplus W_{Q+1} = V_{Q+1}$ requires, each detail function from W_{Q+1} is a linear combination of scaling functions from V_{Q+1}. The allowed choices for these linear combinations are those which satisfy (70) with the $m_\alpha(q)$ defined through (75).

An alternate route to two-scale decomposition is to note directly from $V_Q \oplus W_{Q+1} = V_{Q+1}$ that the $\psi_\alpha(x)$ must be formed from linear combinations of the scaling functions from V_{Q+1}. Then, to ensure that the two-scale and single scale representations are equivalent, one must show that each basis function of V_{Q+1} may be expanded in terms of the basis functions from V_Q and W_{Q+1}. When Fourier transformed, the system of equations which must be solved to find the corresponding expansion coefficients is precisely (69), leading once again to the determinant condition (70) for the acceptable choices for the detail functions.

IV-F Matrix language

To develop a matrix language useful for the application of multiresolution analysis to physical problems, we begin by developing a language for the various descriptions of the functions $f(x)$ in V_N provided by multiresolution analysis. There is the single-scale representation,

$$f(x) = \sum_{p \in C_N} (\vec{F}_N)_p \phi(2^N(x - p)),$$

where we define $\vec{F}_N$ as a column vector whose components are the coefficients associated with the scaling functions of V_N. Note that we index the components of $\vec{F}_N$ by the points p on which the basis functions are centered. Alternately, we may represent $f(x)$ using the multiresolution analysis which starts from a scale $M \leq N$,

$$V_N = V_M \oplus W_{M+1} \oplus \ldots \oplus W_N.$$

This gives instead

$$f(x) = \sum_{p \in C_M} (\vec{F}_{N:M})_p \, \phi(2^M(x - p)) + \sum_{P=M+1}^{N} \sum_{p \in D_P} (\vec{F}_{N:M})_p \, \psi(2^{P-1}(x - p)), \tag{77}$$

where, regardless of its scale, the expansion coefficient associated with the point p of the multiresolution representation spanning scales M through N is indexed as simply $(\vec{F}_{N:M})_p$. Because the expansion coefficient associated with each point depends on the scales present in the multiresolution analysis, it is critical to include the subscript $N : M$ on the vector $(\vec{F}_{N:M})_p$ in order to specify the scales in the multiresolution analysis. Finally, we note that under this convention the single-scale coefficients are also given by $\vec{F}_N \equiv \vec{F}_{N:N}$.

Next, the two-scale relation relation allows us to write both the scaling functions on scale M and the detail functions on scale $M + 1$ as linear combinations of scaling functions on scale $M + 1$. With these replacements, (77) becomes

$$f(x) \quad = \quad \sum_{p \in C_M} (\vec{F}_{N:M})_p \sum_{n \in C_0} c_n \phi(2^{M+1}(x - p) - n))$$

$$+ \sum_{p' \in D_{M+1}} (\vec{F}_{N:M})_{p'} \sum_{n \in Z^d} d_{\alpha(p'),n} \phi(2^{M+1}(x - p') - n))$$
$$+ \sum_{P=M+2}^{N} \sum_{p \in D_P} (\vec{F}_{N:M})_p \, \psi(2^{P-1}(x - p))$$

where the $\alpha(p')$ in the coefficients $d_{\alpha(p'),n}$ in the sum for D_{M+1} are defined so that $p' = p_0 + \eta_{\alpha(p')}/2^{M+1}$ for some p_0 in C_M. By collecting terms, this expression rearranges into the expansion for $f(x)$ in the $(M+1)^{\text{th}}$ scale representation,

$$\begin{aligned} f(x) \;\equiv\; & \sum_{q \in C_{M+1}} (\vec{F}_{N:M+1})_q \phi(2^{M+1}(x - q)) \\ & + \sum_{P=M+2}^{N} \sum_{p \in D_P} (\vec{F}_{N:M+1})_p \, \psi(2^{P-1}(x - p)). \end{aligned} \tag{78}$$

The linear map which this procedure represents between $\vec{F}_{N:M}$ and $\vec{F}_{N:M+1}$ is most compactly represented as a matrix equation,

$$\vec{F}_{N:M+1} \equiv \mathcal{I}_{M+1,M} \vec{F}_{N:M}. \tag{79}$$

The *wavelet transform*, the recovery of the single-scale representation $\vec{F}_N$ from the multiresolution representation $\vec{F}_{N:M}$, is the result of cascading together these representations of the two-scale relation,

$$\begin{aligned} \vec{F}_N \equiv \vec{F}_{N:N} &= (\mathcal{I}_{N,N-1}(\mathcal{I}_{N-1,N-2} \ldots (\mathcal{I}_{M+1,M} \vec{F}_{N:M}))) \\ &\equiv \mathcal{I}_{N:M} \vec{F}_{N:M}. \end{aligned} \tag{80}$$

Note that many authors, particularly in the field of signal processing, refer to the operator $\mathcal{I}_{N:M}$ as the "inverse" wavelet transform. Because the primary mode of operation in physical calculations is to treat the multiscale expansion coefficients as the *independent* variables, in this work we refer to this process of producing a function from its multiscale coefficients as the *forward* transform, which conforms to our usage in Sec. III-C.

The transform operator appearing in (80) may be defined as connecting any two scales $P > Q$,

$$\mathcal{I}_{P:Q} \equiv \prod_{R=P}^{Q+1} \mathcal{I}_{R,R-1}, \tag{81}$$

where in this expression, as throughout this work, we adopt the convention that non-commutative matrix products proceed in order from left to right with the lower index of the product appearing leftmost in the product and the upper index appearing rightmost. A direct result of the definition (81) is that $\mathcal{I}_{M+1:M} \equiv \mathcal{I}_{M+1,M}$. Also,

$$\mathcal{I}_{P:Q} = \mathcal{I}_{P:R} \mathcal{I}_{R:Q} \quad \text{for } (P > R > Q). \tag{82}$$

Finally, to discuss *restricted* multiresolution analyses, where functions are selectively removed from the basis as described in Sec. III-A, we introduce projection matrices which "zero out" coefficients associated with the points not contained in a given grid G,

$$(\mathcal{P}_G)_{pq} \equiv \begin{cases} \delta_{pq} & \text{if } p \in G \\ 0 & \text{if } p \notin G \end{cases} . \tag{83}$$

The product of two such projections is the projection associated with the intersection of the associated grids, and, for disjoint grids, the sum of two such projections is the projection associated with the union of the two,

$$\begin{aligned} \mathcal{P}_{G_1}\mathcal{P}_{G_2} &= \mathcal{P}_{G_1\cap G_2} \\ \mathcal{P}_{G_1}+\mathcal{P}_{G_2} &= \mathcal{P}_{G_1\cup G_2}+\mathcal{P}_{G_1\cap G_2}. \end{aligned} \tag{84}$$

Most statements about the sets of points C_Q, D_Q, B_Q defined in Sec. IV-A may be derived in terms of and translated into identities involving the projections $\mathcal{P}$. Two facts of which we shall make frequent use are that the finer grids contain the coarser grids and that the detail points of level P are contained only in the grids of level $Q \geq P$. In terms of projections, these statements are

$$\begin{aligned} \mathcal{P}_{C_P}\mathcal{P}_{C_Q} &= \mathcal{P}_{C_{\min\,(P,Q)}} \\ \mathcal{P}_{D_P}\mathcal{P}_{C_Q} &= \begin{cases} 0 & Q<P \\ \mathcal{P}_{D_P} & Q\geq P \end{cases}, \end{aligned} \tag{85}$$

respectively. Also, because the linear map represented by $\mathcal{I}_{Q+1,Q}$ replaces scaling functions and detail functions on scales Q and $Q+1$ with scaling functions on scale $Q+1$, it acts independently of the coefficients associated with scales beyond $Q+1$. Thus,

$$\mathcal{P}_{B_{Q+1}}\mathcal{I}_{Q+1,Q} = \mathcal{I}_{Q+1,Q}\mathcal{P}_{B_{Q+1}} = \mathcal{P}_{B_{Q+1}} \tag{86}$$

V Bases for Multiresolution Analysis

Even with the restrictions of multiresolution analysis as laid down in the previous section, significant freedom remains in the choice of the scaling and detail functions. Motivated by differing aspects of the calculations, researchers in electronic structure have employed different multiresolution analyses. Ultimately, the optimal approach may be to use different bases for different phases of the calculation.

The simplicity of working with orthonormal basis sets has led several authors dealing with with electronic structure[WC96, TW97] to use the wavelets of Daubechies[Dau92]. Section V-A below reviews the construction of these bases.

The primary issue in the choice of bases in problems in the physical sciences, however, is the ability of the basis to represent the relevant physical functions, not necessarily the analysis of these functions into separate frequency components. While critical in signal analysis, orthonormality is not as crucial in electronic structure, as illustrated by the great success of the chemistry community with the use of Gaussian bases[FD90]. Several authors therefore have exploited the freedom of not being confined to orthonormal bases to improve the representation of physical problems[ACLT95, LAE98, Yes97, FS94, LAE98, BN96, GI98]. The majority of these applications use multiresolution analyses based upon the scaling functions of Deslauriers and Dubuc[DD89], which were developed independently in several fields[Lem91, CS92, Don92, BS92, SB93, AU93, Uns93, ACLT95, Lew94]. The great advantage of using these scaling functions is that they function as finite element functions and thus provide both good interpolation and transform properties.

Teter[Tet93] was the first in the electronic structure community to recognize the advantage of adapting the ideas of finite elements to bases with a multilevel structure. A key concept from finite element theory is the property of *cardinality*, the condition that each basis function have value zero at every point of the finite element grid except for the one point with which it is associated. Unfortunately, it is impossible to maintain cardinality in a multiresolution analysis because smooth

basis functions from coarse scales cannot oscillate so as to be zero on the grid points of the finer scales. Instead, Teter suggested the construction of bases where cardinality is maintained for the points of coarser scales but sacrificed for finer scales. Section V-B gives the precise definition for such *semicardinal* bases, which developed out of this idea, and describes the nature of multiresolution analyses which are semicardinal.

Such semicardinal bases have the remarkable property that expansion coefficients for a function may be extracted *exactly* from the values of the the function on a finite set of points in space. This property makes these bases ideal for non-linear problems because non-linear couplings such as those in the LDA Lagrangian are computed in real-space on a finite grid and the corresponding expansion coefficients must be extracted from the resulting values. This highly desirable exact extraction property requires the detail functions to have non-zero integral, and thus prevents such bases from being wavelet bases in the technical sense described in [Dau92]. Such semicardinal bases were used in [ACLT95, Ari95, LAE98] and are described in detail in Sec. V-B below.

Finally, Goedecker and Ivanov[GI98] have suggested that the Poisson equation be solved with basis functions with zero integral and higher multipole moments, as formed by linear combinations of cardinal scaling functions according to the lifting scheme of Sweldens[Swe96]. Because working with functions of zero integral extends the range of the basis functions and disrupts the exact reconstruction property which is so useful in treating non-linear interactions, an intriguing possibility for future research would be to use semicardinal basis for the non-linear phases of the LDA calculations and a lifted basis for the solution of Poisson's equation, should lifted wavelets prove superior in the solution of Poisson's equation. (See discussion in Sec. III-F.)

V-A Orthonormal bases

Daubechies was the first to construct orthonormal bases of wavelets with compact support[Dau92]. We now give a brief review of the discussion in [Dau92] within our present conventions and language.

The scaling functions on the coarsest scale of an orthonormal multiresolution basis are themselves orthonormal. This condition may be re-scaled to the scale $Q = 0$, where it becomes

$$\begin{aligned}
\delta_{nm} &= \int d^d x\ \phi^*(x-n)\phi(x-m) \\
&= \int d^d x\ (\int d^d k\ \hat{\phi}(k) e^{ik\cdot(x-n)})^* (\int d^d k'\ \hat{\phi}(k') e^{ik'\cdot(x-m)} \\
&= (2\pi)^d \int d^d k\ \phi^*(k)\phi(k) e^{ik\cdot(n-m)} \quad \text{for all } n, m \text{ in } C_0.
\end{aligned}$$

The entire reciprocal space of vectors k may be partitioned into images of the first Brillouin zone centered on the points G of the reciprocal lattice $2\pi C_0$. Writing the integral in this way gives,

$$\delta_{nm} = (2\pi)^d \int_{B.Z.} d^d k \sum_{G \in 2\pi C_0} \phi^*(k+G)\phi(k+G) e^{ik\cdot(n-m)},$$

where we have used the fact $e^{iG\cdot(n-m)} = 1$ for the reciprocal lattice vectors G. The fact that this is true for all n, m in C_0, combined with the Fourier space version of two-scale relation (59), gives

$$\begin{aligned}
(2\pi)^{-2d} &= \sum_{G \in 2\pi C_0} \phi^*(k+G)\phi(k+G) \qquad (87) \\
&= \sum_{G \in 2\pi C_0} \left(m_0(\frac{k+G}{2})\phi(\frac{k+G}{2}) \right)^* \left(m_0(\frac{k+G}{2})\phi(\frac{k+G}{2}) \right).
\end{aligned}$$

Finally, defining $q \equiv k/2$ and re-expressing the sum over $G/2$ as a sum over the reciprocal lattice and the decoration points $\pi\eta_i$ with η_i defined in (66), gives

$$\begin{aligned}(2\pi)^{-2d} &= \sum_{G' \in 2\pi C_0} \sum_i m_0^*(q + (G' + \pi\eta_i))\phi^*(q + (G' + \pi\eta_i))m_0(q + (G' + \pi\eta_i))\phi(q + (G' + \pi\eta_i)) \\ &= \sum_i m_0^*(q + \pi\eta_i)m_0(q + \pi\eta_i) \sum_{G' \in 2\pi C_0} \phi^*(q + (G' + \pi\eta_i))\phi(q + (G' + \pi\eta_i)) \\ &= \sum_i m_0^*(q + \pi\eta_i)m_0(q + \pi\eta_i)(2\pi)^{-2d},\end{aligned}$$

where we have used the periodicity of m_0 and the first line of (87). We thus conclude that orthonormality among the scaling functions places the following condition on the two-scale symbols,

$$\sum_{i=0}^{2^d-1} m_0^*(q + \pi\eta_i)m_0(q + \pi\eta_i) = 1. \tag{88}$$

In Sec. V-C, we show how to construct functions $M_0(q)$ which obey the constraint

$$\sum_{i=0}^{2^d-1} M_0(q + \pi\eta_i) = 1.$$

Comparing with (88), we see that to construct orthonormal scaling functions, one first finds such an $M_0(q)$ and then takes the "square root" to find the appropriate two scale symbol $m_0(q)$. This procedure is described in [Dau92, Sec. 6.1], which also tabulates the resulting two-scale coefficients.

Next, to construct orthonormal *detail* functions, one must assure that the wavelet ψ_α for each decoration point $\alpha = 1 \ldots 2^d - 1$ be orthogonal to the scaling functions,

$$\begin{aligned}0 &= \int d^d x\ \phi^*(x - n)\psi_\alpha(x - m - \eta_\alpha/2) \\ &= (2\pi)^d \int_{B.Z.} d^d k\ \sum_G \hat{\phi}^*(k + G)\hat{\psi}_\alpha(k + G)e^{ik\cdot(m-n) - i(k+G)\cdot\eta_\alpha/2}.\end{aligned}$$

Through an analogous analysis to that above, we will finally arrive at

$$0 = \sum_i m_0^*(q + \pi\eta_i)\left(e^{-i\pi\eta_i\cdot\eta_\alpha} m_\alpha(q + \pi\eta_i)\right). \tag{89}$$

One must also ensure orthonormality among the $\psi_\alpha(x)$,

$$\delta_{\alpha\beta}\delta_{nm} = \int d^d x\ \psi_\alpha^*(x - n - \eta_\alpha/2)\psi_\beta(x - m - \eta_\beta/2),$$

which leads to

$$\delta_{\alpha\beta} = \sum_{i=0}^{2^d-1} \left(e^{-i\pi\eta_i\cdot\eta_\alpha} m_\alpha(q + \pi\eta_i)\right)^* \left(e^{-i\pi\eta_i\cdot\eta_\beta} m_\beta(q + \pi\eta_i)\right). \tag{90}$$

Finally, we note that three orthonormality conditions (88-90) may be combined into one single condition by simply taking α and β in (90) to vary over the full range $0 \ldots 2^d - 1$.

In one dimension, Eq. (90) represents three independent conditions: orthonormality among the scaling functions, orthonormality among the wavelets $\psi_1(x - n - 1/2)$, and orthogonality between

these two sets of functions. Given a two-scale symbol m_0 satisfying the orthonormality condition, one common choice for the wavelet symbol m_1 which satisfies the remaining conditions in (90) is

$$m_1(k) = m_0^*(k + \pi), \tag{91}$$

as may be confirmed directly by substitution.

For $d > 1$ dimensions, a straight-forward way to satisfy the conditions (90) is to use product functions formed from the symbols m_0 and m_1 of an orthonormal, one-dimensional multiresolution analysis,

$$m_\alpha(q) \equiv \prod_{e=1}^{d} m_{(\eta_\alpha)_e}(q_e),$$

where e varies over the Euclidean dimensions of space, q_e and $(\eta_\alpha)_e$ are the corresponding components of the respective vectors, and, again, we let α vary over the entire range including $\alpha = 0$. With this choice, the condition (90) factors and gives

$$\sum_{i=0}^{2^d-1} \left(e^{-i\pi\eta_i\cdot\eta_\alpha} m_\alpha(q + \pi\eta_i)\right)^* \left(e^{-i\pi\eta_i\cdot\eta_\beta} m_\beta(q + \pi\eta_i)\right)$$

$$= \prod_e \left[\sum_{\eta=0}^{1} \left(e^{-i\pi\eta(\eta_\alpha)_e} m_{(\eta_\alpha)_e}(q + \pi\eta)\right)^* \left(e^{-i\pi\eta(\eta_\beta)_e} m_{(\eta_\beta)_e}(q + \pi\eta)\right)\right]$$

$$= \prod_e \delta_{(\eta_\alpha)_e,(\eta_\beta)_e} = \delta_{\alpha,\beta},$$

as is required. This, coupled with the choice (91), was used to construct the multidimensional basis functions used in the electronic structure calculations of [WC96, TW97]. The particular choice of two-scale symbols m_0 in these works were the D6 and D8 wavelets defined in [Dau92], respectively.

V-B Semicardinal bases

It is highly desirable in the calculation of electronic structure to be able to determine the expansion coefficients of functions from knowledge of their values on a grid of finite resolution. If we insist that at every level of resolution Q, the expansion coefficients of a function depend only upon its values on the grid C_Q, then, as we will now see, it is always possible to find a multiresolution basis in which every basis function has the value zero on all points of the grid of its corresponding scale, except for one, where its value is unity. We refer to such a basis as a *semicardinal* basis.

The following definitions are useful in discussing such bases. The concept of semicardinality may be defined independently of multiresolution analysis, so we couch these definitions in general terms:

1. A *hierarchical basis* is a set of functions, each associated with exactly one point g from a hierarchy of nested grids $G_M \subset G_{M+1} \subset \ldots$.

2. For such a set of grids, $H_{Q+1} \equiv G_{Q+1} - G_Q$.

3. In a hierarchical basis, the *scale* of a point g and it associated basis function is the least value of Q for which g is in G_Q.

4. A function $f(x)$ is *cardinal* on a given grid G if $f(g) = \delta_{gh}$ for all points g and one point h, both in G.

5. A *semicardinal* basis is a hierarchical basis in which each basis function is cardinal on the grid of its own scale.

Note from the second and third definitions that when $Q = M$, G_Q is the set of all points from scale Q and that when $Q > M$, H_Q is the scale of all points from scale Q. In the language of Secs. III-C and IV-F, semicardinality is the condition that the matrix $\mathcal{I}$, whose columns contains the values of each basis function on the finest grid, obeys two simple algebraic identities,

$$\begin{aligned} \mathcal{P}_{G_M}\mathcal{I}\mathcal{P}_{G_M} &= \mathcal{P}_{G_M} \\ \mathcal{P}_{G_Q}\mathcal{I}\mathcal{P}_{H_Q} &= \mathcal{P}_{H_Q} \quad \text{for } Q > M. \end{aligned} \tag{92}$$

Note that a multiresolution analysis is a hierarchical basis on the grids C_Q, with the D_Q playing the role of the H_Q. As an example, consider the multiresolution basis consisting of the basis functions from the top two panels of Figure 8. The basis functions for V_0 are associated only with points of C_0 but not C_1 and thus are of scale $N = 0$. These functions are cardinal on the grid C_0 and thus satisfy their condition for semicardinality. The basis functions for W_1 are associated with the points in $D_1 = C_1 - C_0$, and thus are of scale $N = 1$. But, they are not cardinal on the grid C_1, and thus this two-scale basis fails to be semicardinal. For the basis to be semicardinal, we would have to replace the functions centered on the odd half-integer points with functions which are cardinal on C_1.

V-B.1 Exact extraction

In a hierarchical basis on the scales $N : M$ (by our convention $N > M$), the property of exact extraction means that for *all* scales Q, the expansion coefficients on the scales $Q : M$ for a function $f(x)$ may be determined from knowledge of the values $f(G_Q)$ of the function on the grid G_Q only. This means, in particular that the map from the expansion coefficients on scales $Q : M$ to the values of the function $f(G_Q)$ is *invertible*. We now show that this property of obvious practical utility implies that such a basis may always be chosen to be semicardinal.

Consider functions expanded from the coarsest scale M up to a very fine scale $R >> Q$. By our assumption of the existence of an invertible linear map, the expansion coefficients on the scales $Q : M$ of any function with values $f(G_Q) = 0$ must be zero. Thus, the space of functions satisfying $f(G_Q) = 0$ must be a subspace of span of the basis functions associated with the remaining points, $G_R - G_Q$.

Now, the space of functions $f(G_Q) = 0$ has exactly one degree of freedom for each point of $G_R - G_Q$ and thus has the same dimension as the span of the basis functions associated with the same set of points. Having already established that the former space is contained in the latter, we now see from their dimensionality that the two spaces are in fact the same.

Specifically, this means that all functions $f(x)$ in the span of the basis functions associated with H_{Q+1} must all have zero value on the next coarser grid, $f(G_Q) = 0$. Hence, the invertible linear map which we have supposed to exit between the coefficients of scales $Q + 1 : M$ and the values $f(G_{Q+1})$ induces an invertible map from the span of the basis functions associated with the points H_{Q+1} to the sequences of values $f(G_{Q+1})$ for which $f(G_Q) = 0$. A basis for this latter sequence space is the set of sequences which are zero on all points of G_{Q+1} but for one point in H_{Q+1} where they take the value unity. Applying to each of these sequences the inverse of the aforementioned induced map produces a basis for the span of the functions of scale $Q + 1$ satisfying the conditions of semicardinality. Proceeding in this manner for all scales $N \leq Q \leq M$ produces a semicardinal basis.

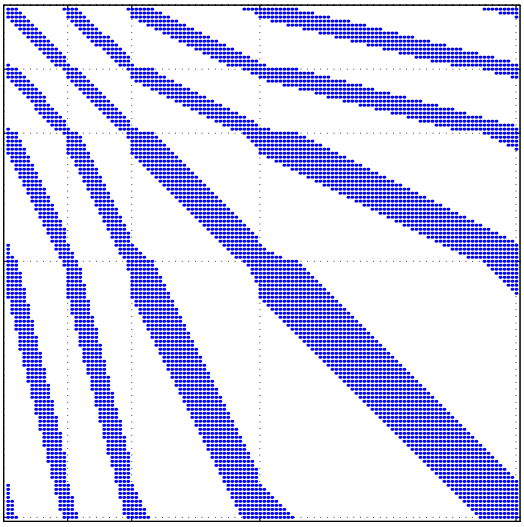

Figure 10: Sparsity pattern of Hermitian operator in a semicardinal basis on $C_0, C_1, \ldots$ in one dimension. (Basis functions grouped into blocks according to scale from coarsest to finest.)

V-B.2 Algorithms

Although semicardinal bases have the desirable property of exact extraction, without the additional structure of multiresolution analysis, it is difficult to develop efficient methods for performing the operations needed in physical calculations.

In particular, without the structure of multiresolution analysis, the operations $\mathcal{L}, \mathcal{O}, \mathcal{I}, \mathcal{I}^\dagger$ must be applied directly as multiplication by the corresponding matrices. When working with the complete grids $C_0, C_1, \ldots$ as defined in (54), these matrices show a sparse, fractal-like pattern. Figure 10 shows the appearance of this pattern in one dimension for L and $\mathcal{O}$ when the basis functions are ordered first according to scale from coarsest to finest and then within each scale by location in space. A similar pattern results for the matrices $\mathcal{I}$ and $\mathcal{I}^\dagger$ except that, because of semicardinality, these matrices are either zero above or below the diagonal, respectively.

After the process of restriction, as defined in Sec. III-A and illustrated in Figure 4, little of this sparsity remains. In calculating electronic structure, the majority of functions surviving the restriction will overlap with one of the nuclei. The matrix elements among these surviving functions thus consist of dense blocks connecting all of the functions associated with each atomic nucleus. Multiplication by matrix blocks of such size requires thousands of operations per basis function and is therefore relatively inefficient.

The inverse transform $\mathcal{J}$ has the potential to require the solution of a general system of linear system of equations and thus become even more problematic. Semicardinality, however, provides just enough structure to allow the inverse transform to be performed in a direct procedure requiring the same work as does $\mathcal{I}$. To see this, let $f \equiv f(G_N)$ be a column vector of the samples of a function on the finest grid and $F \equiv \mathcal{J}f$ be the expansion coefficients we seek. Decomposing F into contributions on different scales and applying the identity $\mathcal{P}_{G_M}\mathcal{I}\mathcal{P}_{H_Q} \equiv \mathcal{P}_{G_M}(\mathcal{P}_{G_Q}\mathcal{I}\mathcal{P}_{H_Q}) = \mathcal{P}_{G_M}\mathcal{P}_{H_Q} = 0$, which follows from the algebraic definition of semicardinality (92) and the facts that $G_Q \subset G_M$ and $G_M \cap H_Q$ for $Q > M$, gives the following result for the values of the function on

the coarsest scale,

$$\begin{aligned} \mathcal{P}_{G_M} f &= \mathcal{P}_{G_M} \mathcal{I} F \\ &= \mathcal{P}_{G_M} \mathcal{I} (\mathcal{P}_{G_M} + \mathcal{P}_{H_{M+1}} + \ldots) F \\ &= \mathcal{P}_{G_M} F. \end{aligned} \tag{93}$$

Thus, the expansion coefficients on the coarsest scale are just the values of the function on the associated points.

Now, proceeding iteratively, suppose the coefficients of F are known up to scale Q and consider the values of f on the next scale. Again using the conditions (92), we have

$$\begin{aligned} \mathcal{P}_{H_{Q+1}} f &= \mathcal{P}_{H_{Q+1}} \mathcal{I} (\mathcal{P}_{G_Q} + \mathcal{P}_{H_{Q+1}} + \mathcal{P}_{H_{Q+2}} + \ldots) F \\ &= (\mathcal{P}_{H_{Q+1}} \mathcal{I} \mathcal{P}_{G_Q} + \mathcal{P}_{H_{Q+1}}) F, \end{aligned}$$

which gives the expansion coefficients on the next scale explicitly as

$$\mathcal{P}_{H_{Q+1}} F = \mathcal{P}_{H_{Q+1}} f - \mathcal{P}_{H_{Q+1}} \mathcal{I} \mathcal{P}_{G_Q} F. \tag{94}$$

Combining (93,94) gives the following recursive procedure for computing $F = \mathcal{J} f$,

$$\begin{aligned} F_M &\equiv f; \\ F_{Q+1} &= F_Q - \mathcal{P}_{H_{Q+1}} \mathcal{I} \mathcal{P}_{G_Q} F_Q; \\ F &\equiv F_N. \end{aligned} \tag{95}$$

Note that the total action of all of the operators $\mathcal{P}_{H_{Q+1}} \mathcal{I} \mathcal{P}_{G_Q}$ is just to connect once each of the columns of $\mathcal{I}$ with all points in the H_{Q+1}. The implementation of (95) is thus precisely as costly as the implementation of $\mathcal{I}$.

Finally, note that the algorithm (95) may be written as the matrix product,

$$\mathcal{J} = \prod_{Q=N-1}^{M} \left(I - \mathcal{P}_{H_{Q+1}} \mathcal{I} \mathcal{P}_{G_Q} \right), \tag{96}$$

from which the procedure to compute $\mathcal{J}^\dagger$ is easily determined.

V-B.3 Semicardinal multiresolution analysis

The key feature of semicardinality, that the expansion coefficients of scale Q for a function $f(x)$ may be extracted from the sample values $f(C_Q)$, is incompatible with the use of standard orthogonal or bi-orthogonal multiresolution analyses. In bi-orthogonal multiresolution analyses[Dau92], one considers both the basis of scaling and detail functions and the *dual* to this basis. The *dual* to any basis is defined as those functions against which any function $f(x)$ may be integrated to determine its expansion coefficients in the original basis. Orthogonal multiresolution analyses are thus a special case of bi-orthogonal bases where the basis is its own dual. For semicardinal bases, the exact extraction property implies that the dual of the functions of scale Q are linear combinations of Dirac δ-functions centered on the points of C_Q. Thus, a semicardinal basis of smooth functions can never be orthogonal, and, because Dirac δ-functions are not square-integrable, such a basis does not technically fit into the bi-orthogonal wavelet framework.

Nonetheless, it is possible to construct multiresolution analyses which are semicardinal. Semicardinality, in fact, nearly completely determines the allowable form for a multiresolution analysis.

To form a semicardinal multiresolution analysis it is necessary and sufficient that the scaling functions be cardinal and that each of the $2^d - 1$ detail functions for scale Q simply be the scaling functions of scale $Q+1$ associated with the corresponding detail points. While this latter property may seem unusual at first, having only one type of function in the multiresolution analysis proves to be of considerable convenience[LAE98].

To show that semicardinal multiresolution analyses must have this form, consider first the requirements which semicardinality places on the scaling functions. The first semicardinality condition of (92) states that the functions spanning the coarsest scale M must appear cardinal on the coarsest grid, which is C_M in the case of a multiresolution analysis. Dilating this condition to the scale $Q = 0$, gives the condition that the scaling functions must be cardinal on the integer grid,

$$\phi(n-m) = \delta_{nm} \quad \text{for } n, m \text{ in } C_0 \equiv Z^d. \tag{97}$$

Section V-C.1(b) discusses the implications of this for functions satisfying the two-scale relation.

Next, we turn to the detail functions. The second semicardinality condition of (92) states that for all $q \in D_Q$ and $p \in C_Q$, the detail function associated with point q must have value $\psi_\alpha(2^{Q-1}(p-q)) = \delta_{pq}$. Enforcing this condition for all p and dilating the condition to scale $Q = 0$, implies that for all α, $\psi_\alpha(n/2) = \delta_{n0}$ for $n \in Z^d$. From this we find that for the detail coefficients of (76) that

$$\begin{aligned} d_{\alpha,n} &\equiv \sum_{k \in Z^d} d_{\alpha,k}\delta_{nk} = \sum_{k \in Z^d} d_{\alpha,k}\phi(n-k) \\ &= \psi_\alpha(n/2) = \delta_{n0}. \end{aligned} \tag{98}$$

Therefore, as stated above, the detail functions $\psi_\alpha(x) = \sum_{k \in Z^d} d_{\alpha,k}\phi(2x-k) = \phi(2x)$ are just the scaling functions from the next finer scale. For a general scale Q this means that the detail functions for the points D_{Q+1} are just the scaling functions on the corresponding points in the single-scale representation of V_{Q+1}.

Finally, we now verify that such a basis satisfies the *two-scale decomposition theorem*. Eq. (98) implies that $m_\alpha(q) = 1/2^d$ for all α and q. Thus the determinant from (70) becomes

$$\begin{aligned} \det &= (\frac{1}{2^d})^{2^d-1} \begin{vmatrix} m_0(q) & \dots & 1 & \dots & 1 \\ \vdots & & \vdots & & \vdots \\ m_0(q+\pi\eta_i) & \dots & (-1)^{\eta_\alpha \cdot \eta_i} & \dots & (-1)^{\eta_{2^d-1} \cdot \eta_i} \\ \vdots & & \vdots & & \vdots \\ m_0(q+\pi\eta_{2^d-1}) & \dots & (-1)^{\eta_\alpha \cdot \eta_{2^d-1}} & \dots & (-1)^{\eta_{2^d-1} \cdot \eta_{2^d-1}} \end{vmatrix} \\ &= \pm(\frac{1}{2^d})^{2^{d-1}} \sum_i m_0(q+\pi\eta_i), \end{aligned} \tag{99}$$

where, we have used the fact, derived in the appendix, that each cofactor in the determinant expansion along the first column has the value $\pm(2^d)^{2^{d-1}-1}$, with a fixed sign for each cofactor. For cardinal scaling functions, we have from (105) in Sec. V-C.1, that the sum over the m_0 appearing in (99) is unity. Thus, as required for two-scale decomposition, the determinant is never zero. The fact that we find a simple constant for the determinant is a direct reflection of the compact nature of the dual basis.

V-C Interpolating, cardinal scaling functions

Because the previous section has already determined the form which the detail functions of a semicardinal multiresolution analysis must take, it remains now only to specify the scaling functions of such multiresolution analyses. Accurate calculations in physical systems require that the reconstructions of physical functions from sample values interpolate well the behavior of those functions between the sampling points. Additionally, in order to limit the processing required for each expansion coefficient, in practice the basis functions should have the minimal spatial extent possible. These conditions represent two additional constraints beyond those we have already imposed, cardinality for exact recovery of expansion coefficients and the two-scale relation to sustain multiresolution analysis. As we shall show in Sec. V-C.1, the four constraints of (1) the two-scale relation, (2) cardinality, (3) minimal support, and (4) interpolation almost uniquely specify the scaling functions. In the interest of brevity, we shall refer to such interpolating, cardinal scaling functions as "interpolets."

Once the two-scale coefficients of the interpolets are determined, the only other information needed to perform physical calculations are the matrix elements of integral-differential operators between scaling functions and the values of the scaling functions in real-space. Sections V-C.2 and V-C.3 describe the determination of these quantities, and Sec. V-C.4 gives examples of specific functions, with tables displaying all information needed in physical calculations.

V-C.1 Construction

We now discuss the mathematical implications of the four constraints outlined above. Because we now consider the very specific class of interpolating cardinal scaling functions, we shall denote these functions as $\mathcal{I}(x)$, in place of the generic $\phi(x)$.

V-C.1(a) Two-scale relation As discussed in Sec. IV-C, we may consider the entire allowable class of scaling functions by considering only functions constructed in Fourier space via

$$\tilde{\mathcal{I}}(k) = \left(\prod_{j=1}^{\infty} m_0(k/2^j) \right) \mathcal{I}(0) \tag{100}$$

with an arbitrary $2\pi C_0$–periodic function $m_0(q)$ satisfying $m_0(0) = 1$.

Each of the remaining conditions thus becomes a condition on the acceptable two-scale symbols $m_0(q)$. Once $m_0(q)$ is known, the two-scale coefficients c_n

$$\mathcal{I}(x) = \sum_n c_n \mathcal{I}(2x - n), \tag{101}$$

used to form the operators $\mathcal{I}_{P+1,P}$ from Sec. IV-F, may be recovered from (60).

V-C.1(b) Cardinality Cardinality is the condition that the scaling functions $\mathcal{I}(x)$ obey

$$\mathcal{I}(n) = \delta_{n,0}, \quad \text{for all } n \in C_0. \tag{102}$$

To transform this into a constraint on the c_n, and thus on the $m_0(q)$, we dilate the two-scale relation by a factor of two,

$$\mathcal{I}(x/2) = \sum_n c_n \mathcal{I}(x - n), \tag{103}$$

and evaluate the result on the points $x = m$ in C_0,

$$\mathcal{I}(m/2) = \sum_n c_n \mathcal{I}(m-n) = \sum_n c_n \delta_{mn} = c_m. \tag{104}$$

Comparing with (102), cardinality determines all "even" terms in c_n,

$$c_{2n} = \delta_{n0}, \quad \text{for } n \text{ in } C_0.$$

To convert this into a condition on the two-scale symbol, we remove all "odd" frequency components of $m_0(q)$ leaving untouched the "even" frequency components by periodizing the sum (60) on the lattice πC_0. Cardinality thus implies that the two-scale symbol obey

$$\sum_{i=0}^{2^d-1} m_0(k+\pi\eta_i) = \sum_{n\in 2C_0} 2^d \frac{c_n}{2^d} e^{-ik\cdot n} = 1, \tag{105}$$

which we used in (99) to confirm that semicardinal multiresolution analyses indeed satisfy the two-scale decomposition theorem.

V-C.1(c) Minimal support From (104) we see that cardinal scaling functions extend at least as far as the range of non-zero elements in the sequence c_n. We thus limit our discussion to sequences with the shortest possible length. Correspondingly, the $m_0(q)$ are to be constructed as the *finite* trigonometric polynomial of the *lowest* order which satisfies all other conditions on the scaling functions.

V-C.1(d) Interpolation By ensuring the equivalence of the multiscale and single-scale representations, multiresolution analysis simplifies the consideration of how well a multiresolution basis interpolates physical functions to the consideration of interpolation for the *single-scale* representation on the finest scale of the analysis. On the finest scale, cardinality of the scaling functions gives

$$\tilde{f}_N(x) = \sum_{p\in C_N} f(p)\mathcal{I}\left(2^N(x-p)\right) \tag{106}$$

as the function $\tilde{f}(x)$ in V_N which matches exactly the sample values $f(C_N)$. To ensure that this estimate interpolate $f(x)$ to order l between the sample points, we insist that it reproduce *exactly* all polynomials up to degree l. By linearity, to do this, we need only impose the reconstruction of all multinomials $\prod_i x_i^{l_i}$ where $\sum_i l_i \le l$ and $0 \le l_i$. Rescaling this condition to the scale $Q = 0$, it becomes

$$\prod_i x_i^{l_i} = \sum_{n\in C_0} (\prod_i n_i^{l_i}) \mathcal{I}(x-n). \tag{107}$$

To determine the constraints which this condition places on $m_0(q)$, we first consider the constraints which it places on $\tilde{\mathcal{I}}(k)$. Condition (107) is a convolution leading to the familiar product form in Fourier space

$$\begin{aligned} \int \prod_i x_i^{l_i} \frac{e^{-ik\cdot x}\, d^d k}{(2\pi)^d} &= \tilde{\mathcal{I}}(k) \sum_{n\in C_0} (\prod_i n_i^{l_i}) e^{-ik\cdot n} \\ \partial_{\{l_i\}}\delta^{(d)}(k) &= \tilde{\mathcal{I}}(k)\cdot(2\pi)^d \sum_{n\in C_0} \partial_{\{l_i\}}\delta^{(d)}(k-2\pi n), \end{aligned} \tag{108}$$

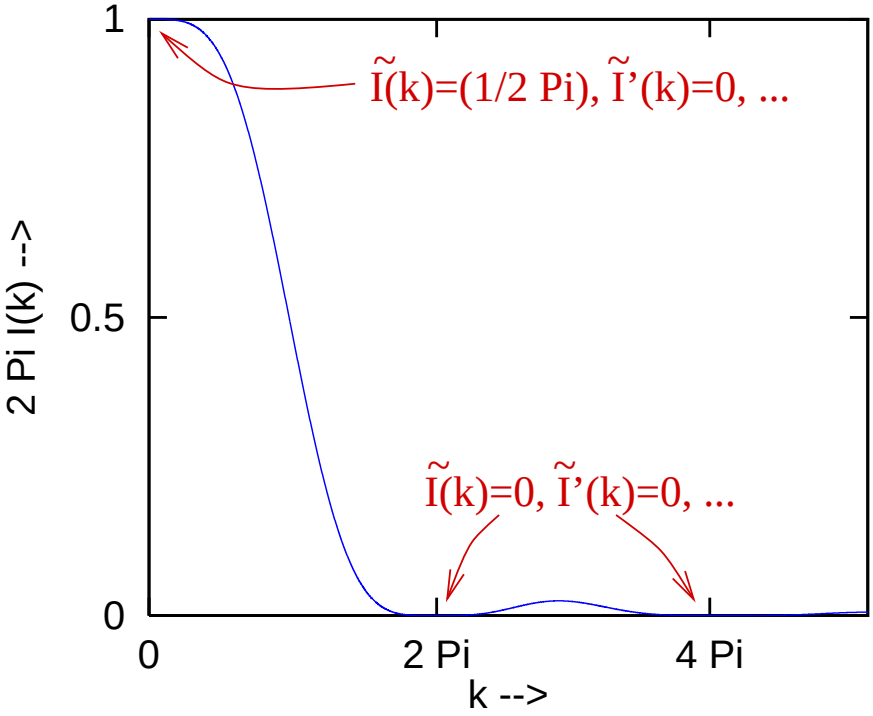

Figure 11: Fourier transform of an interpolating, cardinal scaling function.

where $\delta^{(d)}(q)$ is the d-dimensional Dirac δ-function and $\partial_{\{l_i\}}$ denotes the mixed partial derivative $\prod_i \partial_{x_i}^{l_i}$, and we have used the identity $\sum_n e^{-ik\cdot n} = (2\pi)^d \sum_n \delta^{(d)}(k - 2\pi n)$. Eliminating the singularities at non-zero points in $2\pi C_0$ from the right-hand side of (108) requires a high degree of regularity in $\tilde{\mathcal{I}}(k)$ at these points. Integrating the derivatives of the δ-functions by parts reveals that (108) implies the conditions

$$(2\pi)^d \partial_{\{l_i\}} \tilde{\mathcal{I}}(2\pi n) = \left(\prod_i \delta_{l_i,0} \right) \delta_{n,0} \quad \text{for } \textstyle\sum_i l_i \leq l. \tag{109}$$

Figure 11 illustrates these conditions on $\tilde{\mathcal{I}}(k)$ for one dimension. One important result is that interpolation sets the normalization of the of the scaling functions. The $l = 0$ condition at $n = 0$ is just $\tilde{\mathcal{I}}(0) = 1/(2\pi)^d$, or equivalently,

$$\int d^d x \; \mathcal{I}(x) = 1. \tag{110}$$

The other conditions at $n = 0$ are that the higher order integral moments up to order l be zero,

$$\int d^d x \; (\prod_i x_i^{l_i}) \mathcal{I}(x) = 0 \quad \text{for } \textstyle\sum_i l_i \leq l.$$

The conditions at the *non-zero* points in $2\pi C_0$ are most simply expressed as the condition that $\tilde{\mathcal{I}}(k)$ have an l^{th}-order zero at these points.

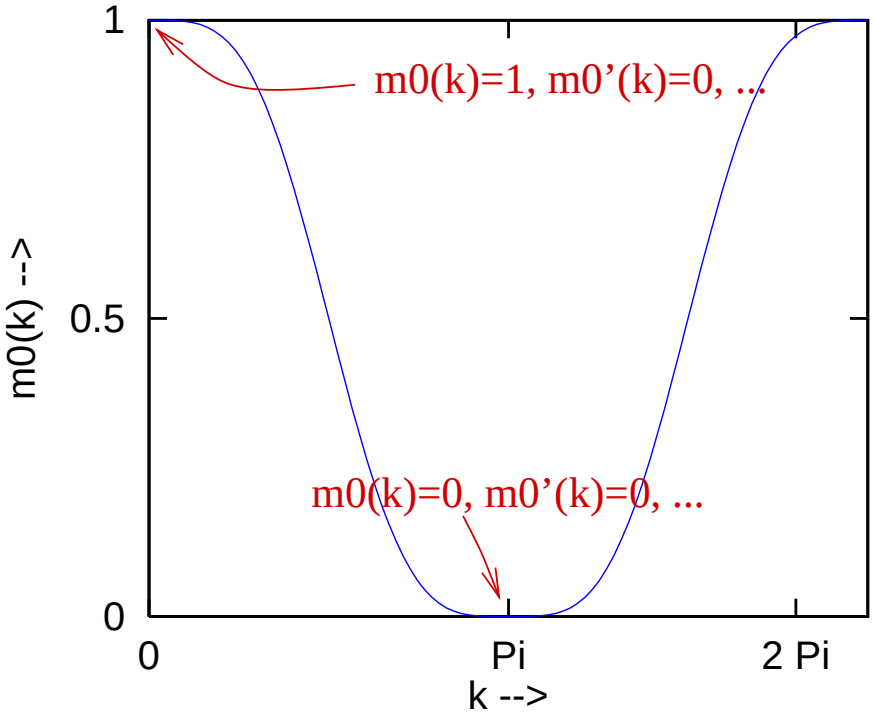

Figure 12: Two-scale symbol m_0 for an interpolating, cardinal scaling function.

The $n = 0$ conditions of (109) constrain the behavior of $m_0(q)$ near $q = 0$. With a finite number of non-zero c_n from the condition of minimal support, we are assured that $m_0(q)$ is analytic. Recalling that $m_0(0) = 1$, we have that near $q = 0$,

$$m_0(q) = 1 + O(q^\beta), \tag{111}$$

for some leading order β. Eq. (100) then ensures that $\tilde{\mathcal{I}}(k)$ has a similar analytic structure near $k = 0$,

$$\begin{aligned} \tilde{\mathcal{I}}(k) &= \tilde{\mathcal{I}}(0) \prod_{n=1}^{\infty} \left(1 + O\left((k/2^n)^\beta\right)\right) \\ &= \tilde{\mathcal{I}}(0) \left(1 + O\left(k^\beta\right)\right). \end{aligned} \tag{112}$$

Thus, we satisfy all $n = 0$ conditions from (109), including the zeroth-order normalization condition, so long as we take

$$\tilde{\mathcal{I}}(k) = \frac{1}{(2\pi)^d} \prod_{j=1}^{\infty} m_0(k/2^j), \tag{113}$$

for some m_0 satisfying

$$\partial_{\{l_i\}} m_0(0) = \prod_i \delta_{l_i,0} \quad \text{for all } \textstyle\sum_i l_i \leq l. \tag{114}$$

The final conditions concern $\tilde{\mathcal{I}}(k)$ at the non-zero points of $2\pi C_0$. From the form of the product (113), we see that if $\tilde{\mathcal{I}}(k)$ is to have an l^{th} order zero at G, then the orders of the zeros of $m_0(q)$

among the points $q = G/2, G/4, \ldots$ must sum to give at least this order. Because all non-zero points in $\pi C_0 = 2\pi C_0/2$ may be expressed in terms of the product of some non-negative power of two with some vector in πD_1, if $m_0(q)$ has an l^{th} order zero at each of the points πD_1, then $\tilde{\mathcal{I}}(k)$ will have the appropriate analytic structure at the non-zero points of $2\pi C_0$. Noting the $2\pi C_0$-periodicity of the $m_0(q)$, the final conditions imposed by interpolation on the two scale symbol are thus

$$\partial_{\{l_i\}} m_0(\pi\eta_\alpha) = 0 \quad \text{for all } \textstyle\sum_i l_i \leq l \text{ and } 1 \leq \alpha \leq 2^d - 1, \tag{115}$$

with the η_α defined as in (66). Figure 12 illustrates these conditions for one dimension.

An interesting alternative to (115) is to note that one could ensure the proper behavior in $\tilde{\mathcal{I}}(k)$ by instead placing l^{th} order zeros in $m_0(q)$ at the points of πD_2. But, this and other such choices demand higher degrees of oscillation in $m_0(q)$ and would to require longer non-zero sequences in c_n. Also, condition (115) has the distinct advantage that when combined with condition (114), the two conditions automatically imply cardinality, condition (105).

To minimize the support of the resulting functions, we thus consider scaling functions constructed according to (113) with $m_0(q)$ satisfying the conditions (114,115) and which therefore satisfy all of our constraints. For a given degree of interpolation l, the conditions (114,115) are equivalent to a system of simple linear equations for the two-scale coefficients c_n. The most compact set of coefficients satisfying these conditions gives the most compact l^{th}-order interpolating cardinal scaling function, or "interpolet". Section V-C.4 details these equations and their solution in several useful cases.

V-C.2 Overlaps

We now present a method for determining matrix elements among the scaling functions directly from the two-scale coefficients c_n. As many of these results are general, we revert temporarily to the notation $\phi(x)$ for the scaling functions. Once we begin to use specific properties of interpolating cardinal functions, we shall return to the notation $\mathcal{I}(x)$. The approach below has been developed by several authors in one dimension and is described in [SN96]. We here give the appropriate generalizations for multiple dimensions.

The specific information needed to apply the overlap matrices $\mathcal{O}$ and L when using the procedures of Sec. VI is the set of matrix elements among the functions of the finest scale,

$$M_{pq} \equiv \int d^d x \, \phi^*(2^N(x-p)) \hat{M} \phi_m(2^N(x-q)) \quad \text{for } p, q \text{ in } C_N, \tag{116}$$

with $\hat{M}$ being the the identity operator $\hat{1}$ (for $\mathcal{O}$) and the Laplacian ∇^2 (for L). To compute these elements we exploit the fact that both $\hat{1}$ and ∇^2 are homogeneous operators.

The *homogeneous operators of order h* are those which may be written in Fourier space as a linear combination of multinomials of order h,

$$\hat{\tilde{M}} = M^{(h)}(k) \equiv \sum_{\sum_{j=1}^d h_j = h} m_{\{h_j\}} \prod_j k_j^{h_j} \tag{117}$$

for some set of coefficients $m_{\{h_j\}}$. In real space, these operators are just

$$\hat{M} = M^{(h)}\left(\frac{\nabla}{i}\right), \tag{118}$$

where $i \equiv \sqrt{-1}$. Taken together, the operators of order h thus form a linear space of dimension equal to the corresponding number of multinomials, $(d-1+h)!/[(d-1)!h!]$. The multinomial coefficients $m_{\{h_j\}}$ for any such operator may be extracted simply by acting with the operator on the multinomial functions of order h,

$$m_{\{h_j\}} = \frac{\hat{M}(\prod_j x_j^{h_j})}{\prod_j h_j!}. \tag{119}$$

Finally, we note that the identity operator $M(k) = 1$ belongs to the one-dimensional space of operators of order $h = 0$ and that the Laplacian operator $M(k) = -\sum_{j=1}^{d} k_j^2$ comes from the space of operators of order $h = 2$, which in $d = 3$ dimensions has dimension six.

For any such homogeneous operator, the required matrix elements (116) for any scale may be related to a single universal set of matrix elements,

$$\begin{aligned} M_{pq} &\equiv \int d^d x\ \phi^*(2^N(x-p)) M^{(h)}\left(\frac{\nabla}{i}\right)\phi(2^N(x-q)) \\ &= \int d^d x\ \phi^*(2^N(x-p)) 2^{Nh}\left(M^{(h)}\left(\frac{\nabla_u}{i}\right)\phi(u)\right)\Big|_{u=2^N(x-q)} \\ &= 2^{N(h-d)}(\vec{M})_{2^N(p-q)}, \end{aligned} \tag{120}$$

where we have changed integration variables to give an expression in terms of overlaps on scale $Q = 0$ only, and where

$$(\vec{M})_{n\in C_0} \equiv \int d^d x\ \phi^*(x-n)\hat{M}\phi(x). \tag{121}$$

Now, to determine $\vec{M}$ in terms of the two-scale coefficients, we generate a recursion by using the two-scale relation to write $\phi(x)$ as a sum of scaling functions from scale $Q = 1$ and then using (120) to re-express the resulting set of overlaps back in terms of $\vec{M}$,

$$\begin{aligned} (\vec{M})_{p\in C_0} &\equiv \int d^d x\ \phi^*(x-p)\hat{M}\phi(x) \\ &= \int d^d x\ \left(\sum_{m\in C_0} c_m^*\phi^*(2(x-p)-m)\right)\hat{M}\left(\sum_{n\in C_0} c_n\phi(2x-n)\right) \\ &= \sum_{m,n\in C_0} c_m^* c_n 2^{h-d}\vec{M}_{2p+m-n}, \end{aligned}$$

which can be rearranged as

$$2^{-h}(\vec{M})_{p\in C_0} = \sum_{q\in C_0}\left(2^{-d}\sum_{n\in C_0} c_{q-2p+n}^* c_n\right)(\vec{M})_q.$$

Thus, for each homogeneous operator of order h for which the vector of matrix elements $\vec{M}$ is well-defined, $\vec{M}$ is an eigenvector of eigenvalue $\lambda = 2^{-h}$ of the two-scale matrix

$$\tilde{M}_{pq} \equiv 2^{-d}\sum_{n\in C_0} c_{q-2p+n}^* c_n. \tag{122}$$

We therefore expect the eigenspectrum of $\tilde{M}$ to consist of clusters of degenerate eigenvalues of value 2^{-h}, with degeneracies equal to the dimensionality of the space of operators of order h and with eigenvectors containing the overlaps for h^{th} order operators.

Determining the overlaps for a specific operator requires additional information in order to select the appropriate vector from the corresponding degenerate subspace of $\tilde{M}$. In the case of interpolating cardinal scaling functions this information comes from the integral normalization of the scaling functions (110) and the interpolation condition (107). To ensure that a given eigenvector represents the correct operator, we verify the values of the multinomial coefficients using the extraction formula (119),

$$\begin{aligned} m_{\{h_j\}} &= \int d^d x\, \mathcal{I}^*(x)\, m_{\{h_j\}} \\ &= \int d^d x\, \mathcal{I}^*(x) \cdot \frac{\hat{M}(\prod_j x_j^{h_j})}{\prod_j h_j!} \\ &= \int d^d x\, \mathcal{I}^*(x) \cdot \frac{1}{\prod_j h_j!} \hat{M} \left(\sum_n \left(\prod_j n_j^{h_j} \right) \mathcal{I}(x-n) \right) \\ &= \sum_n \left(\prod_j \frac{n_j^{h_j}}{h_j!} \right) (\vec{M})_{-n}. \end{aligned} \tag{123}$$

Thus, to determine the vector of overlaps $\vec{M}$ for an operator of order h with coefficients $m_{\{h_j\}}$ one simply forms the linear combination of eigenvectors of (122) with eigenvalue 2^{-h} that satisfies the conditions (123). Because the space of such vectors has one dimension for each multinomial condition in (123), this completely determines the vector $\vec{M}$.

V-C.3 Real-space values

Two approaches are available to compute the values of the interpolets in real space from their two-scale coefficients c_n. The traditional approach, appropriate for any type of scaling function, is to note that the two-scale relation (58), when evaluated at the points $x \equiv m/2^{P+1}$ in C_{P+1}, gives

$$\phi(m/2^{P+1}) = \sum_{n \in C_0} c_n \phi((m - 2^P n)/2^P), \tag{124}$$

a direct formula for the values $\phi(C_{P+1})$ in terms of the values $\phi(C_P)$. Using this, one may proceed iteratively to compute the $\phi(C_Q)$ at any desired level of resolution. To determine the values $\phi(C_0)$ needed to initialize the process, one may generate a self-consistency relation by evaluating the two-scale relation (58) on the points $x = m$ of C_0,

$$\begin{aligned} \phi(m) &= \sum_{n \in C_0} c_n \phi(2m - n) \\ &= \sum_{q \in C_0} c_{2m-q} \phi(q). \end{aligned}$$

The sequence $\phi(C_0)$ thus may be identified as the eigenvector with eigenvalue unity of the matrix $\tilde{C}_{mq} \equiv c_{2m-q}$. For cardinal scaling functions, of course, the cardinality condition (102) prescribes explicitly that the $\mathcal{I}(C_0)$ be a discrete Kronecker δ-function centered on the origin.

For cardinal scaling functions, a more convenient approach exists which does not make large strides through the data-set as does (124). Because $V_0 \subset V_P$, $\mathcal{I}(x)$ may be written exactly in terms of scaling functions on scale P. Moreover, from the interpolation property (106), the proper linear

combination for doing this is just

$$\mathcal{I}(x) = \sum_{p \in C_P} \mathcal{I}(p)\mathcal{I}(2^P(x-p)). \tag{125}$$

Letting $p = m/2^P$, evaluating this relation on the points $x = n/2^{P+1}$ where $n \in C_0$, and using (104) to relate the values $\mathcal{I}(C_1)$ to the c_n gives

$$\mathcal{I}(n/2^{P+1}) \;=\; \sum_{m \in C_0} c_{n-2m}\mathcal{I}(m/2^P), \tag{126}$$

which again may be used iteratively to generate any $\mathcal{I}(C_Q)$ from the known values $\mathcal{I}(C_0)$. A variant of this approach exists for orthonormal functions and is described in [Dau92, Ch. 6.5].

V-C.4 Examples

The simplest interpolating cardinal scaling function we shall consider is the first-order interpolet in one dimension. For $l = 1$ and $d = 1$, the conditions (114,115) on the two-scale symbol are just $m_0(0) = 1$, $m_0(\pi) = 0$ and $m_0'(0) = m_0'(\pi) = 0$. The general appearance of such a function (Figure 12) leads quickly to the *ansatz*, which may be easily verified, that the choice $m_0(q) = \cos^2(2q) = (1 + \cos(q))/2$ satisfies these conditions. From this two-scale symbol, we have immediately the two scale coefficients are $c_0 = 1$, $c_{\pm 1} = 1/2$, and $c_n = 0$ for $|n| > 1$, as listed in Table 1.

Using (126) to compute the real-space values of $\mathcal{I}(x)$, we see that for this interpolet the value on each detail point of D_{P+1} is given simply by the average of the values on the neighboring points of C_P. Using the notation $\{p\}$ to indicate a complete shell of points related by cubic symmetry, so that simply $\{p\} = \pm p$ in this one-dimensional case, Table 1 gives the results of this process. As evident from the table, this first-order interpolating function is the piece-wise linear "triangle" scaling function sketched in Figure 8. Finally, Table 1 also lists the vectors of matrix elements $(\vec{M}^{\{h\}})_n$ computed according to the prescription (121) of the previous section. For the values with $n < 0$, note that $\vec{M}^{\{h\}}_{-n} = (-1)^h \vec{M}^{\{h\}}_n$ in this and all cases below.

Figure (13) illustrates the estimates $\tilde{f}_Q(x)$ for the function $f(x) = \sin(2\pi x)$ afforded by these first-order functions for scales $Q = 2$ and $Q = 3$. The bases for V_Q provide simple linear interpolation between the sample points $f(C_Q)$, and as required by the interpolation condition (107), clearly will reproduce exactly the constant and linear functions. As a quantitative illustration of the linear nature of this interpolation, Figure 14 shows on a logarithmic plot the root mean-square error in reproducing $\sin(2\pi x)$ as a function of the sampling rate 2^Q, as Q varies from one through eight. As expected for linear interpolation, to leading order, the error is second-order and the data fall along a line of slope -2 in the plot.

To construct higher-order interpolets, we note that in one dimension Eq. (105) ensures that the conditions on $m_0(q)$ at $q = \pi$ will be satisfied automatically whenever the conditions (114) at $q = 0$ are satisfied. In terms of the two-scale coefficients, these latter conditions are

$$\frac{1}{2}\sum_n n^\alpha c_n = \delta_{\alpha,0} \quad \text{for } 0 \le \alpha \le l. \tag{127}$$

For second-order scaling functions this gives three independent linear equations,

$$\begin{aligned} c_{-1} + 1 + c_1 + c_3 &= 2 \\ -c_{-1} + c_1 + 3c_3 &= 0 \\ c_{-1} + c_1 + 3^2 c_3 &= 0. \end{aligned}$$

n	0	$\{1\}$
c_n	1	$\frac{1}{2}$

x	0	$\{\frac{1}{4}\}$	$\{\frac{1}{2}\}$	$\{\frac{3}{4}\}$	$\{1\}$
$\mathcal{I}(C_0)$	1				0
$\mathcal{I}(D_1)$			$\frac{1}{2}$		
$\mathcal{I}(D_2)$		$\frac{3}{4}$		$\frac{1}{4}$	
$\mathcal{I}(C_2)$	1	$\frac{3}{4}$	$\frac{1}{2}$	$\frac{1}{4}$	0

n	0	1
$\vec{M}^{\{0\}}$	$\frac{2}{3}$	$\frac{1}{6}$
$\vec{M}^{\{1\}}$	0	$\frac{1}{2}$
$\vec{M}^{\{2\}}$	-2	1

Table 1: First-order interpolating cardinal scaling function in one dimension: non-zero two-scale coefficients (c_n), function values ($\mathcal{I}$), and overlaps of $\partial^h/\partial x^h$ ($M_n^{\{h\}}$, as defined in (121)).

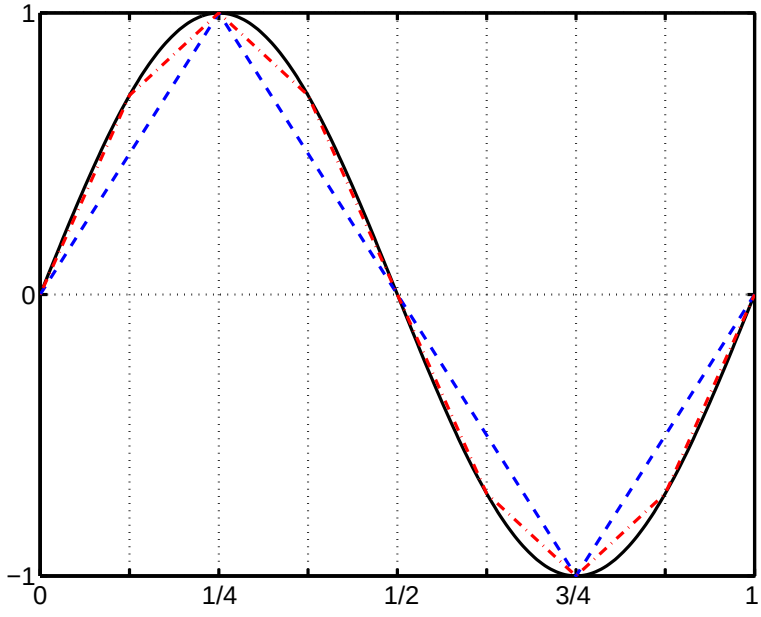

Figure 13: Interpolation with first-order interpolating scaling functions: $\sin(2\pi x)$ (solid curve), representation in V_2 and V_3 (dashed and dot-dashed curves, respectively).

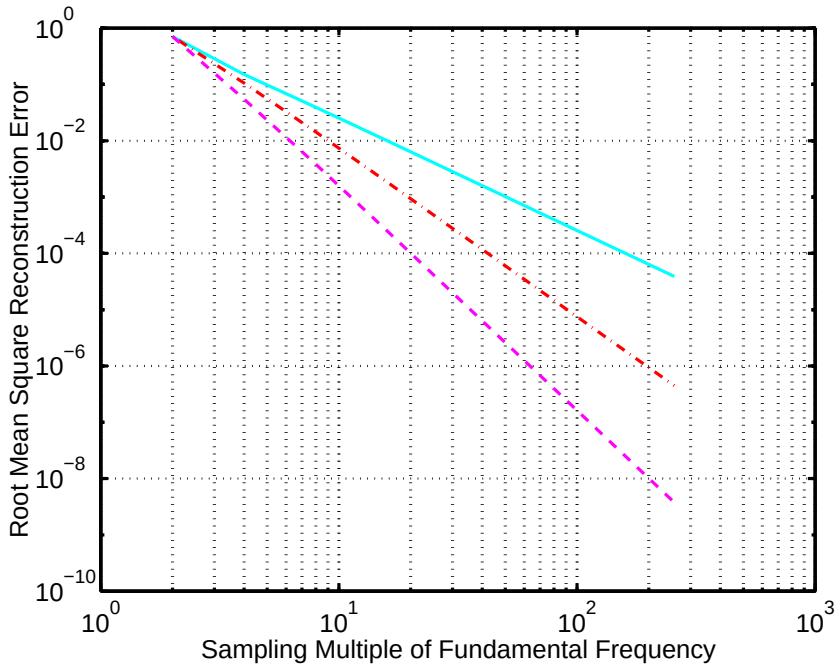

Figure 14: Root mean square error in reconstructing the sine function as a function of the number of samples per period: first- (solid line), second- (dash-dotted line) and third- (dashed line) order interpolating scaling functions, exhibiting exponents of -2, -3 and -4, respectively.

n	-1	0	1	3
c_n	$\frac{3}{8}$	1	$\frac{3}{4}$	$-\frac{1}{8}$

x	-1	$-\frac{1}{2}$	0	$\frac{1}{2}$	1	$\frac{3}{2}$	2	$\frac{5}{2}$	3
$\mathcal{I}(C_1)$	0	$\frac{3}{8}$	1	$\frac{3}{4}$	0	$-\frac{1}{8}$	0	0	0

n	0	1	2	3
$\vec{M}^{\{0\}}$	$\frac{247}{295}$	$\frac{517}{4720}$	$-\frac{17}{590}$	$\frac{3}{4720}$
$\vec{M}^{\{1\}}$	0	$\frac{11}{16}$	$-\frac{1}{10}$	$\frac{1}{240}$
$\vec{M}^{\{2\}}$	$-\frac{30}{11}$	$\frac{397}{264}$	$-\frac{5}{33}$	$\frac{1}{88}$

Table 2: Second-order interpolet in one dimension: non-zero two-scale coefficients (c_n), function values ($\mathcal{I}$), and overlaps of $\partial^h/\partial x^h$ ($M_n^{\{h\}}$, as defined in (121)).

n	0	$\{1\}$	$\{3\}$
c_n	1	$\frac{9}{16}$	$-\frac{1}{16}$

x	0	$\{\frac{1}{2}\}$	$\{1\}$	$\{\frac{3}{2}\}$	$\{2\}$	$\{\frac{5}{2}\}$	$\{3\}$
$\mathcal{I}(C_1)$	1	$\frac{9}{16}$	0	$-\frac{1}{16}$	0	0	0

n	0	1	2	3	4	5
$\vec{M}^{\{0\}}$	$\frac{56264}{70245}$	$\frac{19253}{140490}$	$-\frac{2827}{70245}$	$\frac{6283}{2247840}$	$-\frac{16}{210735}$	$-\frac{1}{6743520}$
$\vec{M}^{\{1\}}$	0	$\frac{3659}{5280}$	$-\frac{731}{6930}$	$\frac{481}{73920}$	$-\frac{4}{10395}$	$-\frac{1}{665280}$
$\vec{M}^{\{2\}}$	$-\frac{20}{9}$	$\frac{9}{8}$	0	$-\frac{1}{72}$	0	0

Table 3: Third order interpolating cardinal scaling function in one dimension: non-zero two-scale coefficients (c_n), function values ($\mathcal{I}$), and overlaps of $\partial^h/\partial x^h$ ($M_n^{\{h\}}$, as defined in (121)).

Table 2 lists the two-scale coefficients which solve this system and the values of the corresponding scaling function on the points of C_1. Figure 15 shows the appearance of the second-order interpolet in real-space. The asymmetry of the function is a direct result of the lack of symmetry in the sequence c_n. Figure 14 shows the reconstruction of the sine function for these interpolets also. The reconstruction is correct to second order and the leading-order error is third-order, as expected.

The final function we consider in one dimension is the third-order interpolet, which was used in the calculations in [ACLT95, Ari95, LAE98] to produce the results shown in Figures 1, 2, 3 and 5. For odd orders of interpolation, the odd-order conditions from (127) are always equivalent to the condition that the interpolet be symmetric, $c_n = c_{-n}$. The remaining conditions for the third-order case are just

$$\begin{aligned} c_1 + c_3 &= \frac{1}{2} \\ c_1 + 9c_3 &= 0 \end{aligned}$$

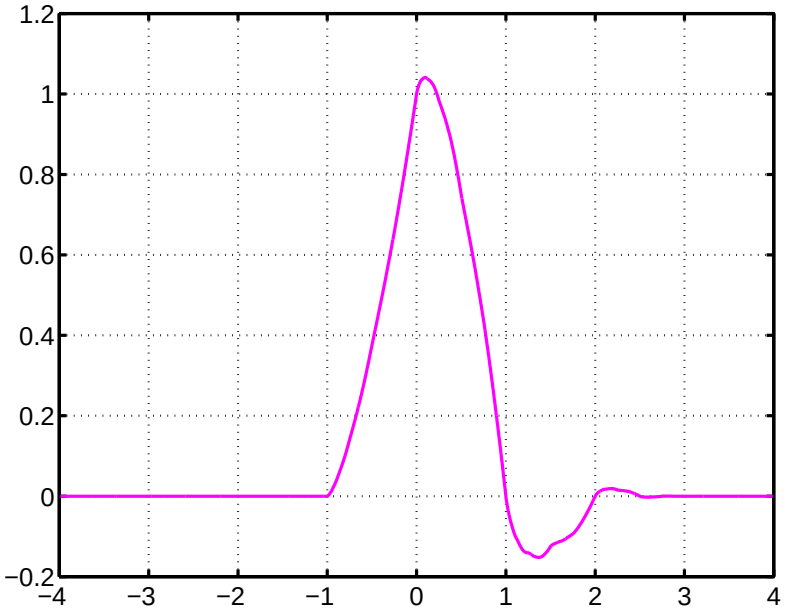

Figure 15: Second-order interpolet in one dimension.

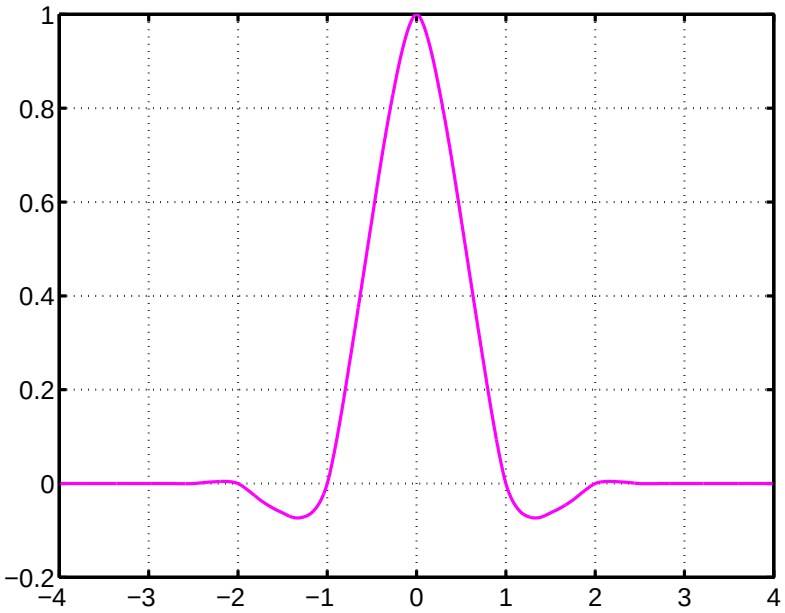

Figure 16: Third-order interpolet in one dimension.

n	000	{001}	{011}	{111}
c_n	1	$\frac{1}{2}$	$\frac{1}{4}$	$\frac{1}{8}$

Table 4: Two-scale coefficients for first-order interpolating cardinal scaling function in $d = 3$ dimensions (product form).

n	{000}	{001}	{011}	{111}	{003}	{013}	{113}	{033}	{133}	{333}
c_n (3d)	1	$\frac{9}{16}$	$\frac{5}{16}$	$\frac{11}{64}$	$-\frac{1}{16}$	$-\frac{1}{32}$	$-\frac{1}{64}$	0	0	0
c_n (pd)	1	$\frac{9}{16}$	$\frac{81}{256}$	$\frac{729}{4096}$	$-\frac{1}{16}$	$-\frac{9}{256}$	$-\frac{81}{4096}$	$\frac{1}{256}$	$\frac{9}{4096}$	$-\frac{1}{4096}$

Table 5: Two-scale coefficients for third-order interpolating cardinal scaling functions in $d = 3$ dimensions: full $d = 3$-dimensional construction (3d), product form (pd).

Table 3 gives the resulting two-scale coefficients, function values on C_1, and vectors of matrix elements for homogeneous integral-differential operators. Figure 16 shows the function in real space, and Figure 14 shows that the leading error in reconstructing the sine function has the expected fourth-order behavior. In one dimension, for each odd order, the minimally supported interpolets are just the scaling functions of Deslauriers Dubuc [DD89].

In higher dimensions, the simplest way to construct interpolets is to take the two-scale symbol to be an outer product $m_0(q) \equiv \prod_{i=1}^{d} m_0^{(1)}(q_i)$ of the two-scale symbol $m_0^{(1)}(q)$ for the one-dimensional interpolet of the corresponding order. The conditions (114,115) then factor into d separate one-dimensional conditions such that if $m_0^{(1)}(q)$ is taken as the two-scale symbol for an l^{th}-order interpolet in one dimension, $m_0(q)$ will be the two-scale symbol for an l^{th}-order interpolet in d dimensions. Because the two-scale coefficients are the Fourier series coefficients of $m_0(q)$, the two-scale coefficients for the d-dimensional interpolet are the outer product of those for the generating one-dimensional interpolet, $c_n \equiv \prod_{i=1}^{d} c_{n_i}^{(1)}$. Finally, from the two-scale relation (113), the scaling function corresponding to $m_0(q)$ is just the outer product of the one-dimensional generating interpolet, $\mathcal{I}(x) \equiv \prod_{i=1}^{d} \mathcal{I}^{(1)}(x_i)$. As an example, Table 4 gives the two-scale coefficients for the first-order interpolet in $d = 3$ dimensions.

Although the outer-product prescription may always be used to generate higher-dimensional interpolets of very simple form, the resulting functions are generally not as compact as possible. To illustrate the fact that working in a full three-dimensional framework can generate more compact functions, we conclude this section by constructing a third-order interpolet in $d = 3$ dimensions which is *not* an outer product of three one-dimensional functions.

For the third-order interpolet in three dimensions, Eqs. (114,115) represent a total of eighty linear conditions on the two-scale coefficients. Considering functions with full cubic symmetry reduces this to just seven conditions, as we now show. The reflection symmetries about the coordinate planes, $c_{n_1,n_2,n_3} = c_{\pm n_1,\pm n_2,\pm n_3}$, ensure that the first- and third-order conditions, as well as the conditions for the off-diagonal second-order multinomials x_1x_2, x_1x_3 and x_2x_3, from (107) are all satisfied, leaving only the zeroth-order condition and the three diagonal second-order conditions, x_1^2, x_2^2 and x_3^2. This set of four conditions has implications for $m_0(q)$ at $q = 0$ and the seven points $\pi\eta_i$. By the permutation symmetries, among these eight total sets of implications, only those for η at (000), (001), (011), (111) need be enforced explicitly. The cardinality condition (105), moreover,

implies that one of these sets is redundant, so that we need not impose the conditions at (011). The zeroth order conditions at the three remaining points appear as the first three conditions in (128). For the diagonal second-order conditions, symmetry renders the three conditions at each of the two points (000), (111) equivalent. One condition from each of these points appears in (128). At the final point, (001), the conditions for x_1^2 and x_2^2 are also equivalent, and so only one of these appears in (128). Finally, the x_3^2 condition at (001) makes up the last of the seven conditions in

$$A \begin{pmatrix} c_{\{000\}} \\ c_{\{001\}} \\ c_{\{011\}} \\ c_{\{111\}} \\ c_{\{003\}} \\ c_{\{013\}} \\ c_{\{113\}} \end{pmatrix} = \begin{pmatrix} 1 \\ 0 \\ 0 \\ 0 \\ 0 \\ 0 \\ 0 \end{pmatrix}, \tag{128}$$

where

$$A \equiv \begin{pmatrix} 1 & 6 & 12 & 8 & 6 & 24 & 24 \\ 1 & 2 & -4 & -8 & 2 & -8 & -24 \\ 1 & -6 & 12 & -8 & -6 & 24 & -24 \\ 0 & 2 & 8 & 8 & 18 & 80 & 88 \\ 0 & -2 & -8 & -8 & -18 & -80 & -88 \\ 0 & 2 & 0 & -8 & 18 & 0 & -88 \\ 0 & -2 & 8 & -8 & -18 & 80 & -88 \end{pmatrix}.$$

Table 5 gives the resulting coefficients along with the coefficients for the outer product of three one-dimensional, $l = 3$ interpolets. Figure 17 illustrates the more compact nature of the result of the three-dimensional construction by comparing the supports of the two functions in the $x_3 = 0$ plane. The three-dimensional volume of the support of the new function is smaller than that of the product form by a factor of two. Finally, Figure 18 shows the appearance of the new function in the $x_3 = 0$ coordinate plane as computed from the recursion (126).

VI Multilevel Methods

As Section V-B.2 discusses, the direct approach of applying the linear operators $\mathcal{I}$, $\mathcal{J}$, $\mathcal{I}^\dagger$, $\mathcal{J}^\dagger$, $\mathcal{O}$, L by multiplying by the corresponding matrices is relatively costly, requiring thousands of operations per coefficient in the restricted multiresolution analyses typical in the calculation of electronic structure. For *unrestricted* multiresolution analyses, more methods more efficient than direct matrix multiplication exist which exploit the structure imposed by the two-scale relation to expend only $O(1)$ floating point operations per expansion coefficient. Many of these methods, however, process information on the unrestricted grid and, thus, in a restricted multiresolution analysis of n_r functions will expend $O(n/n_r)$ floating point operations per expansion coefficient, where n is the number of points in the unrestricted multiresolution analysis. For all-electron calculations, $n/n_r \geq 10^4$, and these approaches are also extremely inefficient.

The recent resolution of this problem has been to find new methods which require only $O(1)$ operations per coefficient but which give results which are *unchanged* when ignoring the $n - n_r$ coefficients associated with functions removed in the restriction of the multiresolution analysis. These methods then attain the goal of expending only $O(n_r)$ operations in a restricted multiresolution analysis of n_r basis functions. We refer to such methods as *restrictable*.

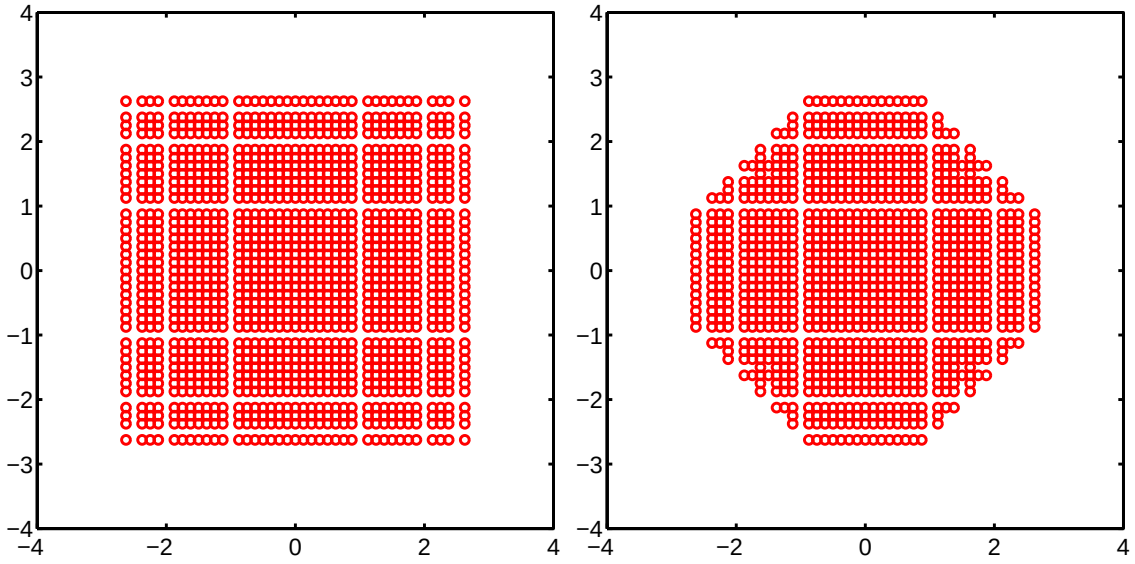

Figure 17: Support in $x_3 = 0$ plane of $d = 3$-dimensional third-order interpolets: product form (left), three-dimensional construction (right).

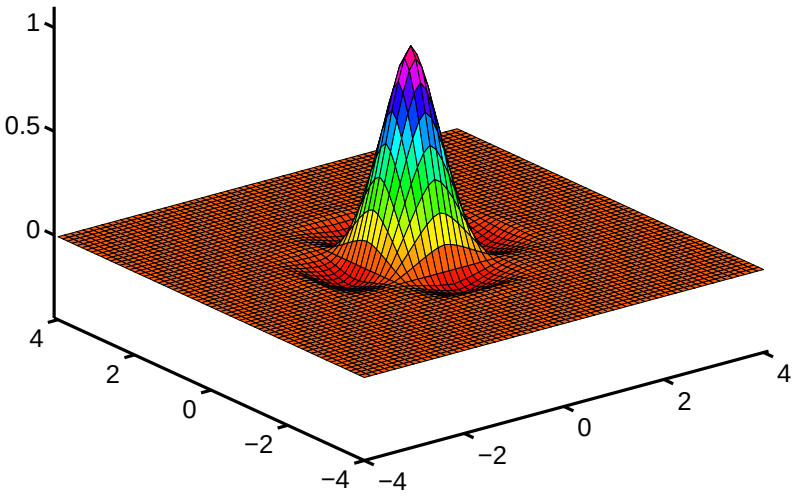

Figure 18: Minimally supported $d = 3$ third-order interpolet in the $x_3 = 0$ plane.

This section reviews the approaches used in the calculation of electronic structure, which included both unrestrictable[WC96, TW97] and restrictable[BCR91, LAE98] methods. For clarity of presentation, we consider in this section only operations in *unrestricted* multiresolution analyses, and dedicate Section VII specifically to the effects of restriction.

VI-A Transforms: $\mathcal{I}$, $\mathcal{I}^\dagger$, $\mathcal{J}$, $\mathcal{J}^\dagger$

VI-A.1 General and orthonormal bases

VI-A.1(a) Forward transform The forward transform of Sec. III-C.1 converts the multiscale expansion coefficients $\vec{F}_{N:M}$ into the values of the function on a set of points in real-space. In a multiresolution analysis, the product $\mathcal{I}_{N:M}\vec{F}_{N:M}$ gives the coefficients $\vec{F}_N$ of the single-scale expansion of the function in V_N. The values of the function on the points p of the real-space grid G are then

$$(\vec{f})_p = \sum_{\alpha \in C_N} \phi(2^N(p-\alpha))(\mathcal{I}_{N:M}\vec{F}_{N:M})_\alpha,$$

or in matrix language,

$$\vec{f} = \Phi\mathcal{I}_{N:M}F_{N:M},$$

where $\Phi_{p\alpha} \equiv \phi(2^N(p-\alpha))$. The forward transform operator $\mathcal{I}$ of (10) is thus

$$\mathcal{I} = \Phi\mathcal{I}_{N:M}. \tag{129}$$

In general, the invariance of the single-scale basis for V_N under the translations of the lattice C_N means that multiplication by the matrix Φ takes the form of a convolution. Multiplication by Φ may thus be carried out using fast Fourier transform techniques with approximately $10\,n\log_2 n$ floating-point operations[Dau92, WC96]. Alternately, when the $\phi(x)$ are products of one-dimensional functions, Φ may be factored into one-dimensional convolutions along each of the coordinate directions, which expend a total of $d(\text{Vol supp }\phi(x))^{1/d}\,n$ operations where d is the dimension of space and Vol supp $\phi(x)$ is the volume of the region of space over which the function $\phi(x)$ is non-zero. For multiresolution analyses with cardinal scaling functions (both semicardinal bases[ACLT95, Yes97] and lifted bases[GI98]), multiplication by Φ is far simpler: cardinality of the scaling functions implies $\Phi = I$, where I is the identity.

Figure 19 illustrates the flow of information corresponding to each factor $\mathcal{I}_{P+1,P}$ in the definition (81) of $\mathcal{I}_{N:M}$. The circles of the upper and lower rows represent coefficients of the multiscale expansions $\vec{F}_{N:P}$ and $\vec{F}_{N:P+1}$, respectively. On the upper row, the larger and smaller open circles represent the coefficients for the scaling functions of scale P and detail functions of scale $P+1$, respectively, and the open circles on the lower row represent coefficients for the scaling functions of scale $P+1$. The filled circles on both rows represent coefficients from finer scales, which are unaffected by $\mathcal{I}_{P+1,P}$. The arrows represent the individual multiply-add operations in the application of $\mathcal{I}_{P+1,P}$ to compute $\vec{F}_{N:P+1} = \mathcal{I}_{P+1,P}\vec{F}_{N:P}$. Each arrow multiplies the expansion coefficient at its base by a constant factor and accumulates the result onto coefficient at its head. The factors which the arrows carry are the two-scale coefficients c_n and d_n, or unity in the case of the dotted arrows. Note that the coefficients $\vec{F}_{N:P+1}$ are taken to be zero before the accumulation begins. Also, for clarity, the figure shows only the connections associated with two-scale coefficients in the range $|n| \le 1$. Figure 20 illustrates, for three levels, the cascading data flow of (80) when the $\mathcal{I}_{P+1,P}$ string together to make the final multiscale operator $\mathcal{I}_{N:M}$.

The translational symmetry of the c_n and d_n coefficients, reflecting the invariance of the two-scale basis for $V_P \oplus W_{P+1}$ under the translations of C_P, implies that the data flow corresponding to

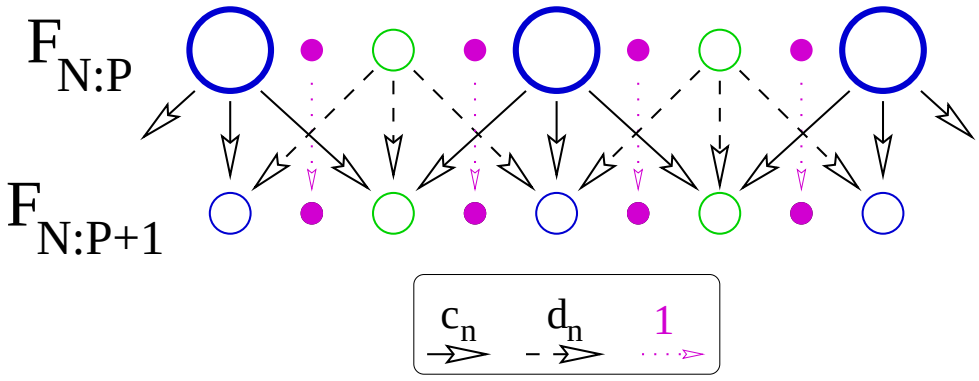

Figure 19: Information flow of the operation $F_{N:P+1} = \mathcal{I}_{P+1,P} F_{N:P}$ (general multiresolution analysis).

$\mathcal{I}_{P+1,P}$ takes the form of a set of convolutions, one for each scaling and detail function of the two-scale basis. As with Φ, these convolutions may be carried out using Fourier transform techniques, or, in the case of product basis functions, factored into sets of one dimensional convolutions along the coordinate directions and treated all at once[Dau92, Ch. 10].

VI-A.1(b) Conjugate forward transform The conjugate forward transform is

$$\mathcal{I}^\dagger = \mathcal{I}^\dagger_{N:M} \Phi^\dagger. \tag{130}$$

The implementation of this expression parallels that of (129). In the general case, $\Phi^\dagger$ is a convolution carried out as described above, and for the case of cardinal scaling functions, $\Phi^\dagger = I$. The component factors $\mathcal{I}^\dagger_{P+1,P}$ of $\mathcal{I}^\dagger_{N:M}$ are again invariant under the translations of C_P and may be either implemented with either Fourier techniques or, for product functions, factored into one-dimensional convolutions.

The information flow for multiplication by $\mathcal{I}^\dagger_{N:M}$ is again a cascade of two-scale connections $\mathcal{I}^\dagger_{P+1,P}$, but now in reverse order. Note that, when written in terms of components, the matrix multiplication $\vec{a} = M\vec{b}$ is $a_i = \sum_j m_{ij} b_j$, and multiplication by the Hermitian conjugate, $\vec{a} = M^\dagger \vec{b}$, is $a_j = \sum_i m^*_{ij} b_i$. This means that multiplication by the Hermitian conjugate simply reverses the direction of and conjugates the factors associated with the arrows. Figure 21 illustrates this information flow for one stage $\mathcal{I}^\dagger_{P+1,P}$ of the cascade for $\mathcal{I}^\dagger_{N:M}$.

VI-A.1(c) Inverse transform For general unrestricted multiresolution analysis and restricted semicardinal multiresolution analyses, the forward transform $\mathcal{I}$ is invertible, and we thus consider the case $\mathcal{J} \equiv \mathcal{I}^{-1}$. Then, the inverse transform is

$$\mathcal{J} = \mathcal{I}^{-1}_{N:M} \Phi^{-1}. \tag{131}$$

For orthonormal wavelets, the inverse convolution Φ^{-1} must be computed using Fourier techniques which require access to the unrestricted grid. The use of cardinal scaling functions removes this complication, for then simply $\Phi^{-1} = I$.

In multiresolution analysis, the condition (70) ensures that the two-scale components $\mathcal{I}^{-1}_{P+1,P}$ of the cascade for $\mathcal{I}^{-1}_{N:M}$ always exist as linear operators. The invariance of $\mathcal{I}_{P+1,P}$ under the

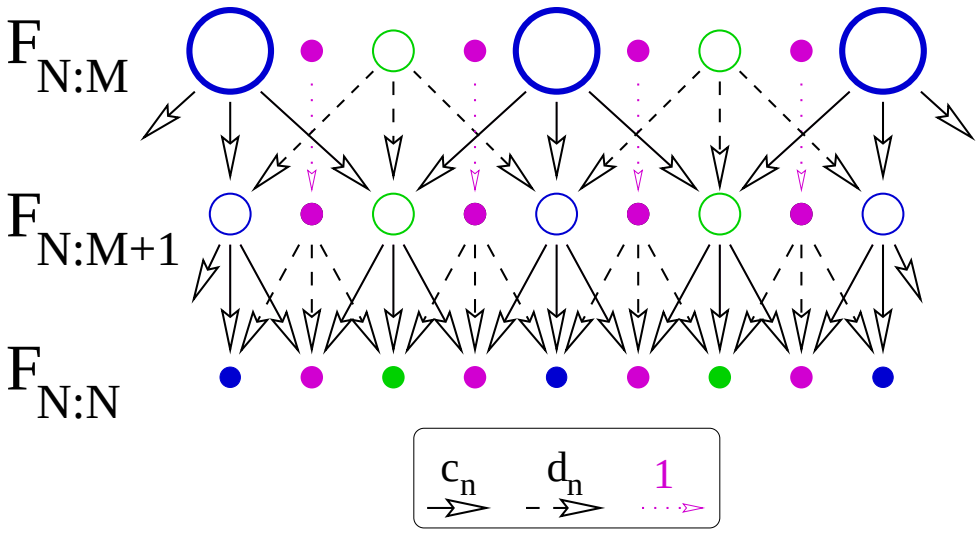

Figure 20: Information flow of the multiscale operation $F_{N:N} = \mathcal{I}_{N:M} F_{N:M}$ (general multiresolution analysis).

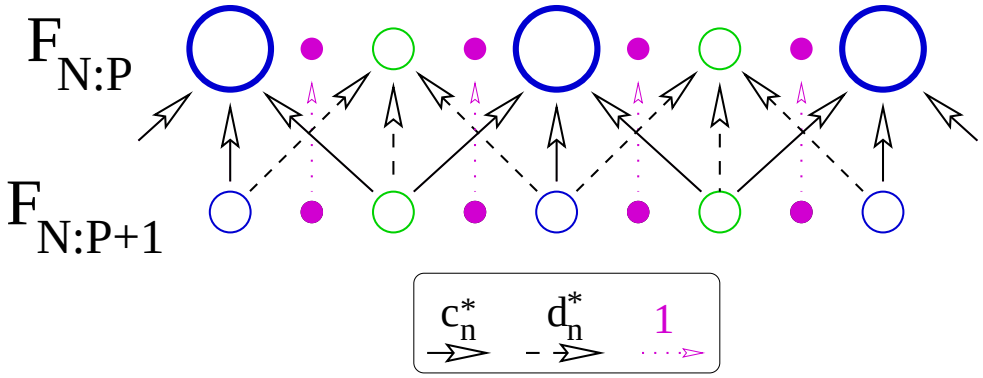

Figure 21: Information flow of the operation $F_{N:P} = \mathcal{I}^{\dagger}_{P+1,P} F_{N:P+1}$ (general multiresolution analysis).

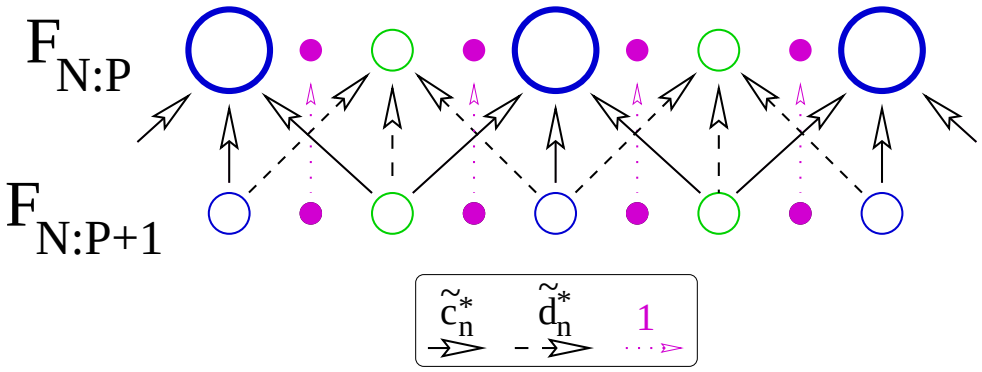

Figure 22: Information flow of the operation $F_{N:P} = \mathcal{I}_{P+1,P}^{-1} F_{N:P+1}$ (general multiresolution analysis).

translations of C_P ensures that the information flow for $\mathcal{I}_{P+1,P}^{-1}$ always takes the form of Figure 22 for some set of *dual coefficients* $\tilde{c}_n$ and $\tilde{d}_n$, defined by convention with the complex conjugation as labelled in the figure. For orthonormal wavelets $\mathcal{I}_{P+1,P}^{-1} = \mathcal{I}_{P+1,P}^{\dagger}$ so that, comparing Figures 21 and 22, the two-scale coefficients and their duals are identical. The dual coefficients also have a special structure in semicardinal bases, which we shall explore in Sec. VI-A.2.

VI-A.1(d) Conjugate inverse transform The remaining transform is the Hermitian conjugate of (131),

$$\mathcal{J}^{\dagger} = \mathcal{I}_{N:M}^{-\dagger} \Phi^{-\dagger}, \tag{132}$$

where for any invertible matrix, $A^{-\dagger} \equiv (A^{-1})^{\dagger} = (A^{\dagger})^{-1}$. In general, the operation $\Phi^{-\dagger}$ may be implemented either by inverting the convolution associated with $\Phi^{\dagger}$ with Fourier techniques. Again, cardinal scaling functions are much simpler and give just $\Phi^{\dagger} = I$. The operations of the cascade for $\mathcal{I}_{N:M}^{-\dagger}$ are obtained by complex conjugation and reversal of the flow of Figure 22. As may be seen from Figure 23, the convention for the definition of the dual coefficients has been established to ensure that the conjugate inverse transform is just the forward transform associated with the dual coefficients. In the orthonormal case, where the coefficients and their duals are the same, this represents the expected result that the conjugate inverse and forward transforms are the same. The next section discusses the form for the $\mathcal{I}_{P+1,P}^{-\dagger}$ in semicardinal bases.

VI-A.2 Semicardinal bases

As we saw in the preceding section, orthonormal bases have the advantage that the *dual* coefficients appearing in the inverse transforms are identical to the two-scale coefficients of the forward transform. The disadvantage is that access to the unrestricted grid of finest resolution is needed to implement the inverse convolutions Φ^{-1} and $\Phi^{-\dagger}$. Because these later operations are trivial for bases with cardinal scaling functions, semicardinal bases will have a great advantage provided the dual coefficients needed for the inverse transforms are simple in form, as we now verify.

The particularly simple form for the dual coefficients for semicardinal multiresolution analyses arises from the structure of the $\mathcal{I}_{P+1,P}$. To elucidate this structure, we analyze $\mathcal{I}_{P+1,P}$ into its effects on different scales, $\mathcal{I}_{P+1,P} = (\mathcal{P}_{C_{P+1}} + \mathcal{P}_{B_{P+1}}) \mathcal{I}_{P+1,P} (\mathcal{P}_{C_{P+1}} + \mathcal{P}_{B_{P+1}})$, where B_{P+1} is the

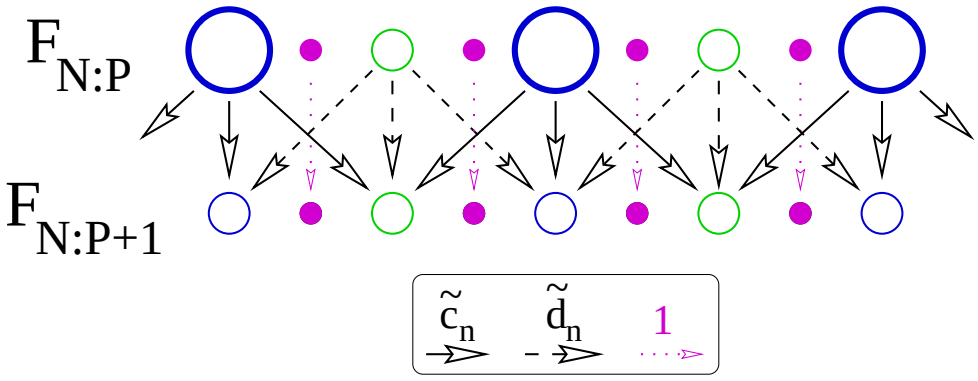

Figure 23: Information flow of the operation $F_{N:P+1} = \mathcal{I}^{-\dagger}_{P+1,P} F_{N:P}$ (general multiresolution analysis).

set of points on scales *beyond* $P+1$ as defined in (56). Because $\mathcal{I}_{P+1,P}$ does not affect functions beyond scale $P+1$, we may use (86) to simplify this to $\mathcal{I}_{P+1,P} = \mathcal{P}_{B_{P+1}} + \mathcal{P}_{C_{P+1}} \mathcal{I}_{P+1,P} \mathcal{P}_{C_{P+1}}$. Next, according to (92), the fact that the two-scale basis for $V_P + W_{P+1}$ is semicardinal on the hierarchy $C_P \subset C_{P+1}$ gives $\mathcal{P}_{C_{P+1}} \mathcal{I}_{P+1,P} \mathcal{P}_{C_P} = \mathcal{P}_{C_P} + \mathcal{P}_{D_{P+1}} \mathcal{I}_{P+1,P} \mathcal{P}_{C_P}$ and $\mathcal{P}_{C_P} \mathcal{I}_{P+1,P} \mathcal{P}_{D_{P+1}} = \mathcal{P}_{D_{P+1}}$. Combining these results, we have

$$\begin{aligned} \mathcal{I}_{P+1,P} &= \mathcal{P}_{B_{P+1}} + ((\mathcal{P}_{C_P} + \mathcal{P}_{D_{P+1}} \mathcal{I}_{P+1,P} \mathcal{P}_{C_P}) + \mathcal{P}_{D_{P+1}}) \\ &= I + \mathcal{P}_{D_{P+1}} \mathcal{I}_{P+1,P} \mathcal{P}_{C_P}. \end{aligned} \tag{133}$$

As Figure 24a illustrates, this means that, apart from the simple copy operation I, the only effect of $\mathcal{I}_{P+1,P}$ in the semicardinal case is to add onto the detail points D_{P+1} information coming from the coarse points C_P.

The full forward transform, given this structure for $\mathcal{I}_{P+1,P}$ and the fact that $\Phi = I$, therefore is

$$\mathcal{I} = \prod_{P=N-1}^{M} \left(I + \mathcal{P}_{D_{P+1}} \mathcal{I}_{P+1,P} \mathcal{P}_{C_P} \right), \tag{134}$$

which corresponds to the following recursive algorithm for computing $f = \mathcal{I} F$,

$$\begin{aligned} F_{N:M} &\equiv F; \\ F_{N:P+1} &= F_{N:P} + \mathcal{P}_{D_{P+1}} \mathcal{I}_{P+1,P} \mathcal{P}_{C_P} F_{N:P}; \\ f &\equiv F_{N:N}. \end{aligned} \tag{135}$$

As we show in Sec. VII, this algorithm is *restrictable* and gives the same results even when completely ignoring points and coefficients eliminated in a restricted multiresolution analysis. Thus, with this approach, the forward transform is extremely efficient and may be computed with only Vol supp $\mathcal{I}(x)$, or $d(\text{Vol supp } \mathcal{I}(x))^{1/d}$ in the case of a product interpolet, operations per coefficient.

As described above, the conjugate to the forward transform (130) must simply reverse the direction of the information flow relative to Figure 24a. In product form, it is

$$\mathcal{I}^{\dagger} = \prod_{P=M}^{N-1} \left(I + \mathcal{P}_{C_P} \mathcal{I}^{\dagger}_{P+1,P} \mathcal{P}_{D_{P+1}} \right), \tag{136}$$

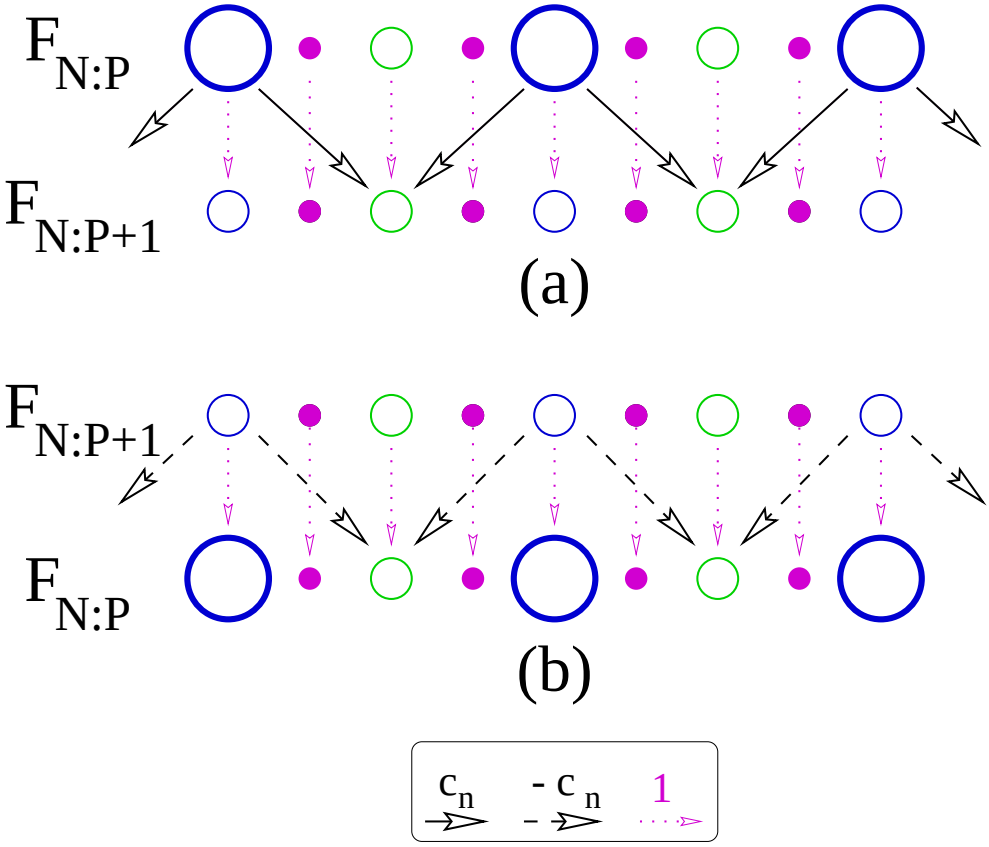

Figure 24: Information flow in a semicardinal basis: (a) forward transform, (b) inverse transform. (For respective conjugate transforms, conjugate and reverse the direction of the arrows.)

corresponding to the following algorithm for computing $F = \mathcal{I}^\dagger f$,

$$\begin{aligned} F_{N:N} &\equiv f; \\ F_{N:P} &= F_{N:P+1} + \mathcal{P}_{C_P}\mathcal{I}^\dagger_{P+1,P}\mathcal{P}_{D_{P+1}}F_{N:P+1}; \\ F &\equiv F_{N:M}. \end{aligned} \tag{137}$$

Despite the fact that information appears to flow in from missing points when reversing the arrows in Figure 24a, we show in the next section that this algorithm is also restrictable and thus also efficient in restricted multiresolution analyses.

Determining the dual coefficients needed to invert each stage $\mathcal{I}_{P+1,P}$ amounts to finding a prescription for undoing the effects of the forward transform. As Figure 24a shows, semicardinality ensures that the forward transform has no effect on the data sitting on the points of C_P, so that in the inverse transform too, these data may be left unmodified. The information flowing diagonally from the points of C_P in the forward transform, however, does corrupt the values on the points of D_P. Because the information which flowed along these links sits on the points of C_P at the start of the inverse transform, to determine the values originally sitting on D_P, one need only carry information along the same diagonal links but with coefficients the opposite sign. Figure 24b illustrates the resulting data flow for the inverse transform. Note that Figures 24a-b are constructed so that the entire diagram may be viewed from top to bottom as the process which first performs the forward transform and then inverts it. Note that, to accomplish this, the sequence of spaces in Figure 24b is reversed relative to that of the preceding diagrams.

Comparing Figure 24b with Figure 22 we see that in semicardinal multiresolution analyses, the dual coefficients are $\tilde{c}^*_n = d_n = \delta_{n0}$ and $\tilde{d}^*_n = 2d_n - c_n$. Expressed in our matrix language, Figure 24b represents

$$\mathcal{I}^{-1}_{P+1,P} = I - \mathcal{P}_{D_{P+1}}\mathcal{I}_{P+1,P}\mathcal{P}_{C_P}, \tag{138}$$

which may be verified algebraically by multiplication with (133) and use of the identity $\mathcal{P}_{C_P}\mathcal{P}_{D_{P+1}} = 0$. The full inverse transform is thus

$$\mathcal{J} \equiv \mathcal{I}^{-1} = \prod_{P=M}^{N-1} \left(I - \mathcal{P}_{D_{P+1}}\mathcal{I}_{P+1,P}\mathcal{P}_{C_P}\right), \tag{139}$$

which may be cast into a recursion to compute $F = \mathcal{J}f$:

$$\begin{aligned} F_{N:N} &\equiv f; \\ F_{N:P} &= F_{N:P+1} - \mathcal{P}_{D_{P+1}}\mathcal{I}_{P+1,P}\mathcal{P}_{C_P}F_{N:P+1}; \\ F &\equiv F_{N:M}. \end{aligned} \tag{140}$$

Section VII verifies that this inverse transform is also restrictable.

Finally, the conjugate inverse transform is

$$\mathcal{J}^\dagger = \prod_{P=N-1}^{M} \left(I - \mathcal{P}_{C_P}\mathcal{I}^\dagger_{P+1,P}\mathcal{P}_{D_{P+1}}\right), \tag{141}$$

which may be computed with the restrictable algorithm,

$$\begin{aligned} F_{N:M} &\equiv F; \\ F_{N:P+1} &= F_{N:P} - \mathcal{P}_{C_P}\mathcal{I}^\dagger_{P+1,P}\mathcal{P}_{D_{P+1}}F_{N:P}; \\ f &\equiv F_{N:N}, \end{aligned} \tag{142}$$

which simply reverses the direction of information flow from that of Figure 24b.

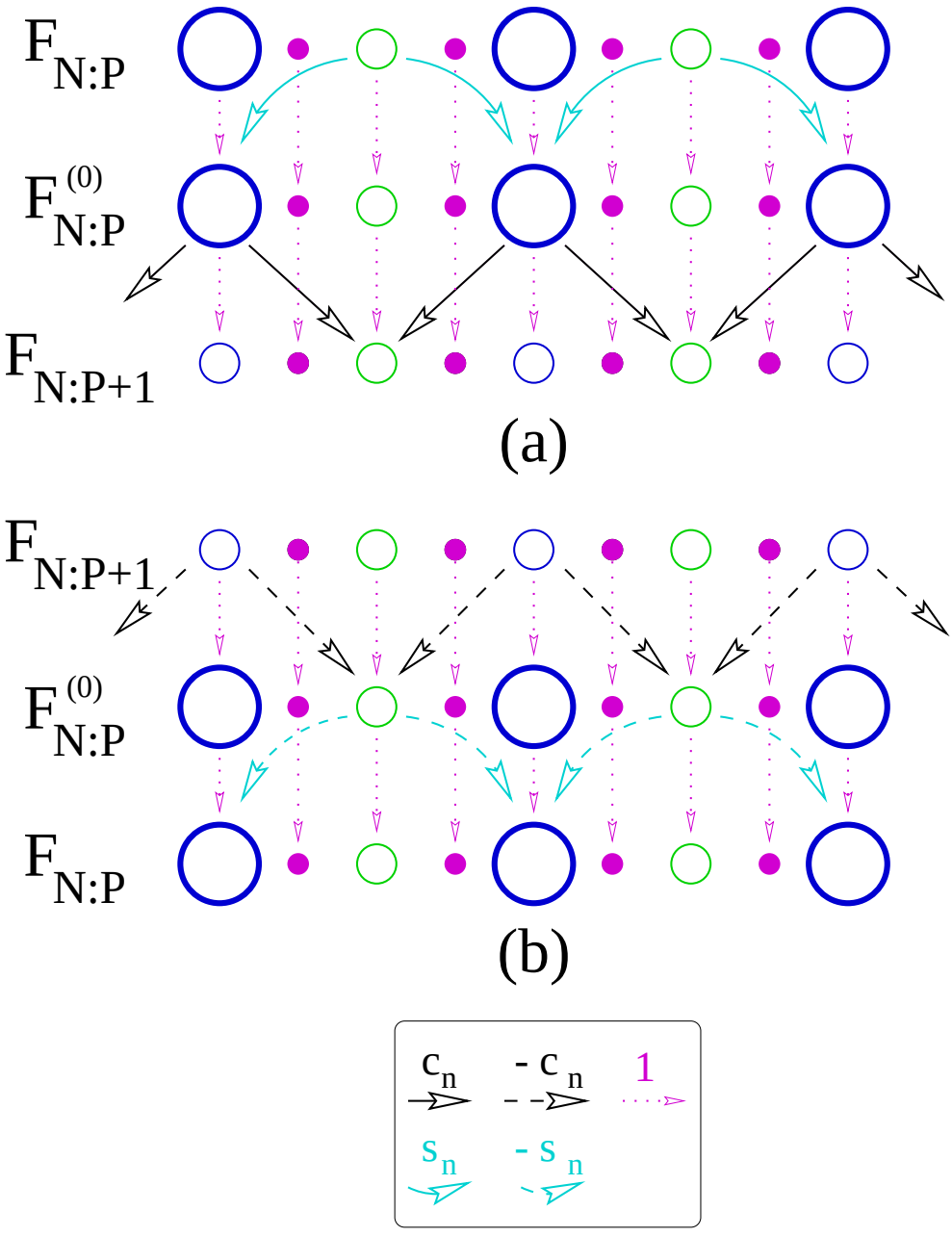

Figure 25: Information flow for a lifted semicardinal basis: (a) forward transform, (b) inverse transform. (For respective conjugate transforms, conjugate and reverse the direction of the arrows.)

VI-A.3 Lifted bases

We close this section with a brief consideration of bases constructed by lifting semicardinal bases through the scheme of [Swe96] as in [GI98]. In the lifting scheme, each detail function $\psi_\alpha(x)$ consists of an original un-lifted detail function $\psi^{(0)}_\alpha(x)$ plus an arbitrary linear combination of scaling functions from the next coarser scale,

$$\psi_\alpha(x - \eta_\alpha/2) \equiv \psi^{(0)}_\alpha(x - \eta_\alpha/2) + \sum_n s_{\alpha,n}\phi(x - n),$$

where the η_α are the decoration points on which the detail functions are centered. (See Eq. (74).) Although a non-zero choice for the coefficients $s_{\alpha,n}$ destroys semicardinality, these coefficients may be chosen to optimize the basis for other purposes. In [GI98], for instance, this combination is taken to produce detail functions with zero integral and zero multipole moments up to some order for use in solving Poisson's equation.

With detail functions of this form, each stage of the cascade for the full forward transform may then proceed in two phases: (1) the lifted multilevel description $F_{N:P}$ of the function is converted to the un-lifted representation $F^{(0)}_{N:P}$ by transferring the weights $s_{\alpha,n}$ from the detail functions of scale $P + 1$ to the scaling functions of scale P; (2) the un-lifted forward transform is carried out on $F^{(0)}_{N:P}$ to produce $F_{N:P+1}$. Figure 25a shows this two-stage process for the component operation $\mathcal{I}_{P+1,P}$ in the forward transform of a lifted a semicardinal basis. The conjugate forward transform just reverses this information flow and conjugates the factors carried by the arrows.

One may apply precisely the same logic as used in generating Figure 24b to invert each of these two stages in sequence to produce the lifted version of $\mathcal{I}^{-1}_{P+1,P}$. Figure 24b shows the resulting information flow. The conjugate to this inverse reverses the information flow and conjugates the factors carried by the arrows in the figure.

Finally, we note that to compute the full transforms, one cascades the above component operations according to (129-132) and uses the fact that, because the scaling functions remain the same, $\Phi = I$ is still true.

VI-B Operators: $\mathcal{O}$, $\mathcal{L}$

When working with *unrestricted* multiresolution analyses, the operation of multiplying by matrices of the form

$$\mathcal{M}_{\alpha\beta} \equiv \int d^d x\, b^*_\alpha(x)\hat{M}b_\beta(x), \tag{143}$$

where $\hat{M}$ is some integral-differential operator, is most easily performed in the finest single-scale representation (V_N) where the matrix elements are invariant under translations of the lattice C_N and thus represent a simple convolution. Substituting the construction formula

$$b_\alpha(x) \equiv \sum_{p\in C_N} (\mathcal{I}_{N:M})_{p\alpha}\phi\left(2^N(x - p)\right)$$

into (143) gives the overlaps in the multiresolution representation as

$$\mathcal{M} = \mathcal{I}^\dagger_{N:M} M \mathcal{I}_{N:M}, \tag{144}$$

where M is the single-scale overlap matrix M on the finest scale defined in (116) of Sec. V-C.2. This immediately gives an $O(n)$ method for applying $\mathcal{M}$, where n is the number of points on the finest grid C_N: transform to the single-scale representation on level N, apply the convolution M,

and transform back to the multiresolution representation with $\mathcal{I}^\dagger$. The main disadvantages of this approach, which is used in [WC96, TW97], are that (a) it is not restrictable and (b) it requires storage and processing of data on the unrestricted grid C_N.

The non-standard multiply approach of Beylkin, Coifman and Rokhlin[BCR91] provides one way of applying operators in multiresolution bases with linear computational effort while circumventing the need to work directly with the V_N representation. A more general approach[LAE98], which includes the non-standard multiply as one special case, is to follow the strategy which underlies Greengard and Rokhlin's fast multipole method[GR89]. The idea is to eliminate the redundancies inherent in the matrix elements of $\mathcal{M}$ by lumping information together into coarse and fine contributions. Only, rather than using multipole moments to summarize fine-scale information in an approximate way, one may exploit the two-scale relation to gather together the fine-scale overlaps *exactly*. And, rather than using Taylor series to summarize smooth information approximately, one may use the two-scale relation to represent smooth-scale information *exactly* in terms of coarse scaling functions. The remaining information on proximate scales then may be handled efficiently by direct, and thus also exact, multiplication.

To define precisely the separation into "fine," "proximate," and "smooth" contributions, we first decompose the operator $\mathcal{M}$ into contributions affecting the results on the different scales $M \le Q \le N$ of the multiresolution analysis,

$$\mathcal{M} = (\mathcal{P}_{C_M} + \ldots + \mathcal{P}_{D_Q} + \ldots + \mathcal{P}_{D_N})\mathcal{M}. \tag{145}$$

For a given term specified by its scale Q, there are contributions which originate from scales R which are either "proximate" ($|R-Q| < \ell$), "finer" ($R \ge Q+\ell$) or smoother ($R \le Q-\ell$), where ℓ is a measure of scale separation. Following this classification, for a given Q, we partition the set of all points in the multiresolution analysis as

$$C_N = S_Q \cup P_Q \cup F_Q. \tag{146}$$

Although the interpretation of S_Q, P_Q and F_Q is clear, the precise nature of these sets of points involves a variety of minor details as Q approaches the coarse and fine limits of the multiresolution analysis. In particular, when $Q-\ell < M$, all of the smoother grids (including C_M) are proximate and S_Q is empty. On the other hand, when $Q+\ell > N$, all of the finer contributions are proximate and F_Q is empty. An additional notational complication is the fact that the points on scale $Q = M$ are the lattice C_Q whereas the points on the finer scales $Q > M$ make up the detail crystals D_Q. To ease the burden of constantly making this distinction, we define

$$L_Q \equiv \begin{cases} C_Q & \text{if } Q = M \\ D_Q & \text{if } Q > M \end{cases},$$

as all points on the "level" Q. With these considerations, the precise definitions for S_Q, P_Q and F_Q are

$$\begin{aligned} S_Q &\equiv \begin{cases} \emptyset & \text{if } Q-\ell < M \\ C_{Q-\ell} & \text{if } Q-\ell \ge M \end{cases} \\ F_Q &\equiv \begin{cases} \emptyset & \text{if } Q+\ell > N \\ B_{Q+\ell-1} & \text{if } Q+\ell \le N \end{cases} \\ P_Q &\equiv C_N - S_Q - F_Q = \bigcup_{R=\max(M,Q-\ell)+1}^{\min(N,Q+\ell-1)} L_R, \end{aligned}$$

where $\emptyset$ is the empty set. With these definitions, the full decomposition of $\mathcal{M}$ is

$$\mathcal{M} = \sum_{Q=M}^{N} \mathcal{P}_{L_Q} \mathcal{M} (\mathcal{P}_{S_Q} + \mathcal{P}_{P_Q} + \mathcal{P}_{F_Q}) \tag{147}$$

Our discussion for the implementation of these various terms will be limited to the semicardinal case, which has been shown to be restrictable[LAE98], and so we return to the specialized notation $\mathcal{I}(x)$ for the scaling functions, in place of the generic $\phi(x)$.

To evaluate the proximate contributions we first define the *inter-scale matrices* of overlaps connecting the scaling functions of V_P with the scaling functions of V_R,

$$(M_{P,R})_{pr} = \begin{cases} \int d^d x \; \mathcal{I}^*(2^P(x-p)) \hat{M} \mathcal{I}(2^R(x-r)) & \text{if } p \in C_P \text{ and } r \in C_R \\ 0 & \text{otherwise} \end{cases} , \tag{148}$$

which, following the same argument which led to (144), take the form

$$M_{P,R} \equiv \mathcal{P}_{C_P} \mathcal{I}^\dagger_{N:P} M \mathcal{I}_{N:R} \mathcal{P}_{C_R}. \tag{149}$$

Note that the $M_{P,R}$ are invariant under the translations of the lattice $C_{\min(P,R)}$ and thus may be implemented as convolutions.

The proximate contributions all involve terms of the form $\mathcal{P}_{L_Q} \mathcal{M} \mathcal{P}_{L_R} \equiv \mathcal{P}_{L_Q} \mathcal{I}^\dagger M \mathcal{I} \mathcal{P}_{L_R}$. To simplify this expression, we use the identity

$$\mathcal{I}_{N:M} \mathcal{P}_{L_R} = \mathcal{I}_{N:R} \mathcal{P}_{L_R}, \tag{150}$$

which may be proven using (81,133). Alternately, Eq. (150) may been seen immediately as the algebraic statement that in a semicardinal multiresolution analysis the basis functions associated with the points p of scale R, whose values are the columns picked out of $\mathcal{I}_{N:M}$ by $\mathcal{P}_{L_R}$ on the left of (150), are just the scaling functions from the single-scale representation of scale R associated with the same points p. With (150), the proximate scale terms are just

$$\begin{aligned} \mathcal{P}_{L_Q} \mathcal{M} \mathcal{P}_{L_R} &= \mathcal{P}_{L_Q} \mathcal{I}^\dagger_{N:M} M \mathcal{I}_{N:M} \mathcal{P}_{L_R} \\ &= \mathcal{P}_{L_Q} \mathcal{P}_{C_Q} \mathcal{I}^\dagger_{N:Q} M \mathcal{I}_{N:R} \mathcal{P}_{C_R} \mathcal{P}_{L_R} \\ &= \mathcal{P}_{L_Q} M_{Q,R} \mathcal{P}_{L_R}, \end{aligned} \tag{151}$$

where on both sides of M in the second line we have used (150) and the fact that always $L_R \subset C_R$ so that $\mathcal{P}_{L_R} = \mathcal{P}_{C_R} \mathcal{P}_{L_R}$.

Unlike the stages of the transforms, the inter-scale matrices here used to apply operators do not convert one multiscale representation into another but rather link together different single-scale representations. We thus introduce a second useful diagrammatic representation for the coefficients of a multiresolution analysis. The horizontal rows of Figure 26 represent the scaling functions for each single-scale representation V_Q. The basis for a semicardinal multiresolution analysis consists of a subset of these functions and includes for each point only the scaling function of the coarsest scale containing that point. These scaling functions are indicated in the figure as filled circles. In practical implementations it is convenient to maintain data structures which include coefficients for the redundant scaling functions from finer scales, which are represented in the figure as open circles. We refer to this as the *redundant representation*. This redundant representation simplifies significantly the implementation of the $M_{Q,R}$ as convolutions and represents only a small increase in storage by a factor of $2^d/(2^d - 1)$, which is just $8/7$ in $d = 3$ dimensions. (See [LAE98].)

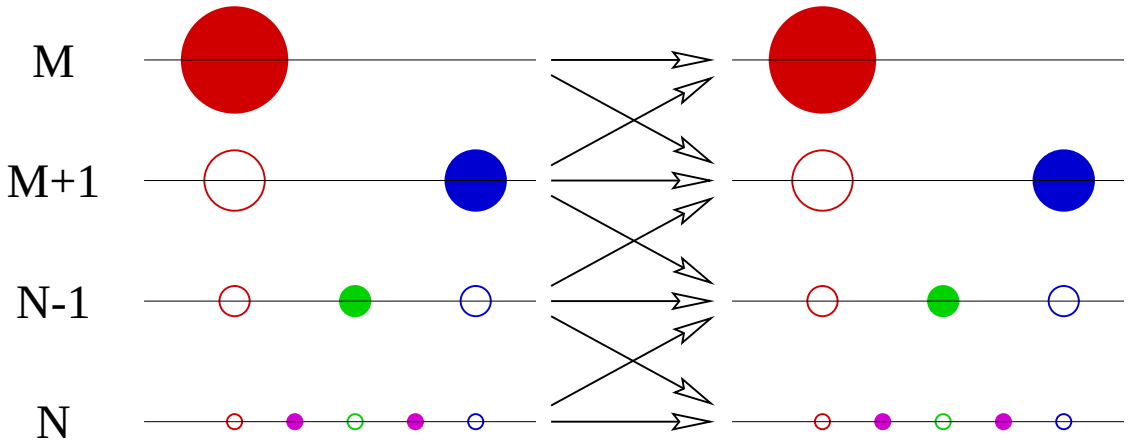

Figure 26: Information flow for proximate contributions to $\mathcal{M}$: inter-scale convolutions $M_{R,Q}$ (arrows).

The arrows in Figure 26 represent the calculation of the proximate contributions according to (147,151). The calculation begins with the coefficients of the vector to which the operator is applied residing on the left of the diagram and with all coefficients residing on the right being initialized to zero. Then, each arrow pointing from a level R on the left to a level Q on the right accumulates onto level Q the result of the convolution $M_{Q,R}$ applied to the information present on level R. Note that the factors $\mathcal{P}_{L_R}$ in (151) imply that the coefficients associated the redundant functions on the left of the figure should be set to zero before performing these convolutions. After the accumulation of the convolutions, the proximate contribution to $\mathcal{M}$ appears on the filled circles on the right side of the diagram. As with all diagrams in this section, the factors $\mathcal{P}_{L_Q}$ in (151) indicate that the final values computed on the empty circles are extraneous and simply may be ignored, or not computed at all.

Next, we turn to the smooth contributions, which need only be computed when $Q - \ell \geq M$. The basic strategy for these terms is to expand the smooth contributions exactly in terms of scaling functions on scale $Q - \ell$. To do this, note that with the expression (144) for $\mathcal{M}$ and the definition $S_Q \equiv C_{Q-\ell}$, $\mathcal{P}_{D_Q}\mathcal{M}\mathcal{P}_{S_Q}$ ends in a product of the form $\mathcal{I}_{N:M}\mathcal{P}_{S_Q} \equiv \mathcal{I}_{N:M}\mathcal{P}_{C_{Q-\ell}}$, which becomes

$$\mathcal{I}_{N:M}\mathcal{P}_{C_{Q-\ell}} \quad = \quad \mathcal{I}_{N:Q-\ell}(\mathcal{P}_{C_{Q-\ell}}\mathcal{I}_{N:M}), \tag{152}$$

after some manipulation of (134). The result (152) also may be seen immediately as the algebraic statement that in a semicardinal multiresolution analysis the multiscale basis functions from scale $Q - \ell$ or coarser, whose values appear in $\mathcal{I}_{N:M}\mathcal{P}_{C_{Q-\ell}}$, may be expanded exactly in the single-scale representation on level $Q - \ell$ with coefficients equal to the values of these basis functions at the corresponding points of $C_{Q-\ell}$. Using (150) on the left, (152) on the right, and the result (149), the smooth contributions become

$$\begin{aligned} \mathcal{P}_{L_Q}\mathcal{M}\mathcal{P}_{S_Q} &= \mathcal{P}_{L_Q}\mathcal{I}_{N:Q}^{\dagger}M\mathcal{I}_{N:Q-\ell}\mathcal{P}_{C_{Q-\ell}}\mathcal{I}_{N:M} \\ &= \mathcal{P}_{L_Q}M_{Q,Q-\ell}\mathcal{I}_{N:M}. \end{aligned} \tag{153}$$

Figure 27 illustrates the information flow for the smooth contributions (153). First, the forward transform $\mathcal{I}_{N:M}$ is carried out using the cascade algorithm (135), as represented by the curved

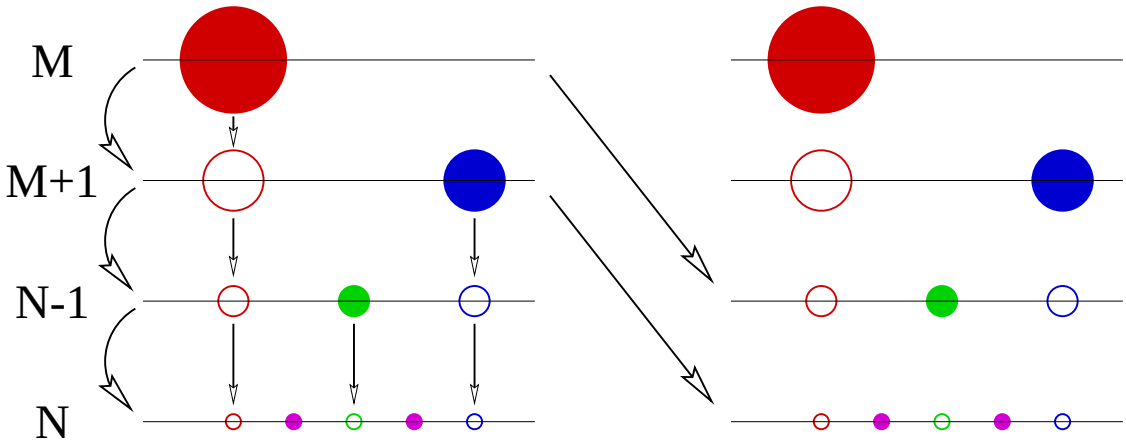

Figure 27: Information flow for smooth contributions to $\mathcal{M}$: cascade algorithm for $\mathcal{I}_{N:M}$ (curved arrows), access to data on multiple scales (vertical arrows), inter-scale convolutions $M_{R,Q}$ (diagonal arrows).

arrows. (In practice, the cascade need not be carried out completely as the results on the finest few levels will not be used.) Next, the vertical arrows indicate that one must ensure that the resulting coefficients are replicated on all finer levels, for they will be accessed also from these levels by the $M_{Q,Q-\ell}$. The final step in computing the smooth contribution is to perform the inter-scale convolutions $M_{Q,Q-\ell}$ represented by the diagonal arrows as in Figure 26.

The strategy for the finer contributions, present whenever $Q - \ell \leq N$, is to gather overlap information from finer scales in the form of the matrix elements,

$$\mathcal{F}_Q \equiv \mathcal{P}_{C_Q} \mathcal{M} \mathcal{P}_{F_Q}. \tag{154}$$

Note that the finer scale contributions in (147) for any scale Q may be extracted from these objects as simply $\mathcal{P}_{L_Q} \mathcal{F}_Q$. To gather the effects of finer scales on these matrix elements, we use the decomposition $F_Q = D_{Q+\ell} \cup F_{Q+1}$ and make the replacement $\mathcal{I}_{N:Q} \mathcal{P}_{C_Q} = \mathcal{I}_{N:Q+1} \mathcal{P}_{C_{Q+1}} \mathcal{I}_{Q+1,Q} \mathcal{P}_{C_Q}$ to convert (154) into the recursion

$$\begin{aligned} \mathcal{F}_Q &= \mathcal{P}_{C_Q} \mathcal{M} \mathcal{P}_{D_{Q+\ell}} + \mathcal{P}_{C_Q} \mathcal{M} \mathcal{P}_{F_{Q+1}} \\ &= M_{Q,Q+\ell} \mathcal{P}_{D_{Q+\ell}} + \mathcal{P}_{C_Q} \mathcal{I}^\dagger_{Q+1,Q} \mathcal{F}_{Q+1}, \end{aligned} \tag{155}$$

which may be solved for $\mathcal{F}_Q$ with $\mathcal{F}_{N-\ell} \equiv \mathcal{P}_{C_Q} \mathcal{M} \mathcal{P}_{D_N}$ as the starting point of the recursion.

Figure 28 illustrates the information flow for this process. The $M_{Q,Q+\ell}$ convolutions may be first computed and then "folded-in" as the recursion (155) proceeds. These convolutions are indicated by the diagonal arrows. As with the proximate contributions, the projections $\mathcal{P}_{D_{Q+\ell}}$ imply that the redundant points associated with the open circles on the left carry zero value for these convolutions. Once the convolutions are precomputed in this manner, the finer scale contributions are computed from the recursive accumulation of the action of $\mathcal{I}^\dagger_{Q+1,Q}$ from each scale onto the next coarser scale in sequence, from the bottom to the top of the figure, as represented by the curved arrows. In practice, the operations $\mathcal{I}^\dagger_{Q+1,Q}$ on the finest few scales work with data with zero value and so need not be computed.

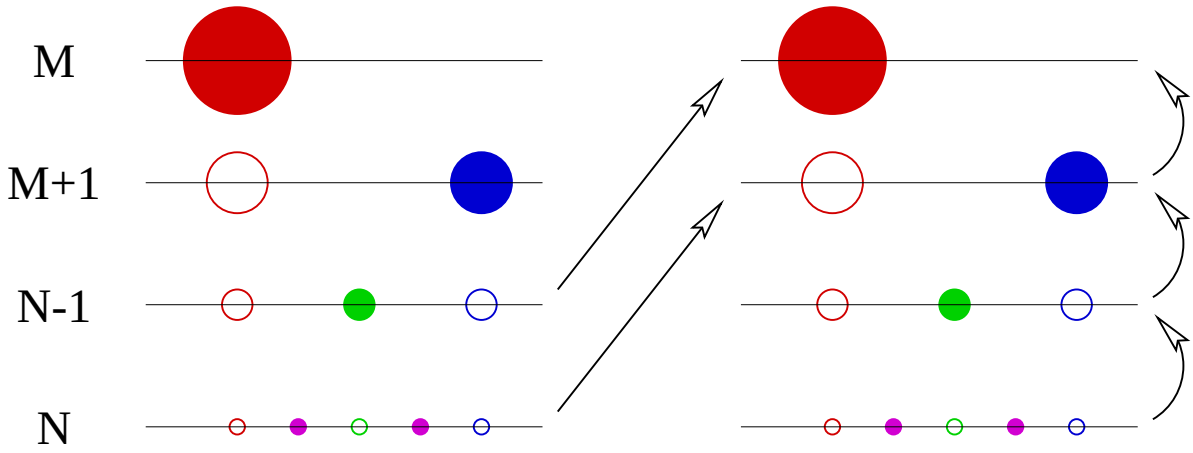

Figure 28: Information flow for fine contributions to $\mathcal{M}$: inter-scale convolutions $M_{R,Q}$ (diagonal arrows), $\mathcal{I}^{\dagger}_{P+1,P}$ stages proceeding in sequence from finest to coarsest (curved arrows).

The sum of the contributions illustrated in Figures 26-28 gives the final result of the application of the operator $\mathcal{M}$. The complete procedure for computing $H = \mathcal{M}G$ for any vector G for the non-trivial cases $N - M \geq \ell$ which involve more than just proximate contributions is thus

$$\mathcal{F}_{N-\ell} = M_{N-\ell,N}\mathcal{P}_{D_N}G, \; g \equiv \mathcal{I}G; \tag{156}$$

$$\mathcal{F}_Q = M_{Q,Q+\ell}\mathcal{P}_{D_{Q+\ell}}G + \mathcal{P}_{C_Q}\mathcal{I}^{\dagger}_{Q+1,Q}\mathcal{F}_{Q+1} \quad (\text{for } Q < N-\ell);$$

$$\begin{aligned} H \;=\; & \sum_{Q=M+\ell}^{N} \mathcal{P}_{L_Q} M_{Q,Q-\ell} \cdot g \\ & + \sum_{Q=M}^{N} \left(\sum_{R=\max(M,Q-\ell+1)}^{\min(N,Q+\ell-1)} \mathcal{P}_{L_Q} M_{Q,R} \mathcal{P}_{L_R} \right) \\ & + \sum_{Q=M}^{N-\ell} \mathcal{P}_{L_Q} \mathcal{F}_Q. \end{aligned}$$

The non-standard multiply approach of Beylkin, Coifman and Rokhlin[BCR91] corresponds to the special case $\ell = 1$ case of this approach. For the restrictions usually encountered in atomic calculations, the case $\ell = 2$ has been shown to improve the speed of calculations by at least a factor of four[LAE98, Lip98].

VII Impact of Restriction

We now consider how the prescriptions (135,137,140,142,156) for operations in semicardinal multiresolution analyses are affected when the analysis is restricted. We show that under relatively mild conditions on how quickly the restriction changes resolutions, it is possible to simply ignore the missing coefficients and yet obtain exactly the results of an unrestricted multiresolution analysis

and thus achieve the ultimate goal of expending $O(1)$ operations per expansion coefficient while, remarkably, introducing no additional approximations beyond the choice of basis set. These issues were first explored in [LAE98], which prompted the study and development of the concept of "S-trees" to appear in a coming work[CD97]. We now present the discussion of [LAE98] using the explicit matrix language introduced in Sec. IV-F.

We begin by introducing the notation $[*]$ as the restriction of the scope of the object "$*$" to the functions and grid points *surviving* the restriction of a multiresolution analysis. The restriction $[S]$ of a set of points S, for example, is defined as the set of those points of S associated with functions which survive the restriction. The set of all surviving points is the restriction of the finest grid in the multiresolution analysis, $[C_N]$. Thus, in general, for any set of points S,

$$[S] \equiv [C_N] \cap S,$$

or in terms of projections,

$$\mathcal{P}_{[S]} = \mathcal{P}_{[C_N]}\mathcal{P}_S = \mathcal{P}_S\mathcal{P}_{[C_N]}. \tag{157}$$

The restriction of any linear operator O is defined so that its matrix elements ignore coefficients that have been restricted from the multiresolution analysis. Algebraically, this is achieved by projection,

$$[O] \equiv \mathcal{P}_{[C_N]}O\mathcal{P}_{[C_N]}. \tag{158}$$

Consistent with this definition, the matrices $\mathcal{O}$ and L used in Sec. III-C.1 involve only overlaps between functions present in the basis.

This simple prescription for the restriction of linear operators, however, is not appropriate in general for the transforms, which relate expansion coefficients on one side with function values at points in real space on the other. Even a smooth function will have significant values in real space on the grid points associated with extremely fine functions. Thus, great care is needed to ensure that the lack of access to this information does not adversely affect the results of expressions involving the transforms. For semicardinal bases, as we shall see, very mild conditions on the restriction of the multiresolution analysis can ensure that the unknown expansion coefficients will have absolutely no impact on the function values computed by the forward transform on the surviving points, so that

$$[\mathcal{I}] \equiv \mathcal{P}_{[C_N]}\mathcal{I}\mathcal{P}_{[C_N]} = \mathcal{P}_{[C_N]}\mathcal{I}, \tag{159}$$

and, most critically, that the missing real-space information has absolutely no impact on the expansion coefficients computed by the inverse transform for the surviving functions,

$$[\mathcal{J}] \equiv \mathcal{P}_{[C_N]}\mathcal{J}\mathcal{P}_{[C_N]} = \mathcal{P}_{[C_N]}\mathcal{J}. \tag{160}$$

Taken together, conditions (159,160) have the remarkable consequence, to which we first alluded in Sec. II-B, that, even in a restricted basis, we may compute the expansion coefficients for any non-linear combination of fields, for example the exchange-correlation energy density $\epsilon_{xc}(r)$, and obtain results identical to what would be obtained by working with an *unrestricted* multiresolution analysis of *arbitrarily* high resolution.

VII-A Transforms

For the transforms, we begin by considering the implications of condition (160) for the allowable restrictions of semicardinal multiresolution analyses. The inverse transform in semicardinal bases (139) has a particularly simple form which is useful for understanding the impact of restriction.

Because $\mathcal{P}_{C_P}\mathcal{P}_{D_{Q+1}} = 0$ for all $P < Q$, the fact that the product (139) orders terms from coarsest to finest from left to right, implies that all but the zero and first order terms in $\mathcal{P}_{D_{P+1}}\mathcal{I}_{P+1,P}\mathcal{P}_{C_P}$ vanish from the product, leaving only the *sum*

$$\mathcal{J} = I - \sum_{P=M}^{N-1} \mathcal{P}_{D_{P+1}}\mathcal{I}_{P+1,P}\mathcal{P}_{C_P}.$$

Inserting this into (160) and using (157) gives

$$\mathcal{P}_{[C_N]} - \sum_{P=M}^{N-1} \mathcal{P}_{[D_{P+1}]}\mathcal{I}_{P+1,P}\mathcal{P}_{[C_P]} \;=\; \mathcal{P}_{[C_N]} - \sum_{P=M}^{N-1} \mathcal{P}_{[D_{P+1}]}\mathcal{I}_{P+1,P}\mathcal{P}_{C_P}.$$

Because the $[D_{P+1}]$ are disjoint, the sums must be equal term by term in $\mathcal{P}_{[D_{P+1}]}$, leading to the condition

$$\mathcal{P}_{[D_{P+1}]}\mathcal{I}_{P+1,P}(\mathcal{P}_{C_P} - \mathcal{P}_{[C_P]}) = \mathcal{P}_{[D_{P+1}]}\mathcal{I}_{P+1,P}\mathcal{P}_{C_P-[C_P]} = 0. \tag{161}$$

Given that all the points in $[C_P]$ must appear in $[C_{P+1}]$, the simplest geometric interpretation of (161) is that no single-scale basis function associated with a point dropped from scale P may have a non-zero two-scale expansion coefficient for any scaling function maintained in the basis on level $P+1$. This is referred to as the *good-grid condition*.

Figure 29 illustrates the effects of the good-grid condition on the progress of a calculation. The figure follows the same conventions as the figures of Sec. VI-A, but now the multiresolution analysis is restricted to provide the resolution of V_M in the left half of the figure, to make a brief transition through V_{M+1}, and finally to attain the resolution of $V_{M+2} = V_N$ on the right. Although the figure shows the information flow which would occur in the full multiresolution analysis, it shows only those coefficients which survive the restriction. Geometrically, the condition (161) states that no arrow in the forward transform (upper half of the figure) which originates from a missing point may terminate on a surviving point. This ensures that the surviving coefficients computed at each stage of the restricted transform are unaffected by the missing coefficients. For semicardinal multiresolution analyses, the pattern of the information flow for the inverse transform (lower half of the figure) is the same as for the forward transform. Thus, the inverse too is unaffected by ignoring coefficients on the restricted points. Finally, the figure illustrates the observation made above that so long as the good-grid condition is maintained, the process of computing expansion coefficients for the results of a local non-linear interaction (represented by the vertical solid connections in the center of the figure) such as $\epsilon_{xc}(\sum_i f|\psi_i(x)|^2)$ remains unaffected by coefficients restricted from the multiresolution analysis.

Figure 30 illustrates the constraints of the good grid condition on allowable restrictions for functions of support ± 2. The presence of the one point on scale $M+2$ in the figure requires the survival, in the restriction of the multiresolution analysis $V_M \oplus W_{M+1} \oplus W_{M+2}$, of all of the other points in the figure. As the figure illustrates, the physical requirement of the good-grid condition is just that the restriction pass through finite regions representing each level of resolution in sequence and that it not not skip discontinuously from level to level. Because the expansion coefficients of physical functions exhibit this behavior naturally (Figure 5), the good-grid condition generally represents little or no additional burden in the restriction of the basis.

To establish algebraically that on good grids the procedures (135,140,137,142) give correct results when working only with data on the surviving points, we first note that on a good grid the separate stages of the transforms individually obey the restriction condition,

$$[\mathcal{I}_{P+1,P}] \;=\; \mathcal{P}_{[C_N]}\mathcal{I}_{P+1,P} \tag{162}$$

$$\left[\mathcal{I}^{-1}_{P+1,P}\right] \;=\; \mathcal{P}_{[C_N]}\mathcal{I}^{-1}_{P+1,P}, \tag{163}$$

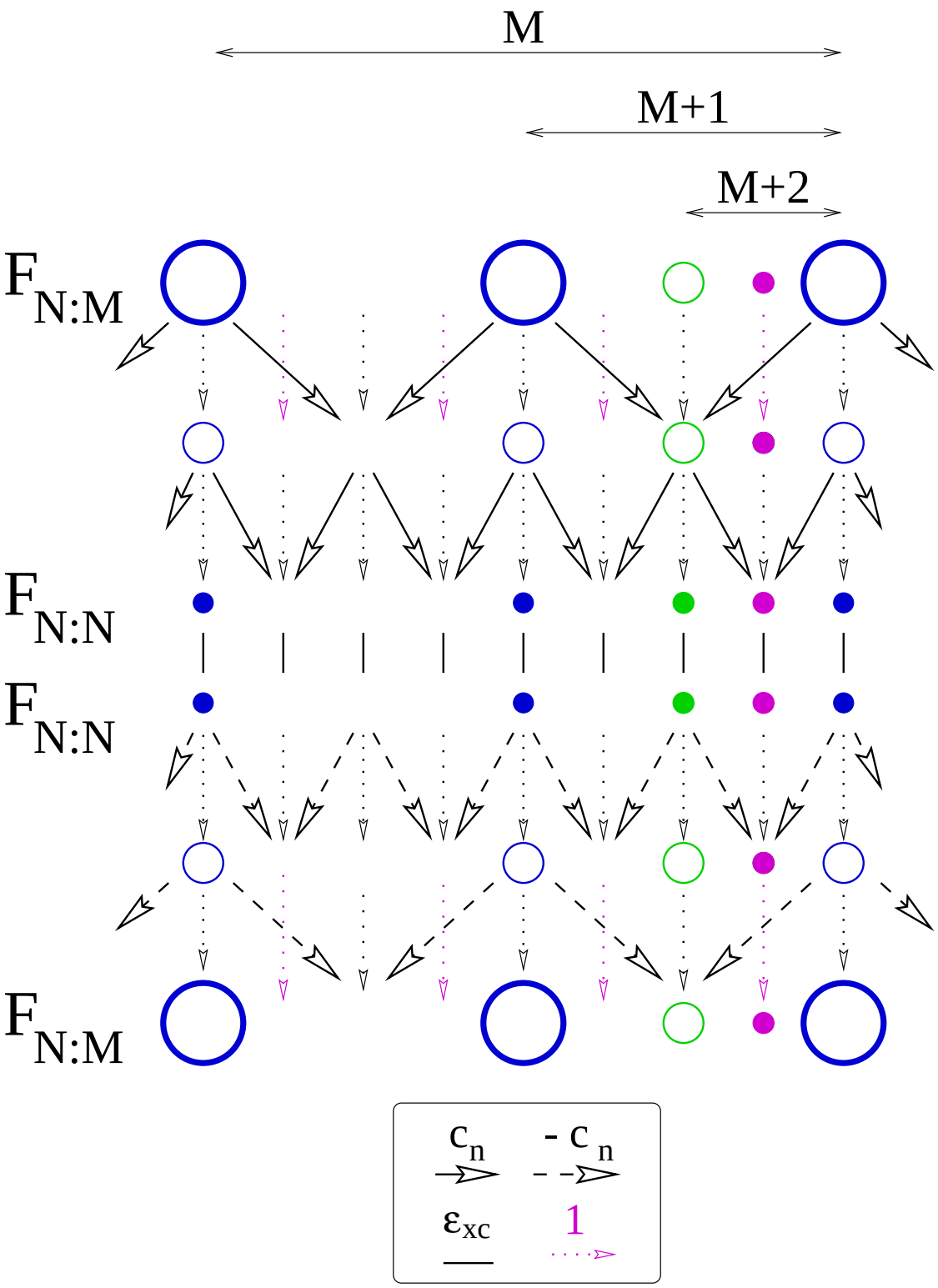

Figure 29: Information flow in the calculation of expansion coefficients for ϵ_{xc} in a restricted semicardinal multiresolution analysis on a good grid: forward transform (upper half), non-linear local interaction (vertical connections in center of figure), inverse transform (lower half).

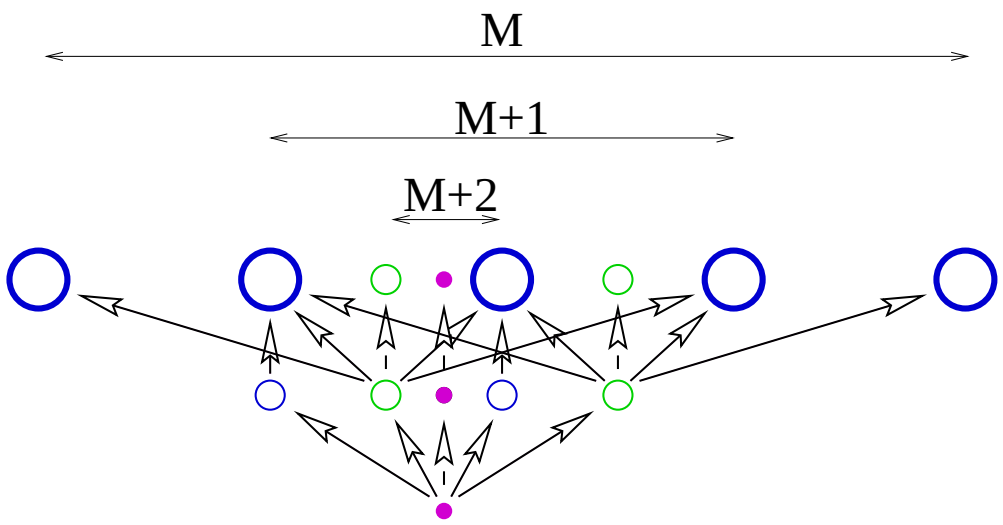

Figure 30: Implications of good grid condition on scales $(M : M+2)$ stemming from a single point (solid circle) on scale $M+2$ for functions of support ± 2: requirements of $\mathcal{P}_{[D_{P+1}]}\mathcal{I}_{P+1,P}\mathcal{P}_{C_P-[C_P]} = 0$ (solid arrows), points already required from lower levels (dashed arrows).

as follows directly from the defining good-grid condition (161) and the decompositions (133,138). Next we note that working with only data on the surviving points amounts to ignoring at each step of a procedure the input from and output onto the restricted points. Algebraically, this corresponds to replacing the factors in the products making up the transforms (134,139,136,141) with their restricted counterparts, $[\mathcal{I}_{P+1,P}]$, $[\mathcal{I}^{-1}_{P+1,P}]$, $[\mathcal{I}^{\dagger}_{P+1,P}]$, $[\mathcal{I}^{-\dagger}_{P+1,P}]$, respectively.

From these considerations, we see that the forward transform (135) executed with only surviving coefficients gives

$$\begin{aligned}\prod_{P=N-1}^{M}[\mathcal{I}_{P+1,P}] &= \mathcal{P}_{[C_N]}\mathcal{I}_{N,N-1}\mathcal{P}_{[C_N]}\ldots\mathcal{P}_{[C_N]}\mathcal{I}_{P+2,P+1}\mathcal{P}_{[C_N]}\mathcal{I}_{P+1,P}\mathcal{P}_{[C_N]}\\ &= \mathcal{P}_{[C_N]}\mathcal{I}_{N,N-1}\mathcal{P}_{[C_N]}\ldots\mathcal{P}_{[C_N]}\mathcal{I}_{P+2,P+1}(\mathcal{P}_{[C_N]}\mathcal{I}_{P+1,P}\mathcal{P}_{[C_N]})\\ &= \mathcal{P}_{[C_N]}\mathcal{I}_{N,N-1}\mathcal{P}_{[C_N]}\ldots(\mathcal{P}_{[C_N]}\mathcal{I}_{P+2,P+1}\mathcal{P}_{[C_N]})\mathcal{I}_{P+1,P}\\ &= \mathcal{P}_{[C_N]}\mathcal{I}, \end{aligned} \tag{164}$$

where we have collapsed the product telescopically using (162). Directly analogous considerations for the inverse transform lead to

$$\prod_{P=M}^{N-1}[\mathcal{I}^{-1}_{P+1,P}] = \mathcal{P}_{[C_N]}\mathcal{J}. \tag{165}$$

Thus, we see that applying the algorithms (135,140) to only the surviving coefficients leads to results on the surviving points which are *identical* to what would be obtained with the unrestricted transforms $\mathcal{I}$ and $\mathcal{J}$. Note that because the left-hand sides of (164,165) are unchanged by post-multiplication by $\mathcal{P}_{[C_N]}$, these results also confirm directly that (159,160) obtain on good grids.

Finally, we note that the conjugate transforms defined in Sec. III-E for any basis are the Hermitian conjugates of the associated forward and inverse transforms. From (159,160) and (164,165),

these are thus simply

$$[\mathcal{I}]^\dagger = \prod_{P=M}^{N-1} [\mathcal{I}^\dagger_{P+1,P}]$$

$$[\mathcal{J}]^\dagger = \prod_{P=N-1}^{M} [\mathcal{I}^{-\dagger}_{P+1,P}].$$

Composed entirely of restricted component operations, these expressions are precisely what the algorithms (137,142) compute when working only with data on surviving points.

VII-B Operators

The procedure (156) for applying physical operators divides the contributions to $\mathcal{M}$ into a sum of three classes of contribution: smooth, proximate, and fine. The proximate contributions call upon $M_{Q,P}$ to collect data from functions present in the basis onto coefficients present in the basis. Thus, regardless of the form of the restriction, the restriction of these parts of $\mathcal{M}$ amounts to ignoring coefficients restricted from the basis, which is precisely what is accomplished when carrying out (156) on data associated with only the surviving points. Algebraically, this corresponds to the fact that restricting (151) leads to corresponding expressions with all component operations replaced by their restricted counterparts. The proximate contributions in (156) are therefore always restrictable.

The smooth contributions, on the other hand, do impose conditions on the restriction. The contributions (153) connect the single-scale basis associated with $C_{Q-\ell}$ through the operator $\mathcal{M}$ onto the multiscale basis functions associated with the points of L_Q. To ensure that no information is lost when computing these contributions, the restriction must be such that all scaling functions associated with the lattice of the scale ℓ levels coarser which overlap with, or *touch*, a function in the basis must also appear in the basis,

$$\mathcal{P}_{[L_Q]} M_{Q,Q-\ell} \mathcal{P}_{C_{Q-\ell}-[C_{Q-\ell}]} = 0. \tag{166}$$

Algebraically, this condition allows the transition from the first to the second line in the derivation

$$\begin{aligned} [\mathcal{P}_{L_Q} M_{Q,Q-\ell} \mathcal{I}_{N:M}] &= \mathcal{P}_{[L_Q]} M_{Q,Q-\ell} \mathcal{P}_{C_{Q-\ell}} \mathcal{I}_{N:M} \mathcal{P}_{[C_N]} \\ &= \mathcal{P}_{[L_Q]} M_{Q,Q-\ell} \mathcal{P}_{[C_{Q-\ell}]} \mathcal{I}_{N:M} \mathcal{P}_{[C_N]} \\ &= [\mathcal{P}_{L_Q}][M_{Q,Q-\ell}][\mathcal{I}_{N:M}], \end{aligned} \tag{167}$$

which establishes that the coarse contributions to $[\mathcal{M}]$ may be computed correctly while processing data on the surviving points only. Figure 31 illustrates the requirements of the this condition for functions of support ± 2 when using the $\ell = 2$ version of the algorithm.

Finally, we turn to the finer contributions. The first term in the recursion (155) for these contributions is of the same generally restrictable form as the proximate contributions and so impose no condition on the restriction. However, proper computation of the second term of (155) requires a condition on the grid which is slightly stronger than (166). Now we must require that all scaling functions from the scales *at least* ℓ levels coarser which touch a function in the basis must also survive the restriction,

$$\mathcal{P}_{C_Q-[C_Q]} \mathcal{M} \mathcal{P}_{[F_Q]} = 0, \tag{168}$$

which, from the definition (154) of $\mathcal{F}$, is equivalent to $\mathcal{F}_Q \mathcal{P}_{[C_N]} = [\mathcal{F}_Q]$. Combining the $Q+1$ case of this condition with the previously established good-grid condition (161), we see that when

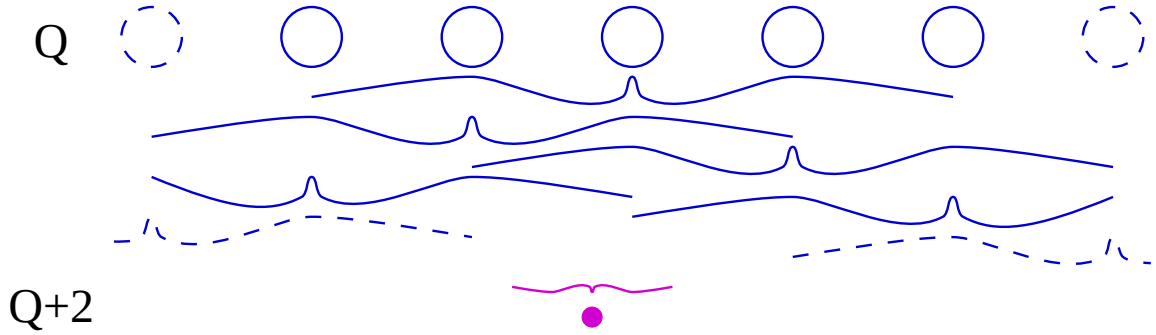

Figure 31: Requirements of the grid-touching condition (168) on scale Q which stem from the presence of a detail function (filled circle) on scale $Q+2$: required points (solid circles), optional points (dashed circles), support of functions (braces). (Illustrated for the $\ell = 2$-level algorithm.)

computing on only surviving coefficients, the second term in (155) gives

$$\begin{aligned}
[\mathcal{P}_{C_Q}][\mathcal{I}^\dagger_{Q+1,Q}][\mathcal{F}_{Q+1}] &= \mathcal{P}_{[C_Q]} \cdot \mathcal{I}^\dagger_{Q+1,Q} \mathcal{P}_{[C_N]} \cdot [\mathcal{F}_{Q+1}] \\
&= \mathcal{P}_{[C_Q]} \mathcal{I}^\dagger_{Q+1,Q} [\mathcal{F}_{Q+1}] \\
&= \mathcal{P}_{[C_Q]} \mathcal{I}^\dagger_{Q+1,Q} \mathcal{F}_{Q+1} \mathcal{P}_{[C_N]} \\
&= [\mathcal{P}_{C_Q} \mathcal{I}^\dagger_{Q+1,Q} \mathcal{F}_{Q+1}],
\end{aligned} \tag{169}$$

precisely the correct restricted result.

We refer to condition (168), which contains (166) as a special case, as the ℓ-level grid-touching condition. Combined with the good-grid condition (161), this condition ensures that the procedure given in Sec. VI-B gives correct results for integral-differential operators even in restricted multiresolution analyses. Note that the ℓ-level grid-touching condition requires that the the situation illustrated in Figure 31 holds not only for the scaling functions on scale Q but also for all coarser scales $R < Q$ as well.

As the scale separation ℓ increases, the detail function on the lower scales appear relatively smaller, and the grid-touching condition becomes weaker. In the limiting case of very large ℓ, the support of the detail functions appears like a single point and the touching condition approaches the good-grid condition. For low ℓ, the differences in the conditions on the restriction can have important consequences. For example, going from $\ell = 1$, which corresponds to the non-standard multiply of [BCR91], to $\ell = 2$ allows for quicker changes in resolution that have been shown to accelerate calculations by over a factor of four for the restrictions typically encountered in atomic calculations[LAE98].

As a closing note, the alternative restriction conditions

$$\begin{aligned}
\mathcal{P}_{C_{Q-\ell}-[C_{Q-\ell}]} \mathcal{I}_{N:M} \mathcal{P}_{[C_N]} &= 0 \\
\mathcal{P}_{[C_Q]} \mathcal{I}^\dagger_{Q+1,Q} \mathcal{P}_{C_{Q+1}-[C_{Q+1}]} &= 0
\end{aligned}$$

would also allow for proper computation of the smooth and fine contributions in (167,169), respectively. These conditions, however, are "finer-looking" in the sense that each function in the basis requires the presence of functions on even finer scales. This leads to an infinite chain of conditions

that ultimately requires the multiresolution analysis to be of infinite resolution. As a result, the ℓ-level touching condition is the appropriate condition to impose in real computations.

VIII Concluding Remarks

Mallat and Meyer's development of multiresolution analysis provides a tool not only of great use in functional analysis and signal processing but also of great potential for the study of physical systems exhibiting behavior on multiple length scales. In particular, multiresolution analysis provides the first practical possibility for a unified, systematic treatment of core and valence behavior in the electronic structure of molecular and condensed-matter systems. The first all-electron density-functional calculations of atoms and molecules carried out with this approach ([ACLT95, Ari95], Sec. I.) have demonstrated that multiresolution analysis provides an extremely efficient means of representing the core and valence electrons simulataneously. Latter work underscores the promising possibilities of combining multiresolution analysis with pseudopotential theory[WC96], developing dynamic restriction schemes[TW97], and using lifted bases for some phases of the calculations[GI98]. Finally, the recent development of the theory of fast restrictable algorithms for semicardinal bases ([LAE98], Sec. VII) now paves the way for the first application of multiresolution analysis to the calculation of the electronic structure of large, complex systems.

In closing, the author would like to leave the reader with the understanding that many opportunities remain for making significant contributions to the field of the multiresolution analysis of electronic structure. The basic groundwork is now in place, but many interesting and important open questions remain. For example, the differing stiffnesses of the core and valence degrees of freedom clearly call for some new form of preconditioning. The significant expense of solving Poisson's equation at each electronic iteration indicates that methods which search directly for the saddle point of the LDA Lagrangian will be more efficient than present approaches. Also, procedures are needed to anticipate accurately the changes in the expansion coefficients of the wave functions as the nuclei move. Finally, there is the intriguing possibility that the weakness of the coupling between the core and valence degrees of freedom will allow the atomic cores to be treated independently and in parallel.

Acknowledgments

This work was supported in part by the MRSEC Program of the National Science Foundation (DMR 94-00334) and the Alfred P. Sloan Foundation (BR-3456). The author is greatly indebted to M.P. Teter for his insights into the utility of cardinal functions, which eventually led to the concept of semicardinality, to S. Ismail-Beigi for his recognition of the restrictability of semicardinal transforms and his most careful reading of the final manuscript, to Dicle Yeşilleten for our first implementation and verification of the restrictable overlap operators, to T.D. Engeness for his reading of the earlier drafts of this work, and to all the others on whose constant intercession the author has relied for help during the preparation of this review.

A Cofactors of the semicardinal two-scale decomposition matrix

In this appendix, we determine the cofactors of the matrix

$$P_{ij} \equiv (-1)^{\eta_i \cdot \eta_j},$$

where, as defined in the text, the η_i range over the set $\{0,1\}^d$.

The central result we use to determine these cofactors is that $P^2 = 2^d I$, which we show by explicit computation,

$$\begin{aligned}
(P^2)_{ij} &= \sum_k P_{ik}P_{kj} \\
&= \sum_{\{\eta_k\}} \prod_{e=1}^{d} (-1)^{(\eta_i)_e(\eta_k)_e+(\eta_k)_e(\eta_j)_e} \\
&= \prod_{e=1}^{d} \sum_{\{(\eta_k)_e=0,1\}} (-1)^{(\eta_k)_e((\eta_i)_e+(\eta_j)_e)} \\
&= \prod_{e=1}^{d} \left(1+(-1)^{(\eta_i)_e+(\eta_j)_e}\right) \\
&= \prod_{e=1}^{d} \left(2\delta_{(\eta_i)_e,(\eta_j)_e}\right) \\
&= 2^d\delta_{ij}.
\end{aligned}$$

With $P^2 = 2^d I$ established, we have $P^{-1} = P/2^d = (\operatorname{cof} P)^T/\det P$, where $\operatorname{cof} P$ is the matrix of the cofactors of the matrix P. To determine $\det P$, we note that $\det P^2 = (2^d)^{2^d}$, so $|\det P| = (2^d)^{2^{d-1}}$. Thus,

$$\operatorname{cof} P = (\det P)(P^{-T}) = \left(\pm(2^d)^{2^{d-1}}\right)\left(\frac{1}{2^d}P^T\right) = \pm(2^d)^{2^{d-1}-1}P^T.$$

Because all entries in the top row of P are unity, the elements of the first column of the cofactor matrix, needed at the end of Sec. V-B.3, all have a single constant value, $\pm(2^d)^{2^{d-1}-1}$.

References

[ACLT95] T.A. Arias, K.J. Cho, Pui Lam, and M.P. Teter. Wavelet transform representation of the electronic structure of materials. In Rajiv K. Kalia and Priya Vashishta, editors, *Proceeedings of the '94 Mardi Gras Conference: Toward Teraflop Computing and New Grand Challenge Applications*, page 23, Commack New York, 1995. Nova Science Publishers.

[AFO85] D. Adler, H. Fritzsche, and S.R. Ovshinsky, editors. *Physics of disordered materials.* Plenum, New York, 1985.

[Aka97] Metin Akay, editor. *Time Frequency and Wavelets in Biomedical Signal Processing.* IEEE Press Series in Biomedical Engineering. IEEE Press, Piscataway, 1997.

[ALM+97] M. Ainsworth, J. Levesley, M. Marletta, W.A. Light, and Epsrc Nu, editors. *Wavelets, Multilevel Methods and Ellipic Pde's.* Numerical Mathematics and Scientific Computation. Oxford University Press, Oxford, 1997.

[And75] O.K. Andersen. Linear methods in band theory. *Phys. Rev. B*, 12:3060, 1975.

[APJ92] Tomás A. Arias, M. C. Payne, and John D. Joannopoulous. *Ab initio* molecular dynamics: Analytically continued energy functionals and insights into iterative solutions. *Phys. Rev. Lett.*, 71:1077–1080, 1992.

[Ari95] T.A. Arias. Interpolets: the wavelet of the future for electronic structure calculation. Annual March Meeting of the American Physical Society, San Jose, California, 1995.

[AU93] A. Aldroubi and M. Unser. Families of multiresolution analysis and wavelet spaces with optimal properties. *Numer. Funct. Anal. Optim.*, 14:417, 1993.

[BBSB97] J. Bernholc, E.L. Briggs, D.J. Sullivan, and C.J. Brabec. Real space multigrid methods for large-scale electronic structure problems. *Int. J. Quantum Chem.*, 65:531, 1997.

[BCR91] G. Beylkin, R.R. Coifman, and V. Rokhlin. Fast wavelet transforms and numerical algorithms. *Commun. Pure and Appl. Math*, 44:141, 1991.

[BK95] G. Beylkin and J. M. Keiser. On the adaptive numerical solution of nonlinear partial differential equations in wavelet bases. *PAM Report*, 262, 1995.

[BK97] G. Beylkin and J. M. Keiser. On the adaptive numerical solution of nonlinear partial differential equations in wavelet bases. *J. Comput. Phys.*, 132:233, 1997.

[BN96] S. Bertoluzza and G. Naldi. A wavelet collocation method for the numerical solution of partial differential equations. *Appl. Comput. Harmon. Anal.*, 3:1, 1996.

[Bra97] Dietrich Braess. *Finite Elements: Theory, Fast Solvers, and Applications in Solid Mechanics*. Cambridge University Press, Cambridge, U.K., 1997.

[BS92] G. Beylkin and N. Saito. Wavelets, their autocorrelation functions, and multiresolution representation of signals. *Expanded abstract in Proceedings ICASSP-92*, 4:381, 1992.

[BSB96] E.L. Briggs, D.J. Sullivan, and J. Bernholc. Real-space multigrid-based approach to large-scale electronic structure calculations. *Phys. Rev. B*, 54:14362, 1996.

[CAJL93] K. Cho, T.A. Arias, J.D. Joannopoulos, and Pui K. Lam. Wavelets in electronic structure calculations. *Phys. Rev. Lett.*, 71:1808, 1993.

[CB97] T.R. Chandrupatla and A.D. Belegundu. *Introduction to Finite Elements in Engineering*. Prentice Hall, Upper Saddle River, N.J., 1997.

[CD97] A. Cohen and R. Danchin. Multiscale approximation of vortex patches. *preprint*, 1997.

[Chu92a] C.K. Chui. *An Introduction to Wavelets*. Academic Press, Boston, 1992.

[Chu92b] T.J. Chung. *Finite Elements in Fluids*. Series in Computational and Physical Processes in Mechanics and Thermal Sciences. John Wiley & Sons, Chichester, N.Y., 1992.

[CIBA98] Gàbor Csányi, Sohrab Ismail-Beigi, and T.A. Arias. Paramagnetic structure for the soliton of the 30^o partial dislocation in silicon. *Phys. Rev. Lett.*, 80:3984, 1998.

[Coh84] M.J. Cohen. Electronic structure of solids. *Phys. Rep.*, 110:293, 1984.

[CS92] C.K. Chui and X. Shi. Mathematical methods in computer aided geometric design ii. In T. Lyche and L.L Schumaker, editors, *Wavelets and multiscale interpolation*, page 111, Boston, 1992. Academic Press.

[Dau92] I. Daubechies. *Ten Lectures on Wavelets*. Number 61 in CBMS/NSF Series in Applied Math. SIAM, Philadelphia, 1992.

[DD89] G. Deslauriers and S. Dubuc. Symmetric iterative interpolation processes. *Constr. Approx.*, 5(1):49, 1989.

[DFB97] Carlos Enrique D'Attellis and E. M. Fernandez-Berdaguer, editors. *Wavelet Theory and Harmonic Analysis in Applied Sciences*. Applied and Numerical Harmonic Analysis. Birkhauser, Boston, 1997.

[DKCJ94] A. Devenyi, T.A. Arias K. Cho, and J.D. Joannopoulos. Adaptive riemannian metric for all-electron calculations. *Phys. Rev. B*, 49:13373, 1994.

[DKO97] Wolfgang Dahmen, Andrew J. Kurdila, and Peter Oswald, editors. *Multiscale Wavelet Methods for Partial Differential Equations*, volume 6 of *Wavelet Analysis and Its Applications*. Academic Press, San Diego, 1997.

[Don92] D. L. Donoho. Interpolating wavelet tranforms. Preprint, Department of Statistics, Stanford University, 1992.

[FD90] David Feller and Ernest R. Davidson. *Basis Sets for Ab Initio Molecular Orbital Calculations and Intermolecular Interactions*, volume 1 of *Reviews in Computational Chemistry*. VCH, New York, 1990.

[FS94] J. Frohlich and K. Schneider. An adaptive wavelet galerkin algorithm for one- and two-dimensional flames. *Eur. J. Mech. B*, 13:439, 1994.

[FS97] J. Frohlich and K. Schneider. An adaptive wavelet-vaguelette algorithm for the solution of pdes. *J. Comput. Phys.*, 130:174, 1997.

[GG95] F. Gygi and G. Galli. Real-space adaptive-coordinate electronic-structure calculations. *Phys. Rev. B*, 52:R2229, 1995.

[GGBB97] Ramesh A. Gopinath, Haitao Guo, C. Sidney Burrus, and L. Sidney Burrus. *Introduction to Wavelets and Wavelet Transforms : A Primer*. Prentice Hall, Upper Saddle River, N.J., 1997.

[GI98] S. Goedecker and O.V. Ivanov. Linear scaling solution of the coulomb problem using wavelets. *Solid State Commun.*, 105:665, 1998.

[GR89] L. Greengard and V. Rokhlin. On the evaluation of electrostatic interactions in molecular modeling. *Chem. Scripta*, 29A:139, 1989.

[Gyg93] F. Gygi. Adaptive riemannian metric for plane-wave electronic-structure calculations. *Europhys. Lett.*, 19:617, 1993.

[Gyg95] F. Gygi. Ab initio molecular dynamics in adaptive coordinates. *Phys. Rev. B*, 51:11190, 1995.

[Ham95] D.R. Hamann. Application of adaptive curvilinear coordinates to the electronic structure of solids. *Phys. Rev. B*, 51:7377, 1995.

[Ham96a] D.R. Hamann. Generalized-gradient functionals in adaptive curvilinear coordinates. *Phys. Rev. B*, 54:1568, 1996.

[Ham96b] D.R. Hamann. Generalized gradient theory for silica phase transitions. *Phys. Rev. Lett.*, 76:660, 1996.

[Ham97] D.R. Hamann. Adaptive-coordinate electronic structure of 3d bands: Tio_2. *Phys. Rev. B*, 56:14979, 1997.

[HK64] P. Hohenberg and W. Kohn. Inhomogeneous electron gas. *Phys. Rev.*, 136:B864, 1964.

[HW96] Eugenio Hernandez and Guido L. Weiss. *A First Course on Wavelets*. Studies in Advanced Mathematics. CRC Press, Boca Raton, 1996.

[IBA98] Sohrab Ismail-Beigi and T.A. Arias. *Ab initio* study of the interplay of edges and surfaces in nanoscale silicon. *Phys. Rev. B*, 57:11923, 1998.

[Kai94] Gerald Kaiser. *A Friendly Guide to Wavelets*. Birkhauser, Boston, 1994.

[KS65] W. Kohn and L. J. Sham. Self-consistent equations including exchange and correlation effects. *Phys. Rev.*, 140:A1133, 1965.

[LAE98] R.A. Lippert, T.A. Arias, and A. Edelman. Multiscale computation with interpolating wavelets. *J. Comput. Phys.*, 140:278, 1998.

[Lem91] P.G. Lemarié. Some remarks on wavelet theory and interpolation. Technical Report 91-13, Univ. Paris Sud, 1991.

[Lew94] R.M. Lewis. Cardinal interpolating multiresolutions. *J. Approx. Theory*, 76:177, 1994.

[Lip98] R.A. Lippert. *Nonlinear Eigenvalue Problems*. PhD thesis, M.I.T., 1998.

[LPT89] J. Liandrat, V. Pierrier, and Ph. Tchamitchian. Numerical resolution of the regularized Burgers equation using the wavelet transform. *Tech. Report CPT-89/P. 2320 - Center of Theoretical Physics, Marseille, France*, 1989.

[LT90] J. Liandrat and P. Tchamitchian. Resolution of the 1d regularized burgers equation using a spatial wavelet approximation. report, Technical Report 90-83, NASA ICASE, December 1990.

[Mal89] S. Mallat. Multiresolution approximation and wavelets. *Trans. Amer. Math. Soc.*, 315:69, 1989.

[MCC97] Yves Meyer, Ronald Coiffman, and Ronald Coifman. *Wavelets : Calderon-Zygmund and Multilinear Operators*, volume 48 of *Cambridge Studies in Advanced Mathematics*. Cambridge Univiversity Press, Cambridge, U.K., 1997.

[Mey86] Y. Meyer. Ondelettes, fonctions splines et analyses graduées. Lectures given at the University of Torino, Italy, 1986.

[Mey90] Y. Meyer. *Ondeletts et Opérateurs*. Herman, Paris, 1990.

[MJ94] Rodolphe L. Motard and Babu Joseph, editors. *Wavelet Applications in Chemical Engineering*. Kluwer Academic Publishers, Boston, 1994.

[MP76] H.J. Monkhorst and J.D. Pack. Special points for brillouin-zone integrations. *Physical Review B*, 13:5188, 1976.

[NC97] A. Nakano and T. Campbell. An adaptive curvilinear-coordinate approach to dynamic load balancing of parallel multiresolution molecular dynamics. *Parallel Comput.*, 23:1461, 1997.

[Pic89] W.E. Pickett. Pseudopotential methods in condensed matter applications. *Comp. Phys. Rep. Lett.*, 9:115, 1989.

[PSU93] Stefan Pittner, Josef Schneid, and Christoph W. Ueberhuber. *The Wavelet Literature Survey*. Institute for Applied and Numerical Mathematics, Vienna, 1993.

[PTA+92] M.C. Payne, M.P. Teter, D.C. Allan, T.A. Arias, and J.D. Joannopoulos. Iterative minimization techniques for *ab initio* total energy calculations: molecular dynamics and conjugate gradients. *Rev. Mod. Phys.*, 64:1045, 1992.

[PZ81] J.P. Perdew and A. Zunger. Self-interaction correction to density-functional approximations for many-electron systems. *Phys. Rev. B*, 23:5048, 1981.

[Ran93] E. Rank. Adaptivity and accuracy estimation for fem and biem. In C.A. Brebbia and M.H. Aliabaldi, editors, *Adaptive Finite and Boundary Element Methods*. Computational Mechanics Publications, Southampton, 1993.

[RJZ94] A. Rieder, R.O. Wells Jr., and X. Zhou. A wavelet approach to robust multilevel solvers for anisotropic elliptic problems. *Appl. Comput. Harmon. Anal.*, 1:355, 1994.

[SB93] N. Saito and G. Beylkin. Multiresolution representations using the auto-correlation functions of compactly supported wavelets. *IEEE Trans. Sig. Proc.*, 41:3584, 1993.

[Sin94] D.J. Singh. *Planewaves, Pseudopotentials and the LAPW Method*. Kluwer Academic Publishers, Netherlands, 1994.

[SN96] G. Strang and T. Nguyen. *Wavelets and Filter Banks*. Wellesley-Cambridge Press, Wellesley, 1996.

[Sut98] Bruce W. Suter. *Multirate and Wavelet Signal Processing*, volume 8 of *Wavelet Analysis and Its Applications*. Academic Press, San Diego, 1998.

[Swe96] W. Sweldens. The lifting scheme: A custom-design construction of biorthogonal wavelets. *Appl. Comput. Harm. Anal.*, 3:186, 1996.

[TB95] K.A. Iyer T.L. Beck, M.P. Merrick. Multigrid method for large scale electronic structure. In A. Tentner, editor, *Proceedings of the 1995 Simulation Multiconference: Grand Challenges in Computer Simulation*, page 141, San Diego, 1995. SCS.

[Tet93] M.P. Teter. Comment on cardinality and inverse transforms. Private communication, 1993.

[TT95a] E. Tsuchida and M. Tsukada. Electronic-structure calculations based on the finite-element method. *Phys. Rev. B*, 52:5573, 1995.

[TT95b] E. Tsuchida and M. Tsukada. Real space approach to electronic-structure calculations. *Solid State Commun.*, 94:5, 1995.

[TT96] E. Tsuchida and M. Tsukada. Adaptive finite-element method for electronic-structure calculations. *Phys. Rev. B*, 54:7602, 1996.

[TW97] C.J. Tymczak and Xiao-Qian Wang. Orthonormal wavelet bases for quantum molecular dynamics. *Phys. Rev. Lett.*, 78:3654, 1997.

[Uns93] M. Unser. Efficient dyadic wavelet transformation of images using interpolating filters. In *Proc. of IEEE Intern. Conf. on Acoustics, Speech and Signal Processing*, volume 5, Piscataway, 1993. IEEE Press.

[VYP97] O.V. Vasilyev, D.A. Yuen, and S. Paolucci. Solving pdes using wavelets. *Computers in Physics*, 11:429, 1997.

[WC96] Siqing Wei and M.Y Chou. Wavelets in self-consistent electronic structure calculations. *Phys. Rev. Lett.*, 76:2650, 1996.

[Wes92] P. Wesseling. *An Introduction to Multigrid Methods*. John Wiley & Sons, Chichester, N.Y., 1992.

[Whi97] J.R. Whiteman, editor. *The Mathematics of Finite Elements and Applications: Highlights 1996*. John Wiley & Sons, New York, 1997.

[WKWF81] E. Wimmer, H. Krakauer, M. Weinert, and A.J. Freeman. Full-potential self-consistent linearized-augmented-plane-wave method for calculating the electronic structure of molecules and surfaces: O_2 molecule. *Phys. Rev. B*, 24:864, 1981.

[WWT89] S.R. White, J.W. Wilkins, and M.P. Teter. Finite-element method for electronic structure. *Phys. Rev. B*, 39:5819, 1989.

[YA98] D. Yesilleten and T.A. Arias. The hopgrid algorithm: multilevel synthesis of multigrid and wavelet theory. xxx.lanl.gov e-Print archive # physics/9806034, 1998.

[Yes97] Dicle Yesilleten. Multiscale modelling in electronic structure calculations. S.B. Thesis, Department of Phyiscs M.I.T., 1997.

[ZMK96] G. Zumback, N.A. Modine, and E. Kaxiras. Adaptive coordinate, real-space electronic structure calculations on parallel computers. *Solid State Commun.*, 99:57, 1996.